Performance of Green Smart-Heat Cured Cementitious Materials

Osama Abdelrahman

A Thesis

In the Department

of

Building, Civil and Environmental Engineering

Presented in Partial Fulfillment of the Requirements

For the Degree of

Master of Applied Science (Civil Engineering) at

Concordia University

Montreal, Quebec, Canada

April 2021

CONCORDIA UNIVERSITY

SCHOOL OF GRADUATE STUDIES

This is to certify that the thesis prepared

By: Osama Abdelrahman

Entitled: Performance of Green Smart-Heat Cured Cementitious Materials

and submitted in partial fulfillment of the requirements for the degree of

Master of Applied Science (Civil Engineering)

Complies with the regulations of the University and meets the accepted standards with respect to originality and quality.

Signed by the final examining committee:

_____ Chair, Examiner
Dr. Michelle Nokken

_____ Examiner
Dr. Biao Li

_____ Supervisor
Dr. Ahmed Soliman

Approved by _____
Dr. Michelle Nokken, Graduate Program Director

April 30th, 2021 _____
Dr. Ashutosh Bagchi, Dean of Faculty

ABSTRACT

Performance of Green Smart-Heat Cured Cementitious Materials

Osama Abdelrahman

During the cold winter season, all in-situ construction activities are halted, leading to economic losses. Hence, shifting to precast elements represents an optimum solution. However, the high energy intensity heat curing process for precast elements represents a challenge. On the other hand, microencapsulated phase change materials (MPCMs) was used to improve cementitious material thermal storage capacity. However, a reduction in mechanical properties and losing thermal efficiency were reported due to MPCMs breakage during the construction process. Hence, this dissertation proposed two solutions: 1) Modifying cementitious mixtures design to reduce MPCMs fracturing risk while maintaining adequate performance and 2) Novel smart external curing sheets. Results reveal that incorporating limestone filler in mixtures was a promising green sustainable solution. Moreover, maintain adequate MPCMs in the mixtures was found to improve the later thermal performance for elements, which is considered additional benefits. The external use of MPCMs in the curing process had resulted in shorting the required curing period to achieve targeted strength. Optimizing thermal capacity and heat curing process for precast elements will increase work efficiency and economic benefits for the precast industry. It will also reduce the energy demand and cut down the precast industry's carbon footprint, leading to a higher level of sustainability.

ACKNOWLEDGEMENTS

I would like to express my sincere appreciation to my supervisor, Prof. Ahmed Soliman, for his support, guidance, and encouragement. Also, I would like to acknowledge the support and guidance provided by my MASc examination committee members Prof. Michelle Nokken and Prof. Biao Li. Moreover, I would like to thank all Concordia staff, especially the technician team. Moreover, I would like to thank my parents, Eng. Ahmed Abouelsoud and Siza Assal and my grandmother, Ms. Souad Ashour and my brothers for their continuous support and prayers. Although I was away from them for a long period, their support was felt as they lived with me. I love you all.

Furthermore, I would like to express my sincere gratitude and appreciation to all companies supporting me with materials: Lafarge CA, Omeya CA, Sika CA, and microteklabs inc.

Table of Contents

List of Figures ix

List of Tables xi

Chapter 1 Thesis Over view 1

1.1 Introduction 1

1.2 Research Objectives 4

1.3 Research Outline 4

1.4 Original Contributions 5

Chapter 2 Literature review 6

2.1 Smart Concrete 6

2.2 Definition of Smart Concrete 6

2.3 Self-Expanding Concrete 7

2.3.1 Theory of Self-Expanding concrete 8

2.3.2 Applications of Self-Expanding Concrete: 9

2.3.3 Applications of Self-Compensating Concrete 10

2.3.4 Applications of Self-Stressing Concrete 10

2.4 Self-Curing Concrete 11

2.4.1 Theory of Self-Curing Concrete 11

2.4.2 Application of Self-Curing Concrete 12

2.5 Self-Shaping Concrete 13

2.5.1 Theory of Self-shaping concrete 13

2.5.2 Applications of Self-Shaping Concrete 14

2.6 Self-Sensing Concrete 15

2.6.1 Theory of Self-sensing concrete 15

2.7 Self-adjusting concrete 16

2.7.1 Phase change materials (PCMs) 17

2.7.2 Types of Phase Change Materials 18

2.7.3 Thermal properties of PCMs 19

2.7.4 Phase change material in construction Materials 21

2.7.5 Incorporating Limestone filler in Self-compacted mortar 23

2.7.6 The physical effect of limestone: 25

2.7.7 Chemical effect of limestone 26

2.7.8 Effect of Steam Curing Temperature 26

Chapter 3 PROPERTIES OF SCM INCORPORTAING LIMESTONE 29

3.1 Experimental Program 29

3.1.1 Materials and mixture design 29

3.1.2 Concrete Mixing 31

3.1.3 Testing methods 32

3.2 RESULTS AND DISCUSSION 33

3.2.1 Flowability 33

3.2.2 Heat of Hydration 35

3.2.3 Thermal Analysis 43

3.2.4 Shrinkage 45

3.2.5 Compressive strength 46

Chapter 4 PROPERTIES OF SCM INCORPORATING LIMESTONE AND PHASE CHANGE MATERIALS 49

4.1 Experimental Program 49

4.1.1 Materials and mixture design 49

4.1.2 Mixing procedure 50

4.1.3 Testing methods 51

4.2 RESULTS AND DISCUSSION 54

4.2.1 Flowability 54

4.2.2 Heat of Hydration 55

4.2.3 Thermal Analysis 57

4.2.4 Compressive strength 59

4.2.5 Shrinkage 61

4.2.6 Heat Flux 62

4.2.7 Thermal conductivity 63

Chapter 5 A NOVEL PHASE CHANGE MATERIALS CURING SHEET 65

5.1 Significance of Research 65

5.2 Experimental Program 65
5.2.1 Materials and mixture design 65
5.2.2 Fabrication of the Curing Sheets 66
5.2.3 Curing regime 67
5.2.4 Testing and Specimen Preparation 68
5.2.5 Methodology 70
5.3 RESULTS AND DISCUSSION 71
5.3.1 Heat Profile 71
5.3.2 Cube Compressive Strength 75
5.3.3 Thermal Camera 77
5.3.4 Scanning Electron Microscopy Analysis 79
5.3.5 Thermal analysis 80
5.3.6 Thermal Conductivity 83
Chapter 6 CONCLUSIONS 85
6.1 Conclusions 85
References 88

List of Figures

Fig 2.1 Examples of the three main categories of concrete printing (a) D-shape, (b) concrete printing, (c) CC (Lim et al. 2012) 14

Fig 2.2 A 3D printing machine was built by ROHACO, a Dutch company (Zhang et al. 2019). 15

Fig.2.3 (a) Energy consumption in each sector; (b) CO_2 emissions from each sector (Frigione, Lettieri, and Sarcinella 2019) 17

Fig 2.4 Latent heat and sensible heat storage (Soares 2016) 20

Fig 2.5 stander PCMs during the melting and solidification cycle with supercooling (Soares 2016) 21

Fig 3.1 Sieve analysis of fine aggregate 31

Fig 3.2 Slump flow of mortar made with various sizes and content of LF as sand and cement replacement. 34

Fig 3.3 V-funnel of mortar made with various sizes and content of LF as sand 35

Fig 3.4 Effect of LF size on the Heat of Hydration for mixtures a) 5% b)10% c) 15% d) 20% sand replacement 37

Fig 3.5 Effect of LF size on the Heat of Hydration for mixtures a) 5% b)10% c) 15% cement replacement 38

Fig 3.6 Effect of LF size on Total Energy Released for mixtures a) 5% b)10% c) 15% d) 20% sand replacement 39

Fig 3.7 Effect of LF size on Total Energy Released for mixtures a) 5% b)10% c) 15% cement replacement 40

Fig 3.8 Effect of LF Content and size on hydration peak 41

Fig 3.9 Effect of LF Content and size on Total energy released 43

Fig 3.10 Effect of LF Content and Size as sand replacement on $Ca(OH)_2$ Content 44

Fig 3.11 Effect of LF Content and Size as cement replacement on $Ca(OH)_2$ Content 45

Fig 3.12 Effect of LF Content and Size on shrinkage of SCM 46

Fig 3.13 effect of LF content and size on compressive strength a) 5% b) 10% c) 15 d) 20% 48

Fig 4.1 Heat flow meter (HFM436, manufactured by NETZSCH) 53

Fig 4.2 Thermal conductivity samples 54

Fig 4.3 Effect of LF and MPCMs on Heat of Hydration 57

Fig 4.4 derivative thermogravimetric analysis (DTG) of mortar with different MPCM content . 59

Fig 4.5 Compressive strength for mixtures incorporating various percentages of MPMCs 60

Fig 4.6 Effect of LF and MPCMs content on shrinkage on SCM 61

Fig 4.7 Heat flow of Mortar made with different percentage of MPCMs 63

Fig 4.8 Thermal conductivity of MPCMs samples 64

Fig 5.1 PCMs curing sheet 67

Fig 5.2 Various curing regime 68

Fig 5.3 Illustration for the curing stages with and without coverage with the sheet (Tc: chamber's temperature, Ts: Specimen's temperature, and Tp: PCM sheet's temperature) 70

Fig 5.4 Temperature profile of the MPCMs sheet and chamber 72

Fig 5.5 Temperature profile for samples at 5 Hrs maximum holding time 73

Fig 5.6 Temperature profile for samples at 10 Hrs maximum holding time 74

Fig 5.7 Temperature profile of samples at different curing regimes 74

Fig 5.8 Compressive strength for mortar under different curing regimes 77

Fig 5.9 the temperature of both sides of the MPCMs sheet 78

Fig 5.10 Thermal image for temperature evolves from specimens covered and not covered by the MPCMs sheet after (a) 1 hr; (b) 3hrs; and (c) 5 hrs 78

Fig 5.11 SEM photograph of mortar at different curing regimes: (a) 10 hrs; (b) 10 hrs + MPCMs sheet; (c) 5hrs; (d) 5hrs + MPCMs sheet 79

Fig 5.12 TG/DTG curves for self-compacted mortar cured at various curing regimes at 1 Day . 82

Fig 5.14 Temperature of Upper and lower plate 84

Fig 5.15 Thermal conductivity of MPCMs Sheet at various mean temperatures 84

List of Tables

Table 2.1: The Advantages and disadvantages of different types of PCM 19

Table 2.2: Maximum Allowable Curing Temperatures (Hwang et al. 2012) 28

Table 3.1:Chemical and physical properties of cement 30

Table 3.2: Physical properties of River Sand 30

Table 3.3: Mix design of tested mixture 31

Table 4.1: MPCM 28°C properties 50

Table 4.2: Mixture design of all tested mixtures 51

Table 4.3: Flowability of SCM incorporating different dosages of MPCMs 55

Table 5.1: MPCM 43°C properties 66

Table 5.2: The total weight loss of SCM during the TGA test 83

Chapter 1 THESIS OVERVIEW

1.1 Introduction

Energy is the driving force of the economy, production, and daily life activities. Energy consumption has become one of the challenging dilemmas the world face now, with the endless growing economy and uprising technologies. The energy demand is rising, along with the limited energy resources, more significant environmental impacts are widening much effort to discover the alternative source of fossil fuel. The building sector consumes around 30% of the total energy consumption and contributes about 30% of total carbon dioxide (CO_2) emissions (Jeon et al., 2013; Frigione, Lettieri, and Sarcinella, 2019). This is attributed to the high-level standard in terms of cooling and heating for both hot and cold climates (Kara, Kurnucß, and Arslanturk 2009; Lu et al. 2017; Frigione, Lettieri, and Sarcinella 2019). Thus, there is a need to increase energy efficiency for buildings.

One way to reduce emissions is using an alternative method to produce electricity; however, most of these sources are intermittent sources of power and depend on the location's climate. For example, solar energy cannot be utilized to regulate cooling and heating on a cloudy day or at night, as there is no sufficient energy stored in the system (Von Paumgartten 2003). A different approach to conserving energy is adjusting the building materials' heat storage through sensible and latent heat storage materials. Sensible heat storage in construction materials transfers heat to the material and increases its temperature throughout the heat storage process. On the other hand, latent heat storage absorbs and releases energy during the phase change without increasing the surroundings' temperature until reaching the maximum storage and then act as sensible heat storage material (Fernandes et al. 2014).

Building energy consumption can be reduced by 30% to 50 % by integrating thermally efficient technologies (Von Paumgartten 2003; Fernandes et al. 2014). Different approaches are available through insulation methods, smart systems and building materials. Researchers are working to implement more new thermal systems to conserve buildings' energy.

Phase Change Materials (PCMs) as thermal storage materials had been studied since 1980 (Castell et al. 2010; Telkes 1975; Abhat 1983a; Lane 1983a; 1983b). PCMs are smart, responsive materials that change their state as the surrounding temperature change. If the temperature increases, PCMs convert from solid to the liquid state and absorb heat (i.e. an endothermic process). However, if the temperature goes down, PCMs convert from liquid to the solid-state and release stored heat (i.e. exothermic process) (Pomianowski, Heiselberg, and Zhang 2013). PCMs can be organic (e.g. paraffin), inorganic (e.g. hydrated salts), and eutectic mixtures materials (i.e. a mix of an organic and inorganic compound) (Waqas and Ud Din 2013; Abhat 1983b; Zalba et al. 2003; Khudhair and Farid 2004; Pasupathy, Velraj, and Seeniraj 2008; Cui et al. 2015). Among those categories, paraffin PCMs is commonly used in construction applications due to their low price, good thermal storage density (i.e. 120 kJ/kg up to 210 kJ/kg), chemically inert, wide melting temperature range (i.e. from 20°C up to 70 °C) and no phase segregation (Baetens, Jelle, and Gustavsen 2010). However, its low thermal conductivity (i.e. 0.2 W/m.K) and large volume change through the transition phase must be considered (Baetens, Jelle, and Gustavsen 2010; Hasnain 1998). PCMs were successfully incorporated in construction materials, such as wallboards, roofs, floors, paste, mortar, and concrete. It had proved high abilities to improve thermal energy storage for different elements (Frigione, Lettieri, and Sarcinella 2019).

Several incorporation methods for PCMs, including impregnation, shape stabilization PCMs, micro-encapsulation, and macro-encapsulation, were proposed (Cui et al., 2015). However, micro-

encapsulated PCMs are recommended for cementitious materials to avoid interfering with the hydration process (Cui et al., 2015; Hasnain, 1998). Previous research had proven that adding PCMs to concrete will improve its heat capacity and heat exchange (Fernandes et al., 2014). These result in better control for temperature fluctuation and consequently avoid thermal cracking and improve freezing-thawing resistance. Conversely, one of the main drawbacks of adding PCMs to concrete is reducing the mechanical properties induced by paraffin leakage and voids induced by broken PCMs capsules during mixing (Hunger et al. 2009).

Self-compacted mortar (SCM) is a special type of mortar that can flow under its weight without bleeding and segregation (Benabed et al. 2012; Okamuara and Ouchi 1999). It is designed to have proper viscosity to ensure homogenous particles and decrease the collision of inner particles that can cause the breakage of PCMs. Previous studies showed that adding fine limestone will improve workability through freeing entrapped water and enhance strength due to the densifying the microstructure (Benabed et al. 2012; Felekoğlu 2008; Aïtcin 2011; Domone and Jin 1999). The low mixing energy and high flowability for SCM make it a potential carrier media for encapsulated PCMs.

During the cold winter season, all in-situ construction activities are halted, leading to economic losses. Hence, shifting to precast concrete represents an optimum solution to maintain construction progress during such harsh environments. However, the heat curing process for precast elements represents a challenge for the precast industry due to its high energy consumption. A novel phase change material curing sheets were developed and tested. Results showed that covering the specimens during the cooling period had significantly enhanced strength development, even for the shorter heating period

1.2 Research Objectives

The purpose of this thesis is to investigate the effect and the mechanism of incorporating limestone filler and microencapsulated phase change materials on the mechanical properties and durability performance of the self-compacted mortar. Therefore, this study examines the feasibility of utilizing phase change materials (PCMs) to optimize the heat curing process that enables the precast industry to produce its work efficiently and economically

This will be achieved through:

1. Inspecting the effect of limestone filler (LF) content and fineness on the hydration products and the hydration kinetics.
2. Evaluating the effect of LF and MPCMs incorporating in SCM under different curing conditions.
3. Proposing a modified curing regime using PCMs sheet that can be adapted in the precast industry to enhance production cost efficiency.

1.3 Research Outline

The research in this thesis was carried out in four stages. Each chapter explores one of the Research Objectives (section 1.2).

- ***Chapter 2*** provides a comprehensive literature review about the different types of smart concrete and their application in building material. Besides, reviewing the physical and chemical effects of limestone on self-compacting mortar.
- ***Chapter 3*** investigates the influence of limestone filler fineness and content on the fresh, harden properties and hydration kinetics of self-compacting mortar.

- ***Chapter 4*** presents a potential solution of using the self-compacting mortar to lower yield stress and reduce the risk of fracturing the capsules. Besides, incorporating limestone filler to improve the cement-based physical and chemical aspects.
- ***Chapter 5*** examines the feasibility of utilizing phase change materials (PCMs) to optimize the heat curing process and propose novel phase change material curing sheets. Two main modifications were applied for the most common steam curing process: i) shortening the maximum temperature holding period (i.e. 5 hrs instead of 10 hrs) and ii) covering specimens by the developed PCMs sheet during the cooling period.

1.4 Original Contributions

1. Developing an extensive database on the different types of smart concrete available and their application in the building sector.
2. Investigate the influence of limestone filler fineness and content on the fresh, harden properties and hydration kinetics of self-compacting mortar.
3. Optimize the percentage of Limestone filler in the self-compacting mortar.
4. Investigating the effects of limestone content on the mechanical performance and thermal properties of self-compacted mortar (SCM), incorporating different percentages of MPCMs.
5. Presenting a potential solution of using the self-compacting mortar to lower yield stress and reduce the risk of fracturing the phase change materials' capsules. Besides, incorporating limestone filler to improve the cement-based physical and chemical aspects.
6. Identify the optimum combination of MPCMs and Limestone to improve concrete thermal properties.
7. Fabricating a curing sheet for the precast industry to increase energy efficiency.

Chapter 2 LITERATURE REVIEW

2.1 Smart Concrete

Concrete is a multiscale and multiphase material. It is composed of different components as cement, aggregates, water, chemical and mineral additives. Concrete includes different phases as solid, liquid, and gas. Its structure includes different sizes, nanometers as Hydration product, micrometres as the binder, and a range from millimetre as mortar and concrete to tens of meters as final structures. Besides, various modification materials such as polymer, powder filler, and fibre filler or different components as actuator and sensors can be incorporated easily. Thus, it is achievable to have smart concrete with multi-functional characteristics (Gambhir 2013; Boyd, Mindess, and Skalny 2002; Newman and Choo 2003; Malier 1992; Gjorv and Sakai 1999; Pacheco-Torgal et al. 2013; Han, Zhang, and Ou 2017a).

2.2 Definition of Smart Concrete

Smart concrete is an intelligent system that has different properties than conventional concrete. For example, it can react under an external stimulus, such as stress or temperature or has self-healing, self-sensing, electrically conductive, electromagnetic, and thermal properties. Smart concrete is designed to achieve a specific requirement by improving its properties to enhance safety, infrastructure function, and durability. Also, to reduce environmental pollution, life cycle cost, and consumption of resources. Smart concrete is achieved through modification in the conventical concrete microstructure or through introducing functional components, composition design (Han, Zhang, and Ou 2017a; Han et al. 2015; Gandhi and Thompson 1992; Schwartz 2008)

Conventional concrete has structure abilities with no smart abilities. On the other hand, smart concrete has structural and intelligent behaviour (i.e. self-adjusting, self-sensing, self-healing, electrically conductive, thermal, and electromagnetic behaviours). Smart concrete is considered a

hybrid system, where multi-functional concrete can be designed according to application requirements.

According to dissipative structure theory, there is no negative entropy input through energy, matter or information exchange with external stimuli during its service period of conventional concrete during its service period. On the other hand, smart concrete can be supplied with energy, matter, or/and information through different approaches such as physical, chemical, biological methods. There is a negative entropy between smart concrete and external stimuli, which has various benefits. Firstly, producing a new generation of multifunction and smart concrete featured with adaptive capabilities and self-organization to external stimuli (e.g. loads or environment) while improving or maintaining mechanical properties. Secondly, the increase in the entropy caused by external interference and damage can be equilibrated so concrete mechanical properties and durability can be maintained or enhanced during service life. (Han, Zhang, and Ou 2017a; S.-K. Lin 1999; Schneider and Kay 1995)

2.3 Self-Expanding Concrete

Self-expanding concrete or expansive concrete mainly consists of Portland cement, water, aggregate and expansive material. It can compensate for the shrinkage of concrete by producing expansion during hydration and drying time or building up chemical prestress inside the concrete structure. There are two types of self-expanding concrete (i.e. self-stressing concrete and self-compensating concrete).

Self-stressing concrete is also called chemically prestressed concrete. An adequate amount of compressive stress can be induced to develop prestress in the concrete structure under particular conditions. In general, self-stressing concrete expansion stress should be more than 2.0 MPa

(Han, Zhang, and Ou 2017d). However, according to American researchers' opinion, self-stress cannot exceed 0.7 MPa (Wu and Zhang 1990).

Self-compensating concrete is also called shrinkage-compensating concrete. Compressive stress can be induced by its expansion, where it can offset stress caused by drying shrinkage in concrete. According to USA and Japan code-technical specifications, self-compensating concrete's expansive stress is ranged between 0.2 to 0.7 MPa (Wu and Zhang 1990). However, the expansive stress is ranged from 0.2 to 1.0 MPa according to the Chinese code-technical specification (JGJ/T 178-2009) (Yuan, Ma, and Cui 2011).

2.3.1 Theory of Self-Expanding concrete

Self-expanding concrete mainly contains expansive materials as expansive agents and expansive cement. A fixed amount of components and certain expansion energy of expansive cement under-designed amount of cement to water ratio is used. According to ASTM, expansive cement is categorized into three types based on original minerals Type K, Type M, Type S (Han, Zhang, and Ou 2017d; Kesler and Pfeifer 1970).

Expansive cement showed drawbacks while developing engineering applications where it is difficult to adjust the percentage of expansive materials, and expansive energy to obtain different degrees of flexible prestress and shrinkage components. In addition to that, expansive cement attack moisture and need protection during transportation and storage which result in short quality guarantee period and higher cost. Also, expansion resulted from ettringite formation consumes a large amount of water. Additionally, ettringite might decompose at high temperatures (i.e. over 70 ºC), resulting in unstable mass concrete under high temperature. Moreover, expansive component particles do not need to be grounded as Portland cement clinker. Thus, the expansive components are ground separately from cement clinker, then

separately mixed as an expansive agent at demand dosage with the concrete mixture to gain designed expanding stress and strain (Han, Zhang, and Ou 2017d).

There are various expansion mechanism theories of self-expanding concrete. Crystal growth theory is spreading out by crystal growth of expansive ingredients (Chatterji and Jeffery 1963; Okushima 1968; Chatterji and Jeffery 1966; Isogai 1975). swelling theory where water absorption results increase in volume gel state expansive ingredients (Povindar Kumar Mehta 1973; Eura, Yamazaki, and Monji 1975). coexisting pores are formed during hydration by disintegrating expansive ingredients (Ramachandran, Sereda, and Feldman 1964). In either case, the formation of gel or formation of pores both required for expansion to coexist with chemical shrinkage. If the expansion due to ettringite or CH formation, at the surface of expansion ingredient topo-chemical reaction is accepted. The primary factor is the compressive force produced from expansive ingredients transmitted from surrounding hydrates, not only the hydration of expansive ingredients. Thus, the hydration of cement and expansive agents must take place simultaneously (Nagataki and Gomi 1998).

2.3.2 Applications of Self-Expanding Concrete:

Self-expanding concrete has been widely used since the 1950s for the purposes of chemical prestressing and shrinkage compensation. The Soviet Union used self-expanding concrete for subway joints. China used Type M expansive cement for tanks and pipe joints in the 1960s. At the same time, self-expanding concrete was used by the US and Japan in various practices as waterproofing, anti-cracking, and anti-leakage. (Han, Zhang, and Ou 2017d; Nagataki and Gomi 1998).

2.3.3 Applications of Self-Compensating Concrete

There are different types of concrete structures fabricated with self-compensating concrete, such as in impervious concrete structures, anti-cracking concrete structures, holes, cracks, joints gaps, sealing engineering, mass concrete structures, shrinkages compensating slabs, expansive concrete reinforcing bands (Wu and Zhang 1990; Nagataki and Gomi 1998).

2.3.4 Applications of Self-Stressing Concrete

Chemical prestress in structure, and members can be established by self-stressing concrete without using complex equipment and tensioning procedures. Self-stressing concrete can be used in thin members and structures such as shell, pipe, tank, and slab. Self-stressing concrete pipe is the most widely used among others. Self-stressed concrete pipe has a great advantage over traditional cast-iron pressure pipe. It provides energy and steel conservation, high durability, and less investment. The self-stressed reinforced pipe has better durability, impermeability, and easier to produce than a mechanical prestressed concrete pipe (Kreston 1970; Mizuma 1972; Iida 1976). Chinese standard (Chang, Huang, and Chen 2009) recommended three types of pipes that have been widely used in municipal, industrial, traffic, conservancy, agricultural infrastructures of urban, mining, industry, and traffic (Han, Zhang, and Ou 2017d).

Recently, self-expanding concrete has been used in steel tube fulling to enhance steel tube concrete structures and members' performance. Steel tubes filled with self-expanding concrete instead of ordinary concrete experienced increasing core strength carrying load capacity and compensating shrinkage (Yan and Pantelides 2011). Hence, these high-performance columns have been used at skyscrapers and arch bridges—for example, Yonghe Bridge in China and Qijia Yellow River Bridge.

2.4 Self-Curing Concrete

Curing concrete is vital after casting concrete to avoid shrinkage, thermal deformation, and settlement during early ages. That is why curing is essential for concrete to achieve the durability and mechanical properties required. Thus, ideal curing conditions require suitable ambient temperature, humidity, moisture, and temperature, which cannot be fulfilled in most projects. However, we can satisfy these conditions through traditional curing methods as spraying, ponding, covering plastic films, or wet burlap. However, curing problems shouldn't be ignored in high-performance concrete (HPC). High-performance concrete is characterized by a high percentage of additives as silica fumes and low water to binder ratio, enabling it to have high density and strength at an early age. Subsequently, it is not easy to penetrate external water through traditional curing methods. Thus, it will be challenging to satisfy the binder's total hydration; serious cracks may be caused by autogenous shrinkage and chemical shrinkage. Consequently, cracks increase degradation of durability and mechanical properties (Han, Zhang, and Ou 2017b).

2.4.1 Theory of Self-Curing Concrete

Curing is divided into two types: internal and external curing. Conventional concrete curing where water is not lost from the surface enables curing to happen outside to inside. However, internal curing, also called self-curing, allows curing from inside to outside. It is achieved by incorporating internal curing materials as pre-saturated components, which act as an internal reservoir. The water inside the curing agent doesn't occur in the chemical reaction until the humidity gradient generates after the early hydration period. The self-curing process occurs at the contact area between cement past and self-curing agent where water is transferred to un-hydrated cement by vapour diffusion, capillary suction, and capillary condensation.

Consequently, avoiding chemical shrinkage and autogenous shrinkage caused by low water to binder ratio (Han, Zhang, and Ou 2017b).

The self-curing agent is a vital component in self-curing concrete. This is because it works as an internal reservoir with a high water absorption capacity in an aqueous solution. For example, pre-saturated porous lightweight aggregate (LWA) and chemical admixtures such as shrinkage-reducing admixture (SRA), superabsorbent polymer (SAP), and wood powder (Ahamed, Pradeep, and Plan 2015). lightweight aggregate (LWA) as ceramsite and pumice contains water by weight of 5-25%. Shrinkage-reducing admixture (SRA), superabsorbent polymer (SAP) are characterized by ultra-high water absorption around 1000 times higher than their weight (Jensen and Hansen 2001).

2.4.2 Application of Self-Curing Concrete

Self-curing concrete has been employed in different engineering applications such as bridge decks and pavements (Han, Zhang, and Ou 2017c). In 2005, a large railway transit yard of about 190,000 m3 of self-cured HPC with LWAs was cast in Texas, USA. Consequently, significant improvement in cement hydration and extreme minimizing in shrinkage cracks were recorded compared to conventical concrete (Villarreal and Crocker 2007). In 2010, the Department of Transportation in New York constructed nine bridges by self-curing concrete where an extra 120 kg/m^3 of fine LWA was added. It was reported an increase of 2-10% in Count Street Bridge's strength and 15% of Bartell Road Bridge at 28 days. However, the initial cost is slightly higher than standard concrete. However, a 63% reduction in the life cost cycle as service life is higher than conventical concrete (Cusson, Lounis, and Daigle 2010).

2.5 Self-Shaping Concrete

The construction industry is one of the significant business drivers. On the other hand, it has been challenging to obtain targets (e.g. less construction time, a lower amount of wastages, and pollution). To take care of this issue, three-dimensional printing technology is developed with self-shaping concrete. Three-dimensional printing (3DP) machine needs only self-shaping concrete as a raw material without the need of formwork, vibration, or any human interaction compared to other conventical concrete, which is environmental and economically friendly. Thus, researchers have done great work to achieve an optimal balance between building mechanical properties and efficiency (Han, Zhang, and Ou 2017e).

2.5.1 Theory of Self-shaping concrete

Designing a building bath for a robotic machine is essential in making self-shaping concrete. 3D-2D slicing software is used to generate a building path that can slice the 3D shape into flat and thin layers thickness where concrete can be layered on top of each other. A Complete 3D structure is finished When all layers at the top of each other. A combination of self-compacting concrete and spray concrete is expected to be employed in 3DP concrete as there is no formwork and vibration (Gosselin et al. 2016). Self-shaping concrete is employed as the ink for the 3D printer, where workability is essential to the printed structure's quality. Concrete should pass pipe–pump–nozzle system easily where concrete characterized by high viscosity and low yield stress to achieve concrete with good plasticity. Self-shaping concrete should also provide high early strength and a short sitting time (Perrot, Rangeard, and Pierre 2016).

2.5.2 Applications of Self-Shaping Concrete

There is various application has been reported worldwide for the 3DP. Currently, D-shape, Contour Crafting (CC), and concrete printing are the three main categories of concrete printing in the public domain, as shown in **Fig 2.1** (Lim et al. 2012).

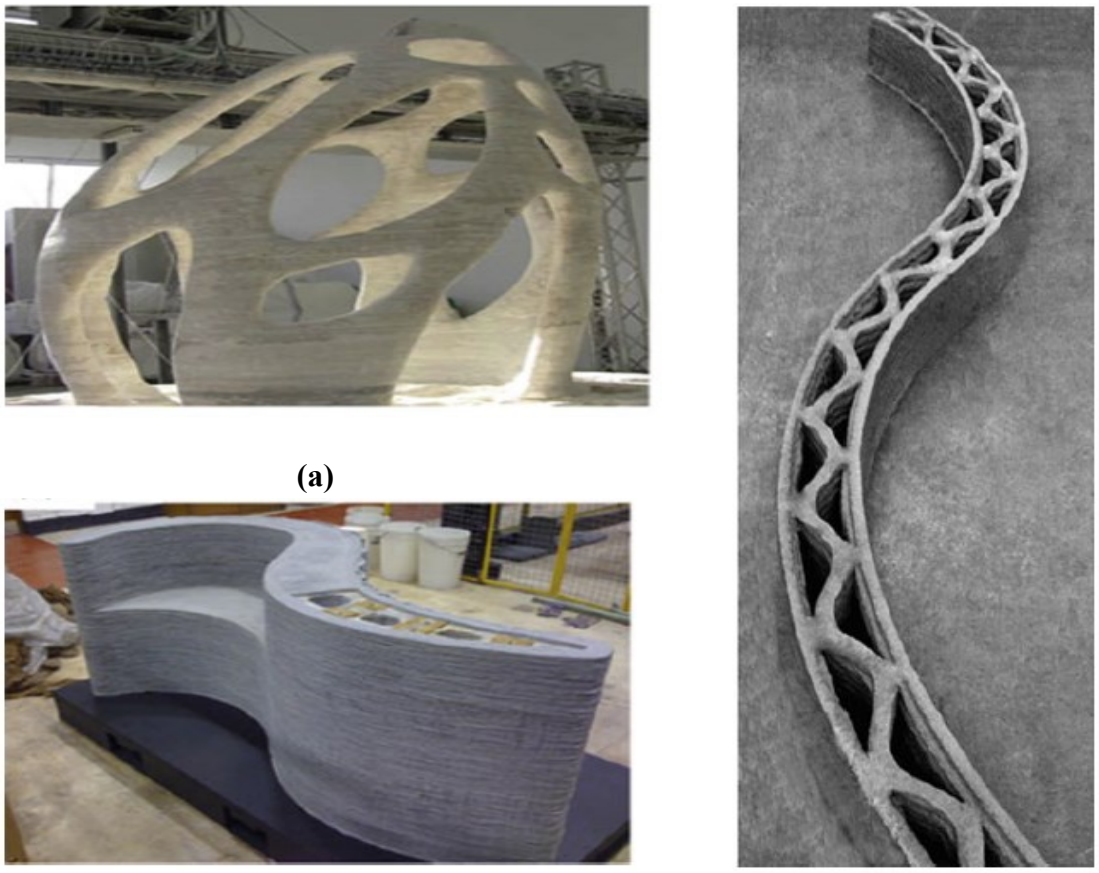

(a) **(b)** **(c)**

Fig 2.1 Examples of the three main categories of concrete printing **(a)** D-shape, **(b)** concrete printing, **(c)** CC (Lim et al. 2012)

It is now possible to Print full-scale constructions, not only large structure components. A 3DP machine can build a 2500 square foot house in 20h (Zhang et al. 2019). In 2015, a group of researchers at the Eindhoven University of Technology in the Netherlands developed a new type of 3DP machine that could provide 11 m × 5 m × 4 m building space with self-shaping concrete with high printing accuracy, as shown in **Fig 2.2.** Also, Chinese company in Shanghai succeeded

in building a five stories apartment block using glass fiber-reinforced concrete as self-shaping concrete (Zhang et al. 2019).

Fig 2.2 A 3D printing machine was built by ROHACO, a Dutch company **(Zhang et al. 2019)**

Self-shaping concrete will save (30%-60%) of construction waste and (50%-80%) of labour cost and will decrease production time by (50%-70%). Hence, self-shaping concrete is forecasted to accomplish significant growth in the upcoming years (Hossain et al. 2020).

2.6 Self-Sensing Concrete

Self-sensing concrete has the capability to sense substantial environmental changes and its conditions, including stain, stress, crack, temperature, damage, and humidity, by incorporating sensing components and functional fillers. It is also called self-diagnosing concrete or self-monitoring. Self-sensing concrete can be classified into intrinsic and non-intrinsic self-sensing concrete.

2.6.1 Theory of Self-sensing concrete

Intrinsic self-sensing concrete is also called piezoresistive, pressure-sensitive, or smart concrete. It is fabricated by integrating different types of filler such as carbon fibre, steel fibre, carbon nanotube, nickel powder into conventical concrete to enhance its ability to sense different

parameter, including stress, strain, temperature, cracks, damage, smoke (Kim 2015), and chloride penetration (Han et al. 2017), while maintaining or enhancing its durability and mechanical properties. A calculated amount of filler is integrated inside the concrete; then concrete becomes conductive. When the hybrid environment's condition is changed due to variation in concrete microstructure, the composite's conductive path is altered. Hence, a change in the electrical properties is occurred (Saafi 2009) (B. Chen and Liu 2008). Different electrical signals can be utilized to determine intrinsic self-sensing concrete's sensing behaviour, including electrical reactance, electrical resistance, relative dielectric constant, capacitance, and electrical impedance tomography. Impedance can be utilized as the sensing signal to identify the sensing behaviour of different geopolymer concrete incorporated with carbon nanotubes (Saafi et al. 2013). Also, electrical impedance tomography can detect concrete damage, producing electrical resistivity maps, which can detect both location and severity of damage by using sand and large aggregate with carbon nanotubes-latex thin films (Gupta, Gonzalez, and Loh 2017).

2.7 Self-adjusting concrete

Concrete material is the first choice for many construction applications. However, from the mining of raw materials until the manufacturing stage, concrete production is a highly intensive energy-consuming process. During concrete production, energy consumption can range from 0.89 to 1.4 MJ/kg (Struble and Godfrey, 2004; Alcorn and Baird, 1996). Many researchers seek new methods to conserve energy in different industries due to the energy recourses limitations and new restrictions on fossil fuel dependency (Marland, Boden, and Andres 2003). Around 77% of the total Canadian energy depletion is from fossil fuels (Brutschin and Fleig 2016). According to the international energy agency shown in **Fig.2.3**, the building sector is on the top energy consumption and responsible for 30% of the energy consumption and about 30% of total carbon-

di-oxide (CO_2) emissions (Jeon et al. 2013; Frigione, Lettieri, and Sarcinella 2019). This is due to the high-level stander in terms of cooling and heating for both hot and cold climates (Kara, Kurnucß, and Arslanturk 2009; Lu et al. 2017; Frigione, Lettieri, and Sarcinella 2019). Thus, there is a need to utilize different renewable energy technology. On the other hand, with the advent of Phase Change Materials (PCMs), many researchers start to examine the potential o adding PCMs in concrete to improve its thermal properties and store energy.

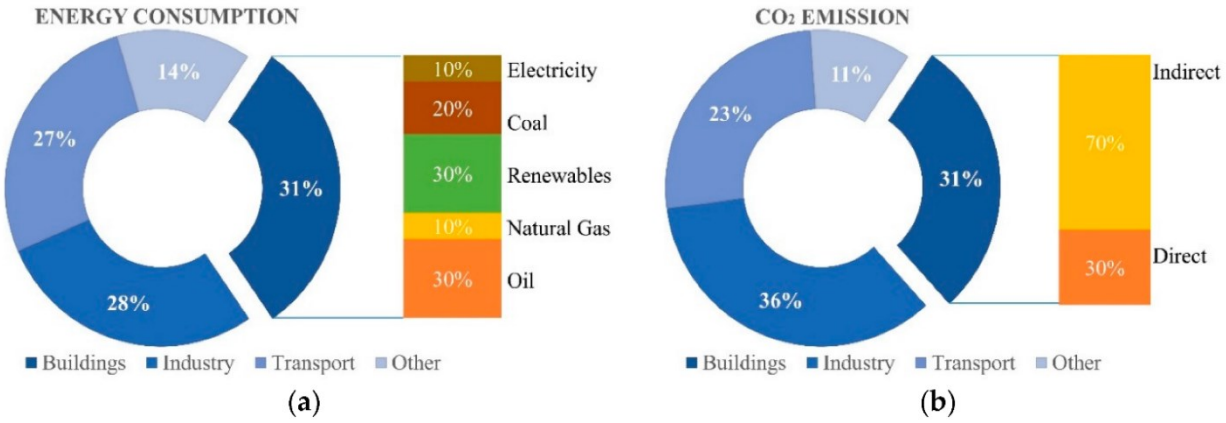

Fig.2.3 (a) Energy consumption in each sector; (b) CO_2 emissions from each sector (Frigione, Lettieri, and Sarcinella 2019)

2.7.1 Phase change materials (PCMs)

Phase change materials are smart, responsive materials that change their state as the surrounding temperature changes (Castell et al. 2010; Telkes 1975; Abhat 1983a; Lane 1983a; 1983b). If the temperature increases, PCMs convert from solid to the liquid state and absorb heat (i.e. an endothermic process). However, if the temperature goes down, PCMs convert from liquid to the solid-state and release the stored heat (i.e. exothermic process) (Pomianowski, Heiselberg, and Zhang 2013).

2.7.2 Types of Phase Change Materials

PCMs can be organic (e.g. paraffin and non-paraffin), inorganic (e.g., hydrated salts), and eutectic mixtures materials (i.e. a mix of an organic and inorganic compound) (Waqas and Ud Din 2013; Abhat 1983b; Zalba et al. 2003; Khudhair and Farid 2004; Pasupathy, Velraj, and Seeniraj 2008; Cui et al. 2015). Among those categories, paraffin PCMs is commonly used in construction applications due to their low price, good thermal storage density (i.e. 120 kJ/kg up to 210 kJ/kg), chemically inert, wide melting temperature range (i.e. from 20°C up to 70 °C) and no phase segregation (Baetens, Jelle, and Gustavsen 2010). Several authors have determined the advantages and disadvantages of various types of PCMs (Khadiran et al. 2016; Baetens, Jelle, and Gustavsen 2010; Cui et al. 2015).**Table 2.1** summarized the main advantages and disadvantages of different types of PCM.

Table 2.1 The Advantages and disadvantages of different types of PCM (Khadiran et al. 2016; Baetens, Jelle, and Gustavsen 2010; Cui et al. 2015)

	Organic	Inorganic	Eutectic
Examples	– Paraffins and non-paraffins	– Hydrated salts	– a mix of an organic and inorganic compound
Advantages	– Available in a wide temperature range – high latent heat of fusion – solidify with minor or no subcooling – no segregation – thermally and chemically stable, – low vapour pressure in the melted form – non-reactive and non-corrosive – compatible with construction materials – recyclable.	– High volume latent heat storage capacity – high latent heat of fusion – low cost – sharp phase-change – high thermal conductivity – non-flammable – low volume change	– High melting temperature – volume thermal storage density a little above organic compounds – no segregation
Disadvantages	– Low thermal conductivity – Low volume latent heat storage capacity – low density – flammable – large volume change	– subcooling – phase segregation during phase transition – not compatible with some construction materials – corrosive and slightly toxic.	– Limited data are available on their properties – some fatty eutectics have a pretty strong odour

2.7.3 Thermal properties of PCMs

Fig 2.4 shows the latent heat storage process. The PCMs starts to melt when it is near PCMs melting temperature. PCMs absorb the heat and store it until it returns to the solid state and releases stored energy to the environment. That is why PCMs can be used for temperature control in the building system. Different studies focused on shifting cooling and heating loads from the peak period to the low peak electricity period by using PCMs (Cui et al. 2015). For

illustration, PCMs absorb heat from the building during changing phase from solid to liquid; thus, reducing loads on the air conditing system during the day and release stored energy into the environment at night when returning to solid again. This will reduce the power generation during peak hours that will help to reduce the cost of electricity (Cui et al. 2015).

It should be noted that the behaviour of the melting temperature of stander PCMs is different from common PCMs. **Fig 2.4** shows the melting temperature peak of the stander PCMs (Tmp) and melting temperature range in the isothermal process of the common PCMs (ΔTm).

Therefore, for the common PCMs, the enthalpy temperature should be described as it includes crucial information for the phase change process.

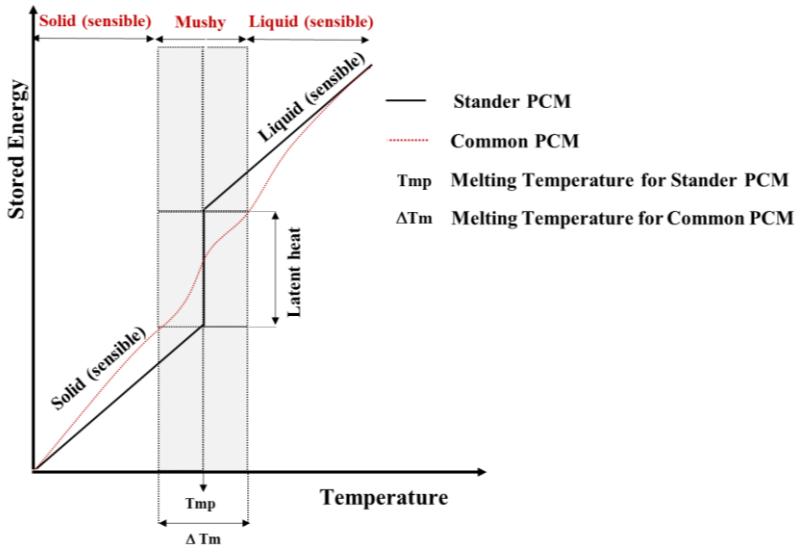

Fig 2.4 Latent heat and sensible heat storage (Soares 2016)

The enthalpy-temperature curve should be the same during the charging and discharging cycles. However, the curve is influenced by the supercooling phenomena (also called subcooling). **Fig 2.5** shows stander PCMs during the melting and solidification cycle with supercooling. The supercooling occurs at a temperature below the PCM's solidification temperature, where it starts to crystallize and release the latent heat stored (Cabeza 2008). If the amount of heat released from the solidification process is more significant than the sensible heat lost from supercooling, the

temperature rises again to PCM's melting peak temperature. However, if the amount of heat lost to the ambient environment is more significant than the heat released from the crystallization process, hysteresis will be caused by supercooling, the temperature will not rise to the solidification temperature. Hence, supercooling can cause significant problems in the technical application of PCMs. Supercooling depends on the type, shape and size of the PCM sample (Cabeza 2008; Soares 2016).

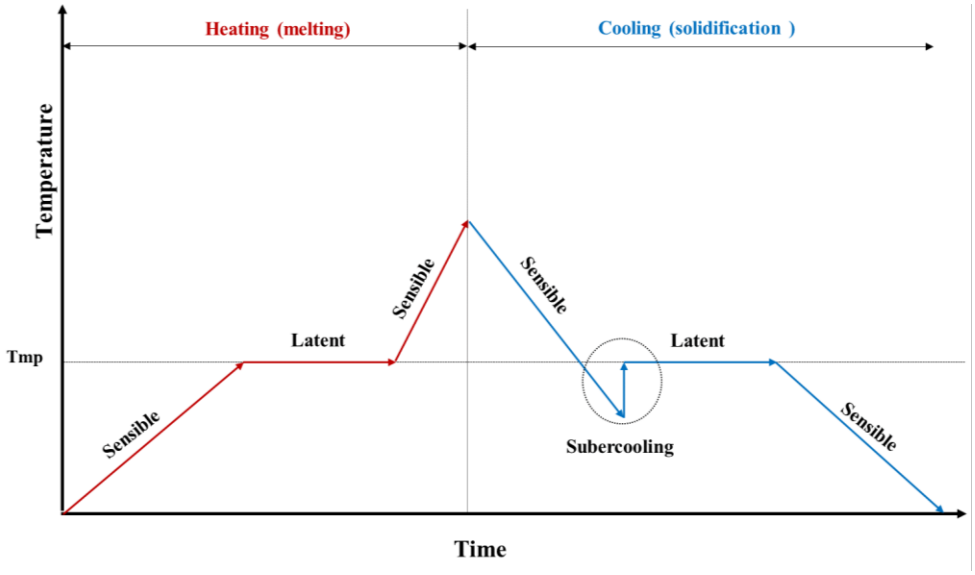

Fig 2.5 stander PCMs during the melting and solidification cycle with supercooling (Soares 2016)

2.7.4 Phase change material in construction Materials

Several incorporation methods for PCMs in construction materials, including direct incorporation, shape stabilization PCMs, immersion and encapsulation, were proposed (Khudhair and Farid 2004). Direct incorporation is the cheapest and the most straightforward approach. PCMs are directly mixed with the construction materials (i.e. concrete, gypsum, plaster)(Cui et al. 2015; Jeon et al. 2013). The immersion impregnates the porous material (i.e. concrete blocks, bricks or gypsum board) into melted PCM and is absorbed by the capillary action. Both direct incorporation

and immersion methods reported some leakage problems, and interactions with building material had been reported (Schossig et al. 2005). Encapsulation is another technique in adding PCM to construction materials. During manufacturing, PCM is encapsulated in a polymer shell then incorporated into the construction material. This methodology reduced leakage and prevent direct contact with construction material (Baetens, Jelle, and Gustavsen 2010; Hawes, Banu, and Feldman 1992). The containment PCM goal includes meeting required strength, avoiding corrosion, thermal stability, and allowing good heat transfer (Regin, Solanki, and Saini 2008). One encapsulation method is microencapsulation, where particles are surrounded by a thin film, a polymeric shell that produces a capsule in the size range of micrometres to millimetres (Regin, Solanki, and Saini 2008). Microencapsulation reduced leakage and prevents direct contact with construction material such as cement, mortar, concrete, paints, and other coatings (Tyagi et al. 2011).

The macro-encapsulation is done by packing PCM into a large container such as tubes, spheres, panels, and then incorporated directly into the building element. The encapsulation helped to overcome the flammability and leakage problems of the PCMs. However, it has some drawbacks: poor thermal conductivity and the tendency to solidify at the edges (Zhou, Zhao, and Tian 2012).

Shapstabilizer PCMs are a new kind of PCMs that have been attracting researchers due to their high thermal conductivity, high specific heat and ability to maintain their shape while changing phase. Shapstabilizer PCMs can be used in many application as building walls, ceiling and floors.

All the techniques above deal with PCM solid-liquid phase change. Solid-solid PCM was proposed by Whitman et al. (Whitman, Johnson, and White 2012) to overcome leakage and expansion problems of the solid-liquid PCMs.

PCMs were successfully incorporated in construction materials, such as wallboards, roofs, floors, paste, mortar, and concrete. It had proved high abilities to improve thermal energy storage for different elements (Frigione, Lettieri, and Sarcinella 2019).

2.7.5 Incorporating Limestone filler in Self-compacted mortar

Self-compacted mortar (SCM) is a special type of mortar that can flow under its weight without bleeding and segregation (Benabed et al. 2012; Okamuara and Ouchi 1999). It is designed to have proper viscosity to ensure homogenous particles and decrease the collision of inner particles that can cause the breakage of PCMs. The low mixing energy and high flowability for SCM make it a potential carrier media for encapsulated PCMs. Superplasticizer (SPs) is used to improve the self-compacted mixture's followability (Benabed et al. 2012; Billberg 1999). Thus, maintaining self-compacting mortar without increasing water/cement ratio, therefore increasing water content drawback is limited. However, optimization of SPs dosage should be maintained to avoid delaying setting time (Benabed et al. 2012; Felekoğlu 2008). Self-compacting concrete has low yield stress, which can reduce the risk of fracturing the PCM microcapsules (Hunger et al. 2009). Previous studies showed that adding fine limestone will improve workability through freeing entrapped water and enhance strength due to the densifying the microstructure (Benabed et al. 2012; Felekoğlu 2008; Aïtcin 2011; Domone and Jin 1999). The effect of fine limestone on the self-compacting mixes' properties was studied by Bosilikove (Bosiljkov 2003). Utilization of limestone in self-compacting mixes will provide a solution in disposal linked with this filler material and reduce the cost of self-compacting mixtures (Benabed et al. 2012; Felekoğlu 2008).

SCC can be used in the construction industry, which has several benefits, including eliminating the need for surface finish, decrease casting time and the number of labourers needed, and enhancing the work environment by reducing noise at the casting location (Ghorpade, Subash, and

Kumar 2015; Erdem, Khayat, and Yahia 2009). Many research focused on limestone's influence on concrete properties at an ambient temperature (i.e. 23°C)(Hooton, Nokken, and Thomas 2007; Tennis, Thomas, and Weiss 2011; Hawkins, Tennis, and Detwiler 1996). However, the results of hardened properties, workability and durability always vary (Hooton, Nokken, and Thomas 2007; Tennis, Thomas, and Weiss 2011). This variation could be due to variations of limestone finesse, composition, percentage, and replacing cement or sand (Knop, Peled, and Cohen 2014).

Limestone is used to increase powder content in SCC mixes (Nishibayashi et al. 2004; Moosberg-Bustnes, Lagerblad, and Forssberg 2004). In addition to that, limestone enhances the chemical and physical effect of the cement-based system. Some of the chemical effects are associated with supplying ions into the phase solution, therefore modifying the hydration products' morphology and hydration kinetics (Naik et al. 2005). Physical factors include the effect of limestone's small particle size, which can reduce voids and enhance packing density; thus, the system's entrapped water is decreased. For illustration, the required powder volume is reduced while using a continuously graded skeleton of powder which ensures adequate concrete deformation (Fujiwara et al. 1996). The use of limestone in SCC mixes can lower the cost of SCC and provide a solution regarding the environmental disposal problems regarding this filler (Fujiwara et al. 1996).

A lot of researchers have been studying the effect of the incorporation of limestone fines in crushed sand on hardened and fresh concrete and mortar for many years. It was found that up to 15% of limestone finesse does not affect the compressive strength performance of limestone concrete(S. Kenai, Menadi, and Ghrici 2006; Nehdi, Mindess, and Aïtcin 1996). Also, 12-18% of fines could be allowed in the sand without a negative effect on mechanical properties of concrete or mortar(Bonavetti and Irassar 1994; Ramirez, Barcena, and Urreta 1987; Bertrandy and Chabernaud 1971; Chi, Wu, and Riefler 2004; Aïtcin and Mehta 1990; Donza, Cabrera, and Irassar

2002; Donza, Gonzalez, and Cabrera 1999; Poitevin 1999; Ramirez, Barcena, and Urreta 1990). Also, the addition of the fines may enhance the performance of concrete. Improving its flexure and compressive strength and decrease the porosity, adsorption, and permeability of concrete (Felekoğlu 2008; Aïtcin 2011; Domone and Jin 1999).

When cement is replaced by limestone, the behaviour of cement is influenced through physical and chemical effects. The physical effect is caused by particle size distribution, heterogeneous nucleation and dilution. Limestone particle sizes and heterogeneous nucleation can enhance the concrete properties. However, dilution has an adverse effect.

2.7.6 The physical effect of limestone:

a) Particle size distribution

Limestone has low hardness properties compared to cement clinker. Thus, a wide range of particle size distribution is produced compared to cement clinker (Tennis, Thomas, and Weiss 2011; Gunnelius et al. 2014). Limestone fills the voids between sand and cement particles, decreasing pores volume in concrete and increasing concrete density (Camiletti, Soliman, and Nehdi 2013; J. J. Chen, Kwan, and Jiang 2014). Some of the water is replaced by limestone during its fresh state. Therefore, The workability increased due to reduced internal friction (Hawkins, Tennis, and Detwiler 1996; Vance et al. 2013). However, the improvement in workability is insignificant due to increased water adsorption when the limestone's finesse is increased (Felekoğlu et al. 2006). Also, limestone can reduce bleeding in concrete at a replacement level greater than 5 % (Bentz et al. 2015).

b) Dilution effect

Dilution occurs when replacing cement with a reactive material by less reactive or inert material such as limestone (Bentz et al. 2015). The volume of hydration product is decreased when cement

content is reduced by more than 5%, which negatively affects the porosity, compressive strength and permeability of concrete. On the other hand, when limestone is less than 5% replacement of cement, the dilution effect is minimized. The dilution effect is mainly observed at later ages (i.e. after 3-7 days). However, limestone's heterogeneous nucleation effect compensates dilution effect before 3-7 days (Said Kenai, Soboyejo, and Soboyejo 2004).

c) heterogeneous nucleation

limestone depends mainly on its finesse which acts as a nucleation site for the hydration products, which accelerate cement hydration process (Berodier and Scrivener 2014; Irassar 2009; Ezziane et al. 2010). Also, the hydration product's thickness is reduced by coating underrated cement particles with increasing surface area of limestone, which accommodates precipitation of some of the hydration products (F. Lin and Meyer 2009). Hence, acceleration in the hydration process allows the inner part of unhydrated cement to hydrate faster.

2.7.7 Chemical effect of limestone

Limestone is not considered as an inert material, but it is partially reactive (Hawkins, Tennis, and Detwiler 1996; Lothenbach et al. 2008a). Limestone reacts with monosulfate and calcium aluminate hydrates in the presence of water to form calcium monocarboaluminate. Limestone fineness influences the reaction; the greater the finesse, the more limestone is consumed (Hooton, Nokken, and Thomas 2007).

2.7.8 Effect of Steam Curing Temperature

Curing is an important processing step in the precast industry to ensure adequate early-age performance and durability properties. During curing, Specimens are exposed to elevated temperature (50–70 °C) and high relative humidity (above 95%). This process is considered an energy-intensive process due to its steam-generating component. However, it is a widely used

approach for precast curing increasing sustainability challenges for the precast industry (Berodier and Scrivener 2014; Hwang et al. 2012).

Curing parameter and mixture composition are the main factors that affect early age compressive strength in heat curing concrete. Once the chamber attains its maximum temperature, the curing temperature is held for a constant period, following a temperature cool to ambient temperature. **Table 2.2** summarizes the heat curing regime's regulation and recommendation to secure the required mechanical properties and minimize surface cracking and defects.

In general, maximum chamber temperature improves early age mechanical properties. However, mechanical properties could be reduced compared to moist cured concrete (Heritage, Khalaf, and Wilson 2000; De Weerdt et al. 2012). The maximum curing temperature ranges from 40 ºC to 85 ºC according to various codes. A wide range of various temperatures with different targeted 18-hours compressive strength and diversity of physical and chemical characteristics of the supplementary cementitious materials and cement used (Hwang et al. 2012). Recent studies suggested using low curing temperatures (50 °C – 70°C) (Taylor, Famy, and Scrivener 2001; Escadeillas et al. 2007; Nguyen et al. 2013). Canadian Standards Association (CSA A23.4) sets the maximum curing temperature at 60°C for wet exposure and 70°C for dry exposure to avoid delayed ettringite formation. However, Washington and New York DOT specified a maximum limit of 0.75% and 0.70% on cement alkali content, respectively (Manual 2002; Transportation (WSDOT) 2010). Thus, this explains the high curing temperature allowed.

Table 2.2 Maximum Allowable Curing Temperatures (Hwang et al. 2012)

Code	Preset period	Maximum rate of heating °C/hr	Maximum temperature °C	Maximum rate of cooling °C/hr
Canadian Standards Association (CSA A23.4 2009 reaffirmed 2014)	After the initial set, at least 3 hours after final placement	20°C	- 60°C for wet exposure - 70°C for dry exposure	15°C
Texas DOT 2004	After the initial set, at least 3 hours after final placement	20°C	- Do not exceed 77°C - do not exceed 71°C for more - than one cumulative hour during - curing period	Not Defined
Portland Cement Association (2006)	3 to 5 hours after initial setting, at least 3 hours after final placement	11°C to 22°C	- 71°C - 60 °C is recommended	22°C
AASHTO LRFD Bridge Design Specifications (2004)	After the initial set	22°C	71°C	22°C
Washington DOT (2002)	After the initial set, heat concrete to no more than 38°C during the first 2 hours after placement	14°C	80°C	14 until the concrete temperature reaches 38°C
New York State DOT (2002)	After the initial set	20°C	Maintain temperature between 40°C and 85°C for a period of not less than 12 hours.	20°C

Chapter 3 PROPERTIES OF SCM INCORPORTAING LIMESTONE

This chapter's primary purpose is to investigate the influence of limestone filler fineness and content on the fresh, hardened properties and hydration kinetics of self-compacting mortar. Limestone filler with three nominal particles sizes of 3μm, 12μm, and 17μm, which correspond to Blaine finenesses of 1125, 1049, 475 m^2/kg, respectively, were used as a partial replacement of sand and cement with a percentage of 5%, 10%, 15%, and 20%. Hardened properties, including compressive and shrinkage, were also evaluated under ambient condition (i.e. temperature (T) = 20℃ ± 2℃ and relative humidity (RH) = 50% ± 5%). The hydration kinetics was examined using thermal analysis and heat of hydration. Thermo-gravimetric analysis (TGA) and Differential thermal analyses (DGA) were used to measure the amount of formed hydration products.

3.1 Experimental Program

3.1.1 Materials and mixture design

General use hydraulic cement, according to CSA-3001-03, was used as the main binding material. **Table 3.1** illustrates the chemical and physical properties of used cement. Omya, Canada supplied four LFs with different nominal particle sizes (3 μm, and 12 μm and 17 μm). The fine aggregate was natural riverside sand with specific gravity, fineness modulus, and water absorption of 2.51, 2.70, and 2.73 were used as a fine aggregate, respectively—sieve analysis for the sand according to ASTM C33 (2018) shown in **Fig 3.1.** Mixtures were divided into two groups based on the replaced materials. The first ground is the sand replacement and the second group is the cement replacement. The LF replacement ratio ranged from 0% to 20% by volume. The water-to-cement ratio of 0.4 and a sand-to-cement ratio of 2 were used for all tested mixtures. The mixture proportions are presented in **Table 3.2**. Each mixture's code has a charter "S" referring to the sand

replacement group and "C" referring to the cement replacement group. Then followed by two numbers, the first one is the replacement rate, and the second one is the size of LF.

Table 3.1:Chemical and physical properties of cement

	Cement
SiO_2 (%)	19.60
Al_2O_3 (%)	4.80
CaO (%)	61.50
Fe_2O_3 (%)	3.30
SO_3 (%)	3.50
Na_2O (%)	0.70
C_3S (%)	55.00
C_2S (%)	15.00
C_3A (%)	7.00
C_4AF (%)	10.00
Loss on ignition (%)	1.90
Specific gravity	3.15
Surface area (m^2/kg)	371

Table 3.2: Physical properties of River Sand

Properties	**River Sand**
Specific gravity	2.51
Fineness modulus	2.70
Water absorption (%)	2.73

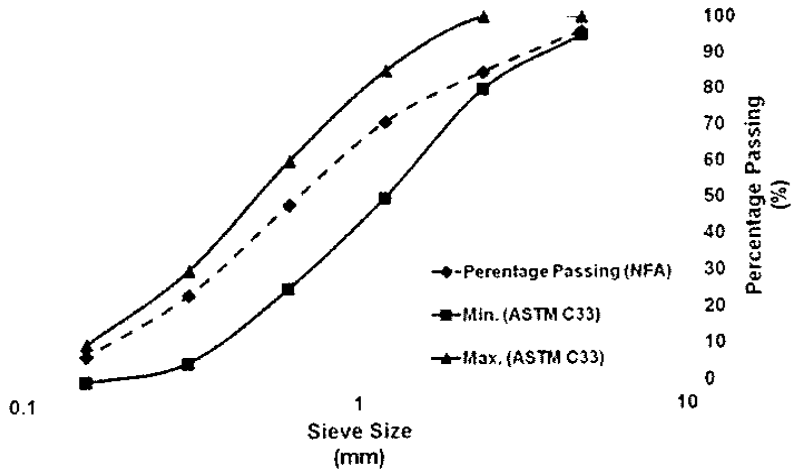

Fig 3.1 Sieve analysis of fine aggregate

3.1.2 Concrete Mixing

The mixing procedure consists of four main stages. Firstly, all solid materials were mixed together for half a minute. Then, 90 % of the total water amount is added and continues mixing for two minutes (Valcuende et al. 2012). After that, the remaining amount of water and superplasticizer was added. **Table 3.3** illustrates the tested mixture. Slump flow Test, V-Funnel test were performed to evaluate the filling ability of each mixture.

Table 3.3 Mix design of tested mixture

Group ID	Mixture ID	Cement (%)	Sand (%)	LF Content (%)	LF Size (µm)
	C	100	100	0	
G1	C.5	95	100	5	3, 12, 17
	C.10	90	100	10	
	C.15	85	100	15	
	C.20	80	100	20	
G2	S.5	100	95	5	3, 12, 17
	S.10	100	90	10	
	S.15	100	85	15	
	S.20	100	80	20	

3.1.3 Testing methods

Flowability was evaluated using the mini-slump cone test to ensure meeting the EFNARC guideline for self-compacting mortar. After removing the filled mini-cone, the final spread diameter (D_f) of the fresh paste sample was taken as an average of two measurements made in two perpendicular directions. Cubic specimens 50 mm were used to evaluate the compressive strengths at ages 3, 7, and 28 days following the ASTM C 109-20 "Standard Test Method for Compressive Strength of Hydraulic Cement Mortars (Using 2-in. or [50-mm] Cube Specimens". For drying shrinkage measurements, prismatic specimens, 25 × 25 × 285 mm, were made according to ASTM C 157/C127-17 "Standard Test Method for Length Change of Hardened Hydraulic-Cement Mortar and Concrete." After demolding, each mixture's specimens were exposed to dry at the ambient laboratory conditions to evaluate the total shrinkage. The unrestrained one-dimensional deformations were measured using a comparator provided with a dial gauge with an accuracy of 10 μm/m.

Thermo-gravimetric analysis (TGA) combined with derivative thermo-gravimetric (DTG) was used to monitor the formation of different hydration products (i.e. Calcium hydroxide (CH)) and measure non-evaporable water contents. At the selected testing age, hydration of samples was stopped by submerging in isopropanol. Then, chunks taken from the centre of the specimens were ground to powder and sieved on No. 200 sieves. Samples weighing approximately 40 mg were heated from 23°C to 650°C at a heating rate of 10 °C/min. Collected data and curves were analyzed using TA Instruments thermal analysis software. The percentage of CH (i.e. approximately the mass loss between 450–500 °C and degree of hydration (mass loss between 23 °C and 550 °C with respect to the maximum theoretical non-evaporable water (i.e. 0.23)) were used to compare the degree of hydration between various mixtures. This indirect method to quantify the degree of

hydration has been commonly used by many researchers (Loukili et al., 1999; Mounanga et al., 2004). Isothermal calorimetry was used to assess the thermal power from different mixtures by using calorimeter apparatus (Calmetrix I-CAL 2000 HPC).

3.2 RESULTS AND DISCUSSION

3.2.1 Flowability

Fig 3.2 and **Fig 3.3** show the flowability (i.e. mini-slump and V-funnel test) of SCM incorporating various sizes and dosages of LF as sand and cement replacement. All SCM slump flow values were within the recommended range between (250-300 mm) (Domone and Jin 1999). Besides, they maintained flow time value in the range between (2-10s) as recommended by (Felekoğlu et al. 2006). In general, the flowability was enhanced by increasing the percentage and size of limestone. Also, it was reported a decrease in flow time when limestone fineness and size increased. For instance, for S.17µm mixtures, the flowability improved by 13% when the LF percentage increased from 0% to 20%. This improvement in workability was due to replacing LF some of the water inside the voids, which further reduced the internal friction (Aqel 2016; Hawkins, Tennis, and Detwiler 1996; Vance et al. 2013). Also, a slight decrease in flowability of mortar was reported when using smaller particle sizes of limestone. For example, for S.3µm mixtures, there was around a 4% reduction in flowability than S.17µm mixtures. This is due to increased water adsorption with increased limestone fineness (Aqel 2016; Felekoğlu et al. 2006). SCM's flowability is related to the incorporated powder's particular size distribution, particular shape, fineness, packing and internal-particle fraction between materials (Felekoğlu et al. 2006). Besides, using finer powder increases surface area and water demand. As a result, viscosity and yield stress increased, leading to a lower flowability (Benachour et al. 2008; Esping 2008).

On the other hand, cement replacement mixtures showed the same trend as sand replacement mixtures. However, the increase in flowability is not significant between different particle sizes. To illustrate, for C.17µm mixtures, there was up to 4% improvement in flowability compared to C.3µm. This can be due to balancing the reduction in water demand and the increase in the inter-friction .

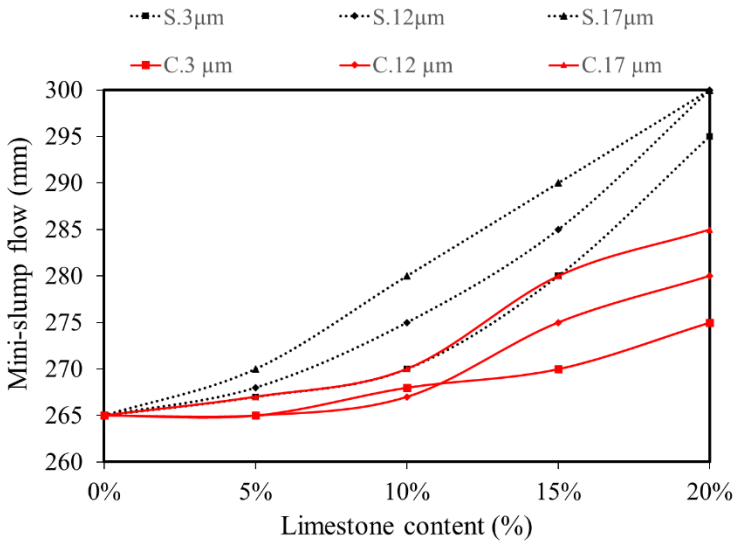

Fig 3.2 Slump flow of mortar made with various sizes and content of LF as sand and cement replacement.

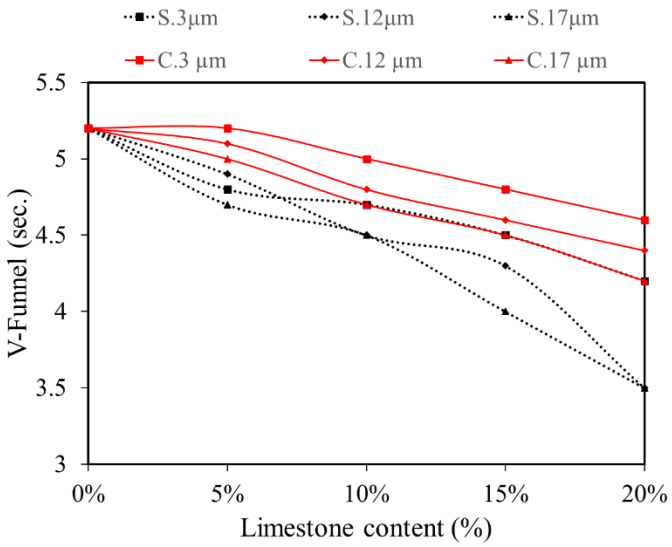

Fig 3.3 V-funnel of mortar made with various sizes and content of LF as sand and cement replacement.

3.2.2 Heat of Hydration

The hydration process is a chemical reaction between binder and water that starts with the first second of mixing. LF is not considered an inert material, but it is partially reactive (Hawkins, Tennis, and Detwiler 1996; Lothenbach et al. 2008b). Incorporation LF influences hydration kinetics. The hydration peaks increase and occur sooner. Mixtures with different LF sizes and content were studied at 23℃ for 48 hrs to capture the hydration peaks of the hydration process. In general, an exothermic peak was reported immediately after mixing due to a rapid initial chemical reaction between Tricalcium silicate (C_3S) and water (Costoya Fernández 2008). Also, it can be attributed to the dissolution of the C_3S (Bullard et al. 2011). After that, an induction period has been reported for 1-2 hours. This can be explained due to the fall down in growth and nucleation of calcium silicate hydrate (C-S-H) (Costoya Fernández 2008). Subsequently, the heat continues to evolve and reach its maximum peak. This is due to the ongoing reaction of calcium silicate hydrate and calcium hydrate, which depend on the particle's size and the rapid formation of

hydrates, which reached their peak after 10 -12 hrs (Scrivener 1984). Then, the hydration reaction goes through a deceleration period. After that, a second shoulder peak is reported, which is linked to ettringite formation, where the hydration product is accelerated in the aluminate phase (Juilland et al. 2010).

Fig 3.4 and **Fig 3.5** presented the effect of LF content and size for sand and cement replacement, respectively, on the heat of hydration. Moreover, **Fig 3.6** and **Fig 3.7** presented the total energy released calculated from the heat of hydration curves. The hydration heat was increased as LF content increased and LF sizes decreased compared to the control mixtures. Limestone filler small particles and higher surface area work as a physical catalyst for the chemical reaction (Zeng et al. 2013). Hence, LF smaller size stimulates cement hydration and space-filling (Li et al. 2015). The effect of LF was more pronounced in sand replacement mixture than in cement replacement mixture. Hence, The hydration peak and total energy released for the first 48 hrs of different percentages and sizes of LF were compared to each other as presented in **Fig 3.8** and **Fig 3.9** The first 48 hr of hydration was selected as a comparison base of the hydration heat released in this period.

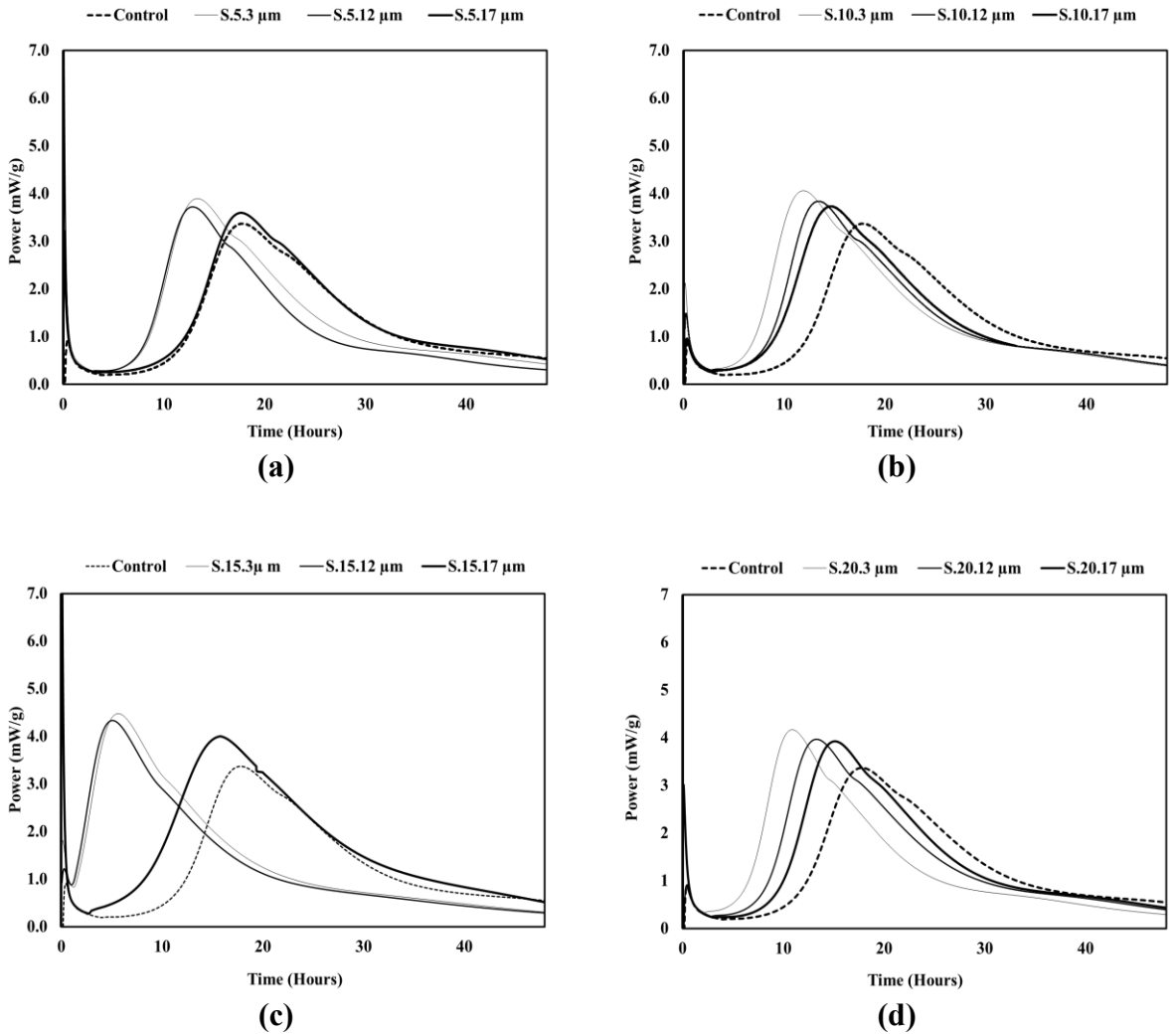

Fig 3.4 Effect of LF size on the Heat of Hydration for mixtures a) 5% b)10% c) 15% d) 20% sand replacement

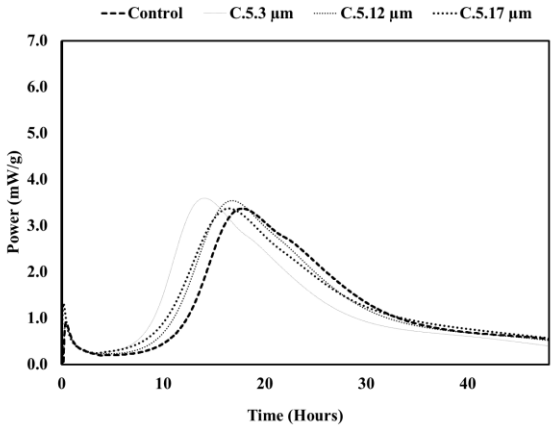

(a)

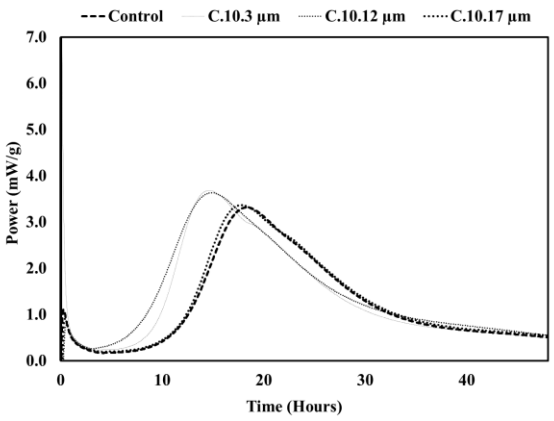

(b)

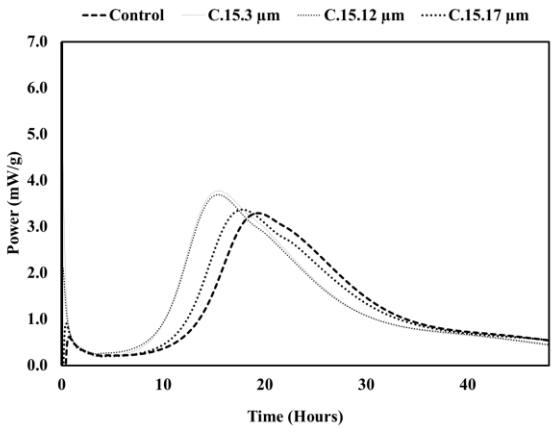

(c)

Fig 3.5 Effect of LF size on the Heat of Hydration for mixtures a) 5% b)10% c) 15% cement replacement

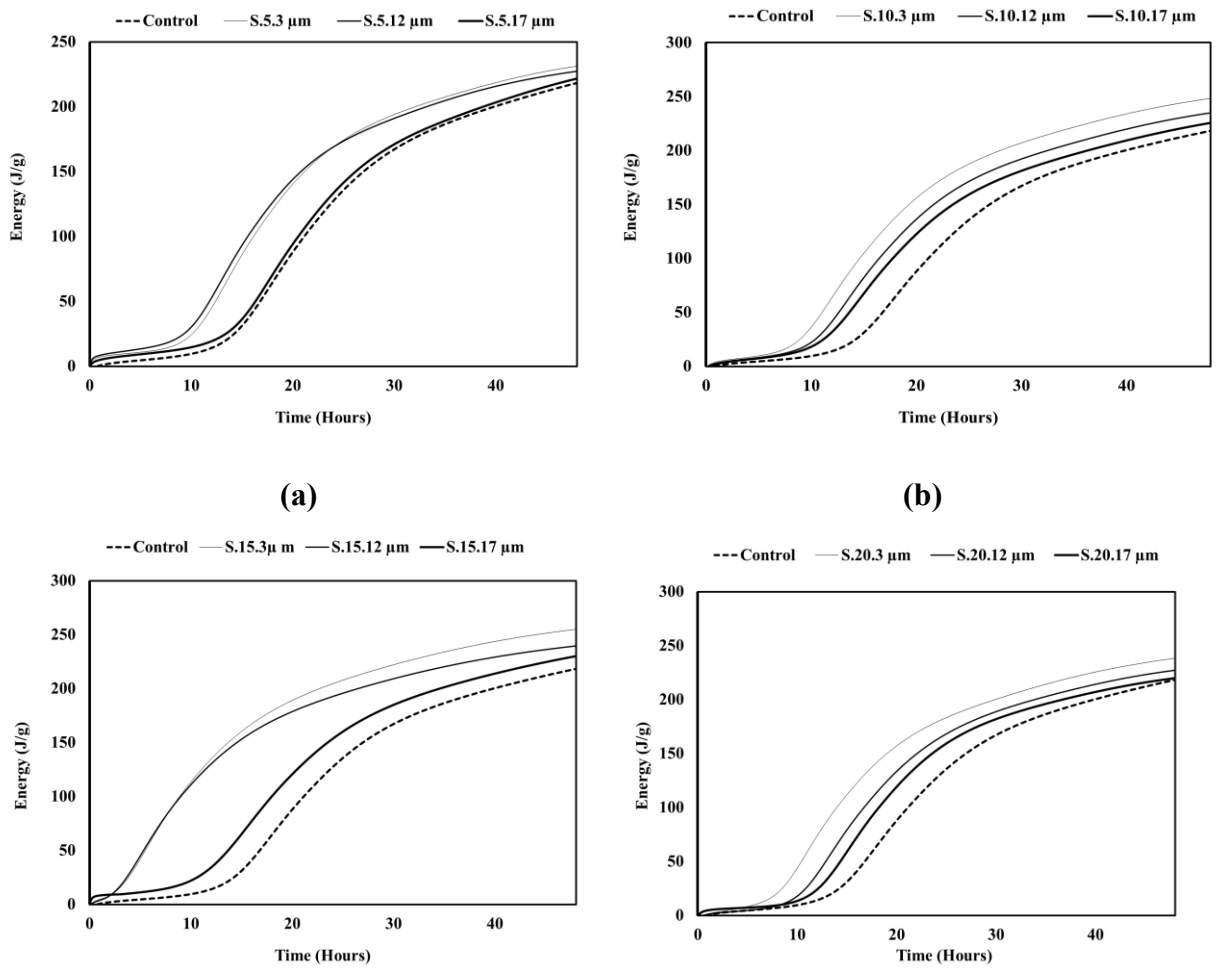

Fig 3.6 Effect of LF size on Total Energy Released for mixtures a) 5% b)10% c) 15% d) 20% sand replacement

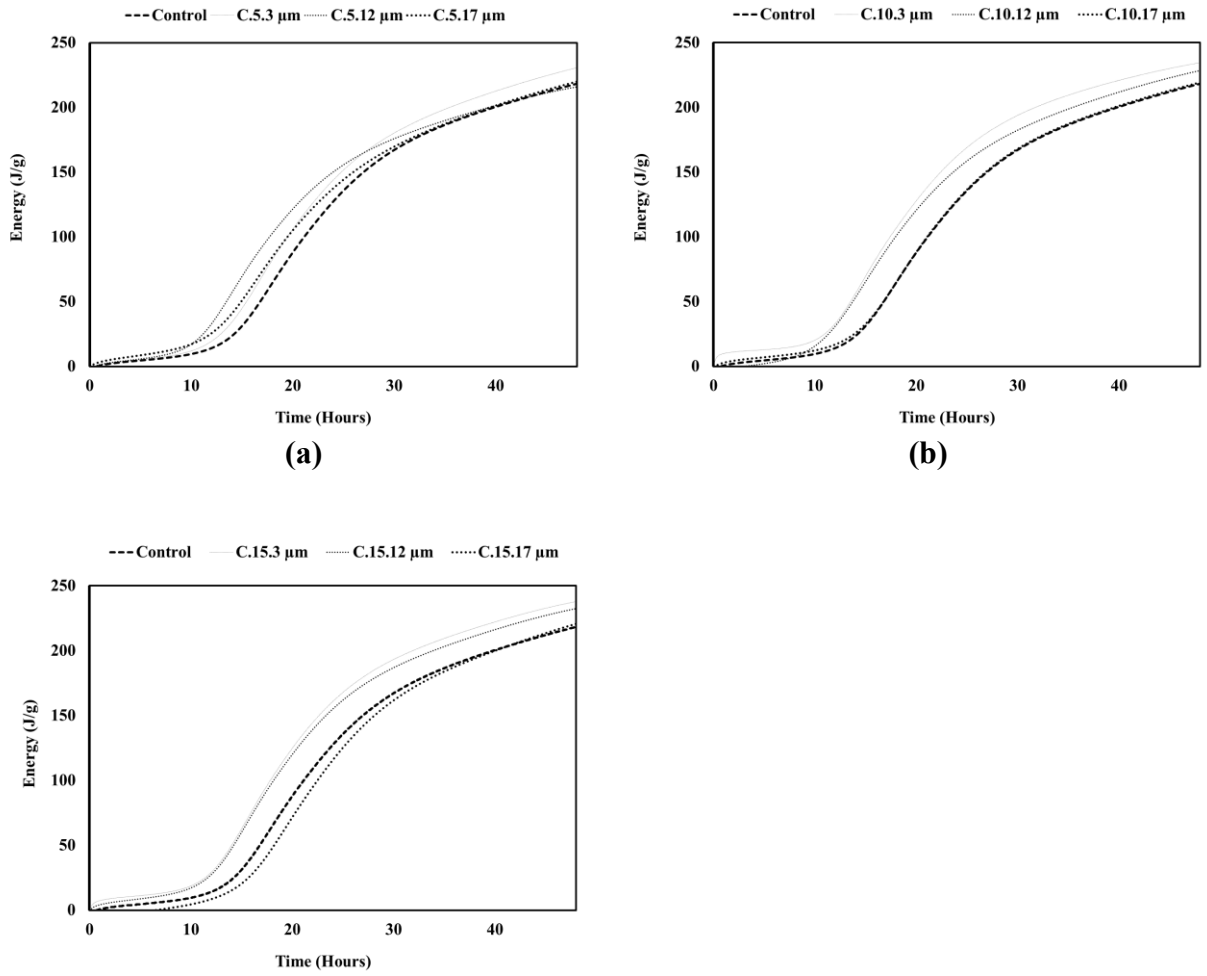

Fig 3.7 Effect of LF size on Total Energy Released for mixtures a) 5% b)10% c) 15% cement replacement

a) Hydration Peak

Fig 3.8 presented the effect of LF content and size on the hydration peak. Each point in the curve is the average of three tests with a coefficient of variation of less than 3%. In general, in all mixes made with LF, the hydration peak increased and occurred sooner with the smaller size and higher LF content than the control mix. This can be explained due to the acceleration effect of LF (Lothenbach et al. 2008b; De Schutter 2011). In general, the increase in hydration peak was more pronounced at sand replacement mixtures, with particle sizes 3 µm; the highest peak was recorded

at 15% sand replacement. This is due to the greater surface, which surges the acceleration effect of LF in the hydration process. To illustrate, mixtures with 3, 12, 17 µm LF, the hydration peak improved by 33%, 30%, 19%, respectively, when the added dosage of LF increased from 0 to 15% as sand replacement. When the dosage of LF increased up to 20%, the hydration peak started to decrease. For example, mixtures with 3, 12, 17 µm LF, the hydration peak improved by 24%, 18%, 16% when the added dosage of LF increased up to 20%. In mixtures made with LF as a cement replacement, the hydration was less pronounced than sand replacement. Mixtures made with 3 and 12 µm showed a higher hydration peak, followed by 17 µm LF compared to control mixtures. Also, the hydration peak increased as the percentage of LF increased.

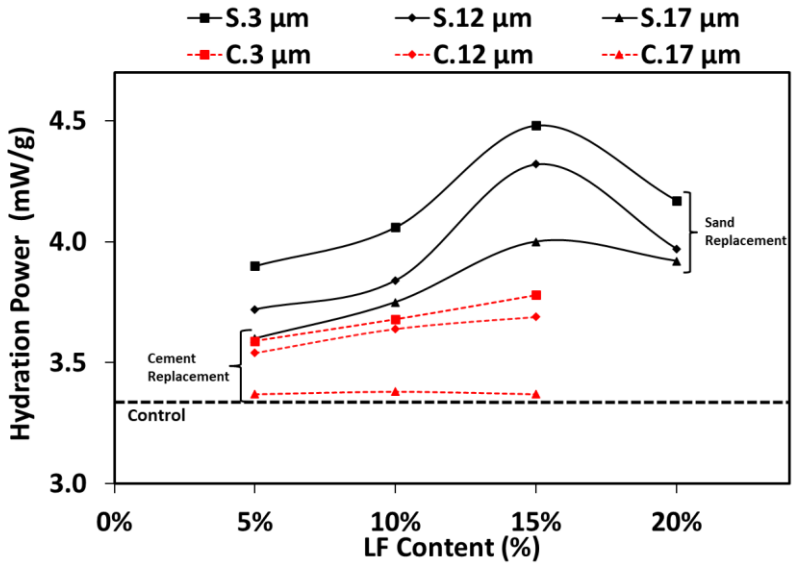

Fig 3.8 Effect of LF Content and size on hydration peak

b) Total energy released

The total energy released was measured from the first moment of mixing the binder with water to 48 hrs for each mixture and compared to the control mix, as shown in **Fig 3.9**. Each point in the curve is the average of three tests with a coefficient of variation of less than 3%. The total energy was calculated as the area under the power curves shown in **Fig 3.4** and **Fig 3.5.** Generally, the total energy released increased with smaller LF sizes and higher content than the control mix.

Incorporating LF as sand or cement replacement increased total energy released in the first 48 hrs of hydration, which agrees with the literature review of accelerating the hydration reaction and formation of calcium monocarboaluminate, which fill the pores between cement particles (Lawrence, Cyr, and Ringot 2003; Liu et al. 2012; Heikal, El-Didamony, and Morsy 2000).

Incorporating LF as sand replacement reported greater total energy released than mixtures made with LF as a cement replacement. Moreover, using LF size, 3 μm significantly increased the total energy released in sand and cement replacement. This shows the vital role of increasing mixture fineness in enhancing the hydration rate. The total energy released in 3, 12, 17 μm was increased by 19%, 11%, 7%, respectively, when the added dosage of LF increased from 0 to 15% as sand replacement. When the dosage of LF increased up to 20%, the amount of heat released starts to decrease. For example, in mixtures with 3, 12, 17 μm LF, the hydration peak improved by 9%, 5%, 2% when the added dosage of LF increased up to 20%. In mixtures made with LF as a cement replacement, the heat released was less significant than sand replacement. Mixtures made with 3 and 12 μm showed higher energy released, followed by 17 μm LF compared to control mixtures.

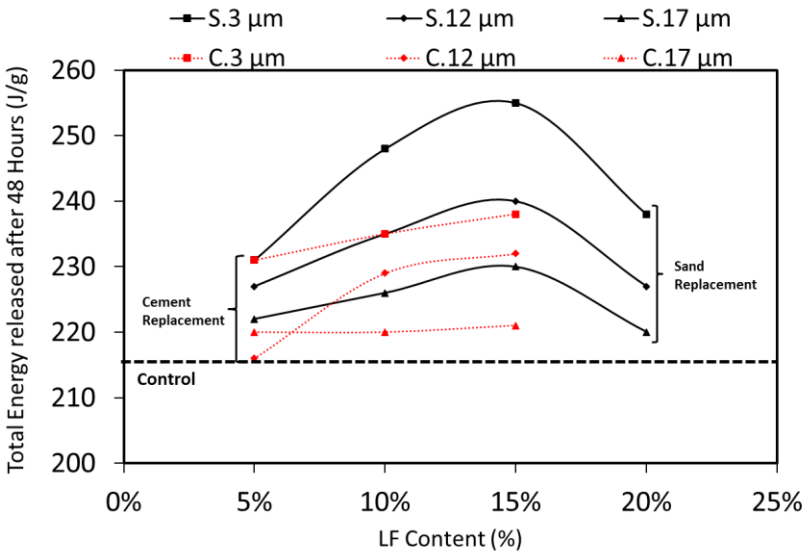

Fig 3.9 Effect of LF Content and size on Total energy released

3.2.3 Thermal Analysis

$Ca(OH)_2$ Content

Fig 3.10 and **Fig 3.11** presented the measured $Ca(OH)_2$ content for pastes made with various sizes and dosages of LF as sand and cement replacement at age 3 and 28 days, respectively. Each point is the average of three tests, and the coefficient of variation was less than 3% for all mixtures. At 3 days, increasing the LF content and decreasing LF sizes increases the $Ca(OH)_2$ content. The increase in $Ca(OH)_2$ content is due to the presence of LF, which increases the heat of hydration and consequently increases the hydration products, including $Ca(OH)_2$. To illustrate, as shown in **Fig 3.10**, when LF content increased to 20% replacement of sand and particle sizes decreased. It was reported that $Ca(OH)_2$ content significantly increased compared to the control mixtures. Besides, S.3µm mixtures showed an increase in $Ca(OH)_2$ content compared to bigger LF sizes. For example, S.3µm mixtures at 15% replacement of sand showed up to a 6% increase in the $Ca(OH)_2$ content compared to S.17 mixtures. The increase in $Ca(OH)_2$ Content is due to the

presence of LF, which increases the heat of hydration and consequently increases the hydration products, including $Ca(OH)_2$.

On the other hand, **Fig 3.11,** increasing LF's content by (10%) cement replacement, increased $Ca(OH)_2$ compared to the control mix. However, there was no significant improvement in $Ca(OH)_2$ when LF content increased by 15%. The is due to the dilution effect, which is more significant at 28 days.

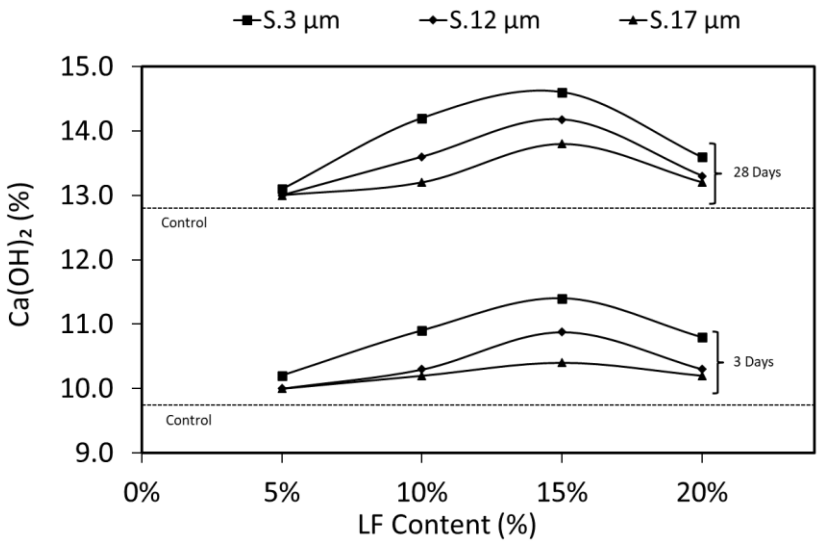

Fig 3.10 Effect of LF Content and Size as sand replacement on $Ca(OH)_2$ Content

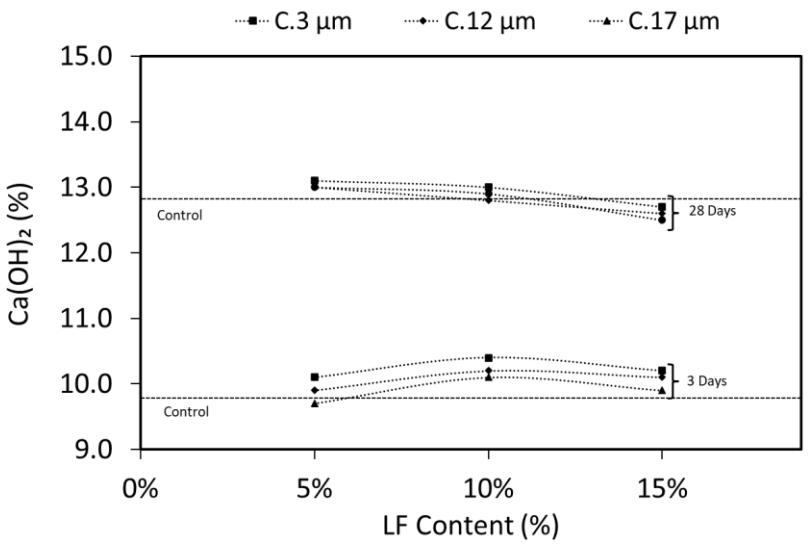

Fig 3.11 Effect of LF Content and Size as cement replacement on $Ca(OH)_2$ Content

3.2.4 Shrinkage

Fig 3.12 illustrates the effect of the shrinkage test on various LF content and sizes at 28 days. Each point in the curve is the average of three tests. After 28 days, the shrinkage values tend to converge. Generally, The addition of LF as cement replacement reduced shrinkage. The reduction in shrinkage is related to decreasing cement content (Valcuende et al. 2012; Kang et al. 2019). Also, shrinkage decreased when LF sizes increased from 3 µm to 17 µm. This can contribute to the acceleration in cement hydration and the pore structure's improvement that changes the binder's particle packing (Kang et al. 2019). Conversely, incorporating LF as sand replacement increase shrinkage. The increase of shrinkage can be related to the acceleration of hydration or formation carboaluimate at an early age, which increased the volume of cement gel (Malhotra and Carette 1985; Adams and Race 1990).

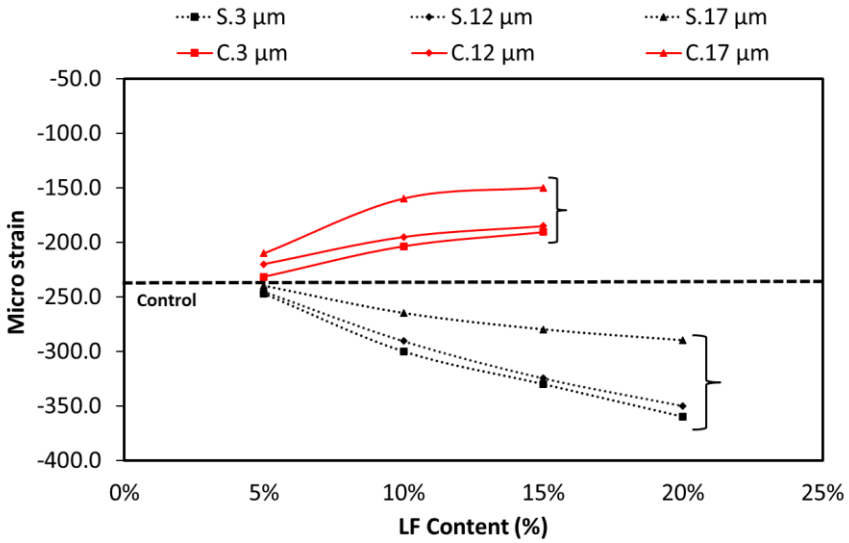

Fig 3.12 Effect of LF Content and Size on shrinkage of SCM

3.2.5 Compressive strength

The compressive strength results of different content and sizes of LF are presented in **Fig 3.13.** Each point is the average of three tests, and the coefficient of variation was less than 5% for all mixes. Results show that LF enhances mechanical properties at the early ages of SCM made with LF as sand and cement replacement. However, at 28 days, the effect of LF was different when comparing mortar used LF as cement than sand replacement. For mortar with LF cement replacement, LF causes a reduction in compressive strength after 28 days. In contrast, the compressive strength increased at all ages for mortar with LF sand replacement.

For mortar with LF cement replacement, the effect of LF was less pronounced than mortar made with LF as sand replacement. Generally, no significant improvement in the compressive strength when 5% LF was used as cement replacement at all ages. The compressive strength enhanced at the early ages for mixtures with 10% to 15% LF cement replacement. However, at age 28 days, the strength with LF cement replacement slightly decreased by 3% than the control mix. The

reduction of compressive strength was greater in the mortar made with higher content and larger LF size.

For mortar with LF sand replacement, replacing 5% sand with LF did not cause a significant improvement in mechanical properties at all ages. Increasing the LF content from 5% to 15% significantly increased compressive strength at all ages. The effect of LF size was more pronounced when the size of LF decreased from 17 μm to 3 μm. This result agrees with the thermal analysis and heat of hydration. The improvement of early age is attributed to the early production of monocarboaluminate and acceleration of hydration.

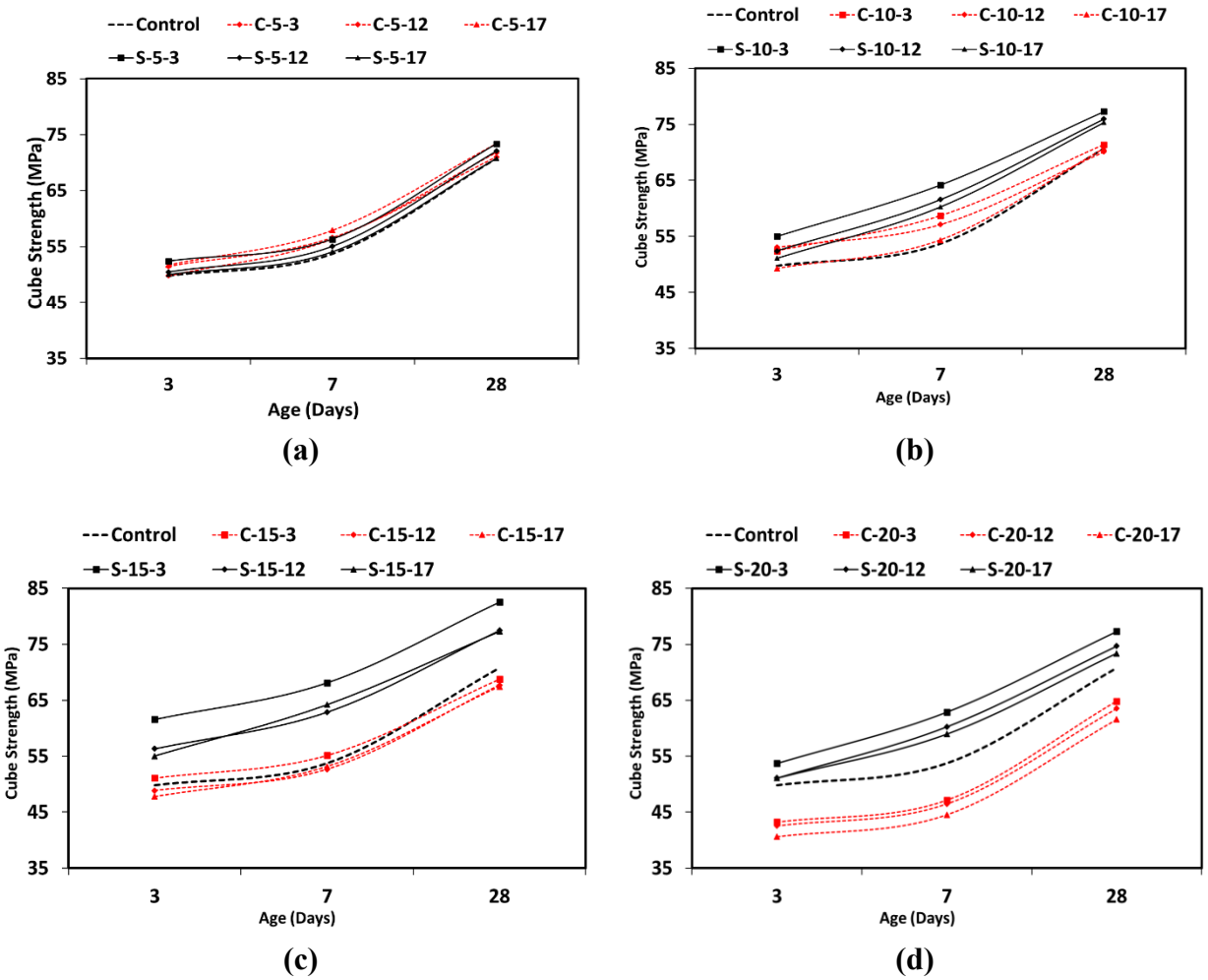

Fig 3.13 effect of LF content and size on compressive strength a) 5% b) 10% c) 15 d) 20%

Chapter 4 PROPERTIES OF SCM INCORPORATING LIMESTONE AND PHASE CHANGE MATERIALS

The building sector is the primary consumer for energy, either as operating or embodied energy. Nowadays, there is a trend to reduce energy consumption in buildings by providing adequate insulation. Many researchers attempted to implement new technologies to save energy, such as phase change materials (PCMs). However, the addition of PCMs can lead to a reduction in mechanical properties. This chapter presents a potential solution of using the self-compacting mortar to lower yield stress and reduce the risk of fracturing the capsules. Besides, incorporating limestone filler to improve the cement-based physical and chemical aspects. Previous studies recommended microencapsulated Phase change material (MPCMs) with particle size range (5-30 μm) to achieve a balance between thermal, mechanical performance, and cost (Richardson, Heniegal, and Tindall 2017; S. S. Lucas, Ferreira, and De Aguiar 2013). Hence, this study investigates the effects of limestone content on the mechanical performance and thermal properties of self-compacted mortar (SCM) incorporating different percentages of MPCMs.

4.1 Experimental Program

4.1.1 Materials and mixture design

General use hydraulic cement, according to CSA-3001-03, was used as the main binding material. Limestone filler with 15% sand replacement sand and particle size 3μm was used, as this mixture showed good mechanical properties as discussed in the previous chapter (i.e. chapter 3). MPCM with melting points of 28℃ was used. **Table 4.1** summarizes the properties of used MPCM according to the manufacturer. The used MPCM has a paraffin core and polymeric outer shell (i.e. the capsule), and particle sizes ranged from 3 to 30 μm was used MPCMs were added at different dosages (0%, 3%, 6%, 12%) as a replacement of sand. The first ground MPCMs were incorporated

as a replacement of sand, and the second group MPCMs and LF were incorporated in SCM as sand replacement. The water-to-cement ratio of 0.4 and a sand-to-cement ratio of 2 were used for all tested mixtures. Each mixture's code has a charter "P" referring to the phase change material group and "S" referring to the sand replacement group. Then followed by two numbers, the first one after charter "P" is the percentage of MPCM used, and the second one after charter "S" is the percentage of LF used.

Table 4.1 MPCM 28°C properties

Manufacture properties	**MCPCM 28**
Melting Point (°C)	28
Latent Heat Capacity (J/g)	185
Moisture (%)	< 1 %
Appearance	White Powder

4.1.2 Mixing procedure

Initially, all solid materials (cement, sand, and limestone) were mixed for half a minute. Then, 90 % of the total water amount is added and continues mixing for two minutes(Jeon et al. 2013) . Meanwhile, the superplasticizer was added to the mixture after water to ensure mixing time is sufficient for the superplasticizer to be homogeneous. For mixtures incorporating MPCMs, MPCM was added in the last stage to shortens their mixing time and avoid breaking the encapsulated particles. After that, the remaining amount of water and superplasticizer was added. The mixture proportions are presented in **Table 4.2.** Finally, the visual inspection of the mortar took place. Slump Flow Test, V-Funnel test were performed to evaluate the filling ability of the mixture.

Table 4.2 Mixture design of all tested mixtures

Group ID	Mixture ID	Cement (%)	Sand (%)	MPCMs (%)	LF Content (%)
	C	100	100	0	0
G1	P.3	100	97	3	0
	P.6		94	6	
	P.12		88	12	
G2	S.15-P.3	100	82	3	15
	S.15-P.6		79	6	
	S.15-P.12		73	12	

4.1.3 Testing methods

Mini-Slump flow test was used to evaluate the workability and filling ability of self-compacting mortar. The fresh mortar sample was placed in the cone without tamping, located in the steel plate's centre. After filling the cone with mortar, the cone is lifted vertically upwards, the mortar spread over the steel plate, and the average diameter was measured in two perpendicular directions using the calliper (EFNARC 2002).

V-funnel Test was used to measure the viscosity of mortar. The funnel was filled up with fresh mortar; then, the gate was opened. Simultaneously, the gate was opened, and timing started till the first light appeared from the above (EFNARC 2002).

Compressive strengths at ages 3, 7, and 28 days were evaluated for all tested mixtures using 50 mm cubic specimens according to ASTM C 109 (Standard Test for compressive strength for cement mortar). Moreover, the drying shrinkage test for mixtures was tested according to ASTM C 596 (Standard Test For Drying Shrinkage Of Mortar). Measurement was taken for the first week, then after 14, 21,28 days.

All specimens were demolded after 24h and stored at temperature = 20 °C ± 2 °C and relative humidity = 50% ± 5%.

The derivative thermo-gravimetric (DTG) was used to monitor the formation of different hydration products (i.e. Calcium hydroxide (CH)) and measure non-evaporable water contents. At the selected testing age, hydration of samples was stopped by submerging in isopropanol. Then, chunks taken from the centre of the specimens were ground to powder and sieved on No. 200 sieves. Samples weighing approximately 40 mg were heated from 23°C to 650°C at a heating rate of 10 °C/min. Collected data and curves were analyzed using TA Instruments thermal analysis software. The percentage of CH (i.e. approximately the mass loss between 450–500 °C and degree of hydration (mass loss between 23 °C and 550 °C with respect to the maximum theoretical non-evaporable water (i.e. 0.23)) were used to compare the degree of hydration between various mixtures. This indirect method to quantify the degree of hydration has been commonly used by many researchers (Loukili et al., 1999; Mounanga et al., 2004). Isothermal calorimetry was used to assess the thermal power from different mixtures by using calorimeter apparatus (Calmetrix I-CAL 2000 HPC).

Thermal conductivity was measured according to ASTM C518 (Materials 2017). A heat flow meter (HFM436, manufactured by NETZSCH) was used to measure the mortar thermal conductivity as shown in **Fig 4.1**. The samples with dimensions 300 × 300 mm and thickness 40 mm shown **Fig 4.2** were placed in contact with hot and cold plates. Thus, heat flow from the hot to the cold plate. The temperature of both plates was taken every minute from sensors embedded inside. Heat flow was calculated according to the Fourier heat flow equation (1). Heat flux q [W/m²] depends on several factors. The rate of heat flow Q [W], the specific area A [m²] where

heat flows, the thermal conductivity of the sample (λ), the temperature difference of the sample (ΔT), and the thickness of the sample (Δx)

$$q = \frac{Q}{A} = \lambda \frac{\Delta T}{\Delta x} \qquad (1)$$

The test for each sample was repeated three times, and the results were averaged. Each test waited 24 hours after the previous test finished to ensure heat dissipated from the machine and the MPCMs samples.

Isothermal calorimetry was used to assess the heat generated from different mixtures by using calorimeter apparatus (Calmetrix I-CAL 2000 HPC).

Fig 4.1 Heat flow meter (HFM436, manufactured by NETZSCH)

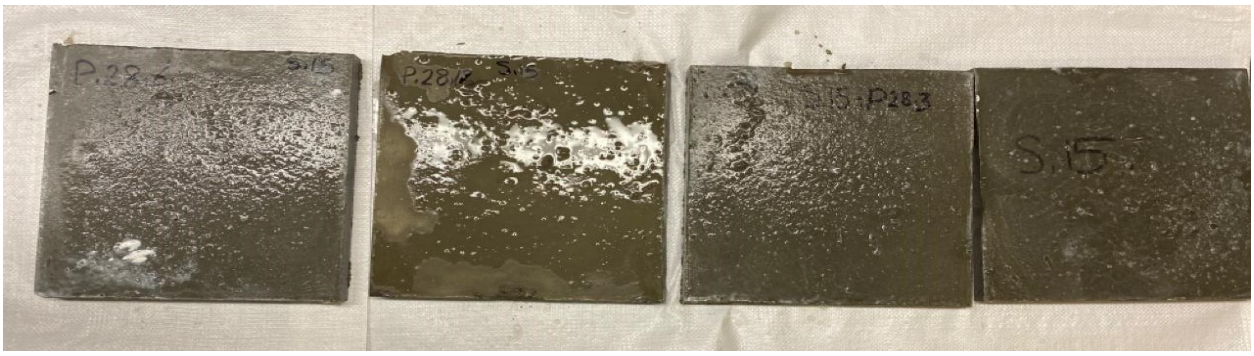

Fig 4.2 Thermal conductivity samples

4.2 RESULTS AND DISCUSSION

4.2.1 Flowability

Self-compacting mortar was designed to lower the yield stress and reduce the risk of fracturing the capsule during pouring and compaction. **Table 4.3** shows the flowability (i.e. mini-slump and V-funnel) of SCM incorporating different dosages of MPCMs as a sand replacement with and without LF. All SCM gave slump flow in the recommended range between (250-300 mm) (Domone and Jin 1999). Besides, they maintained flow time value in the range between (2-10s) as recommended (Felekoğlu et al. 2006). In general, all mixes show good self-compacting properties. Increasing the percentage of MPCMs increase the viscosity of SCM. For instants, in S.15 - P.12 mixtures, the flow time increased by 110% when the MPCMs percentage increased from 0% to 12%. This is due to the reduction of free water in the presence of fine particles(S. Lucas et al. 2010; Sanfelix et al. 2019). This indicates MPCMs enhance the viscosity of SCM.

Table 4.3 Flowability of SCM incorporating different dosages of MPCMs

Mixture ID	Mini-Slump (mm)	V-Funnel (sec.)
C	260	5
P.3	270	5.5
P.6	275	6.5
P.12	275	8
S.15-P.3	285	6
S.15-P.6	285	7
S.15-P.12	295	9

4.2.2 Heat of Hydration

The hydration process is a chemical reaction between binder and water that starts with the first second of mixing. LF is not considered an inert material, but it is partially reactive (Hawkins, Tennis, and Detwiler 1996; Lothenbach et al. 2008b). Incopreation LF and MPCMs influence hydration kinetics. The hydration peaks increase and occur sooner. Mixtures with 15% LF and various percentages of MPCMs (i.e. 3%, 6%, 12%) were studied at 23℃ for 48 hrs to capture the hydration peaks of the hydration process. In general, an exothermic peak was reported immediately after mixing due to a rapid initial chemical reaction between Tricalcium silicate (C_3S) and water (Costoya Fernández 2008). Also, it can be attributed to the dissolution of the C_3S (Bullard et al. 2011). After that, an induction period has been reported for 1-2 hours. This can be explained due to the fall down in growth and nucleation of calcium silicate hydrate (C-S-H) (Costoya Fernández 2008). Subsequently, the heat continues to evolve and reach its maximum peak. This is due to the ongoing reaction of calcium silicate hydrate and calcium hydrate, which depend on the particle's size and the rapid formation of hydrates, which reached their peak after 10 -12 hrs (Scrivener 1984). Then, the hydration reaction goes through a deceleration period. After that, a second

shoulder peak is reported, which is linked to ettringite formation, where the hydration product is accelerated in the aluminate phase (Juilland et al. 2010).

Fig 4.3 presented the effect of LF and MPCMs content on the hydration of heat. The first 48 hr was selected as a comparison base of the hydration heat released in this period. The hydration peaks increased and occurred sooner by incorporating LF and increasing content MPCMs content compared to the control mixtures. For instance, in mixtures S.15-P.12 and S.15-P.3, the hydration peak occurred sooner by 6.85 hrs and 6.71 hrs, respectively, compared to the control mix and sooner than mixtures with no LF by 5hrs and 4.8hrs. Moreover, the hydration peak showed 21% and 7% improvement, respectively, compared to the control mix and 16 % and 7% compared to samples with no LF. Limestone filler and MPCMs small particles (i.e. LF particle size 3µm and MPCMs ranged from 3-30µm) compared to 4 mm fine aggregate enhance heterogeneous nucleation at low energy levels where it works as a physical catalyst through activation of cement hydration (Zeng et al. 2013; Luo et al. 2013; Jayalath et al. 2016). The LF and MPCMs particle sizes located in the smallest cement particles family (i.e. less than 10µm) have a higher surface area, enhancing hydration products' development. Consequently, using LF and MPCMs with smaller sizes stimulates cement hydration and improves the space-filling properties compare to mixtures without LF and control mix (Li et al. 2015; Jayalath et al. 2016).

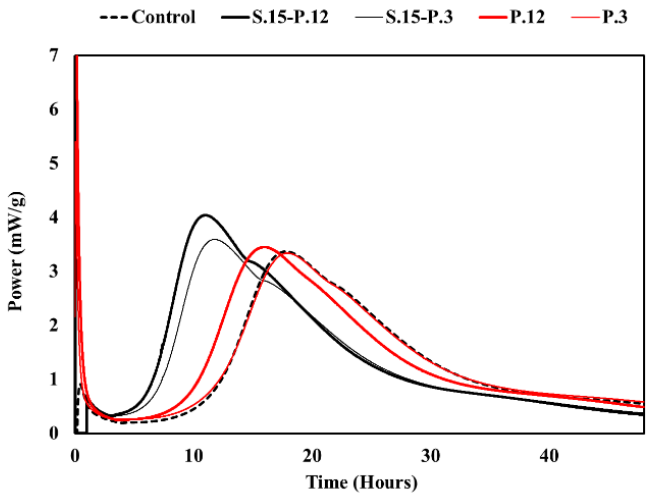

Fig 4.3 Effect of LF and MPCMs on Heat of Hydration

4.2.3 Thermal Analysis

Cement past consists of four significant compounds: dicalcium silicate (C_2S), tricalcium silicate (C_3S), tetracalcium aluminoferrite (C_4AF) and tricalcium aluminate (C_3A). The calcium silicate hydrate (C-S-H) and calcium hydroxide, (CH) is the most critical product of the hydration reactions (Sha, O'Neill, and Guo 1999).

Different researchers pointed out the reactions that occur with increasing temperature in the cement past as follow (Noumowe 1995; 1995; Nonnet, Lequeux, and Boch 1999):

- Between 30 - 105 ℃: most of the bound water evaporates. All the water evaporates at temperature 120℃.
- Between 110- 170 ℃: gypsum and ettringite decomposed.
- Between 180 – 300 ℃: bound water is lost from the decomposition of calcium silicate and carboaluminate hydrates.
- Between 450 – 550 ℃: Calcium hydroxide (portlandite) is dehydroxylated.

- Between 700 -900: calcium carbonate is decarbonated.

Fig 4.4 presents the derivative of thermogravimetric (DTG) curves incorporating different percentages of MPCM in SCM. The DGA curves present the heat flow in (mj/s) during the heating process. There are two prominent peaks reported at a temperature around 110 ℃, 500 ℃ and a shoulder peak at 170℃. The first peak corresponds to dehydration of C-S-H gel and ettringite (Le Saoût et al. 2013). The second peak account for the dehydration of calcium hydroxide, which occurred between 450 ℃ and 550 ℃. The shoulder peak can be related to dehydration of monosulfoaluminate (Trauchessec et al. 2015; Martinelli, Koenders, and Caggiano 2013).

The decomposition occurred in all samples; however, its intensity depends on the percentage of MPCMs, as shown in **Fig 4.4**. The peak value at 110 ℃ and 500 ℃ increased with the increased MPCMs content. The amount of the C-S-H gel and CH increased with the increased content of phase change material. Moreover, the weight loss derivative for S.15-P.12 mixture showed a slightly higher peak at temperature range 200℃ to 450℃. This can be related to the part of C-S-H gel transformed into a more stable state requiring dehydrating at a higher temperature. Thus, this indicates MPCM and LF influence the CH content. This is due to the small size of the PCM particles and LF, which stimulate the hydration reaction and CH content (Jayalath et al. 2016). Also, MPCM and LF were used as sand replacements. Hence, the dilution effect is neglected.

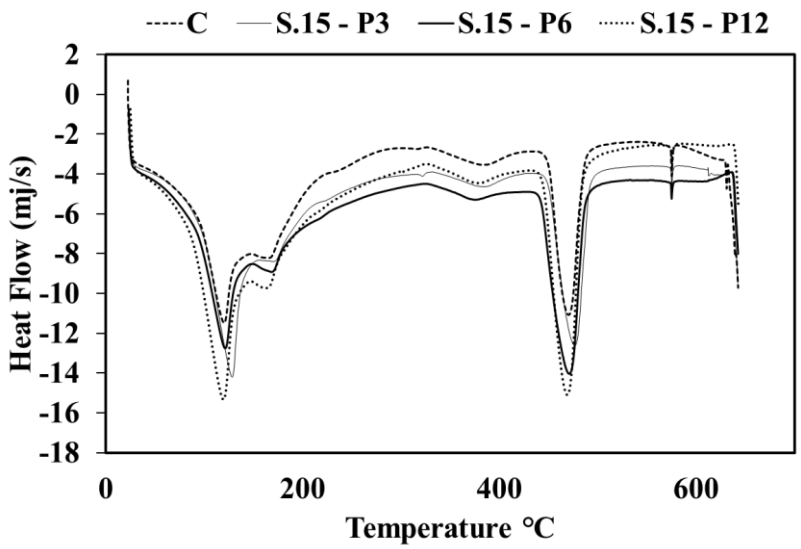

Fig 4.4 Derivative thermogravimetric analysis (DTG) of mortar with different MPCM content

4.2.4 Compressive strength

The compressive strength test was executed to evaluate the mechanical properties of incorporation MPCMs in SCM. **Fig 4.5** illustrates the compressive strength for mixtures incorporating various percentages of MPMCs. Each point is the average of three tests, and the coefficient of variation was less than 4% for all mixes. Generally, MPCMs dosage effect the mechanical properties of SCM. On the other hand, adding LF enhances the mechanical properties of SCM made with MPCMs.

For mortar with LF and MPCMs, replacing 15% of sand with LF and 3% of MPCMs significantly increased compressive strength at all ages by 7% compared to the control mix. For S.15-P.6 mixture, Increasing the MPCMs content up 6% and LF 15% did not induce a considerable change in the compressive strength than the control mix. Conversely, When the percentage of MPCMs increased up to 12%, the compressive strength of mixtures reduced by 15%.

For mortar with MPCMs and without LF, replacing 3% sand with MPCMs did not cause a significant effect in mechanical properties at all ages. On the other hand, Increasing the MPCMs content by 6% and 12% significantly decreases mechanical properties by 15% and 22%, respectively.

Through DGA analysis and heat of hydration results, micro-size particles of LF and MPCM increase the hydration product and accelerate hydration reaction. However, the compressive strength results showed a loss in strength. The reduction in compressive strength can be attributed to the soft nature of the MPCMs compared with hard particles of sand, which can not sustain loads, and capsules act as a void (Drissi et al. 2014). However, the small particle size of LF and MPCM increased the nucleation sites of hydration products, increasing strength increment. Also, limestone filler enhanced the cement-based chemical and physical characteristics and fill the voids between sand and cement particles, decreasing pores volume in the SCM (Camiletti, Soliman, and Nehdi 2013; J. J. Chen, Kwan, and Jiang 2014; Jayalath et al. 2016).

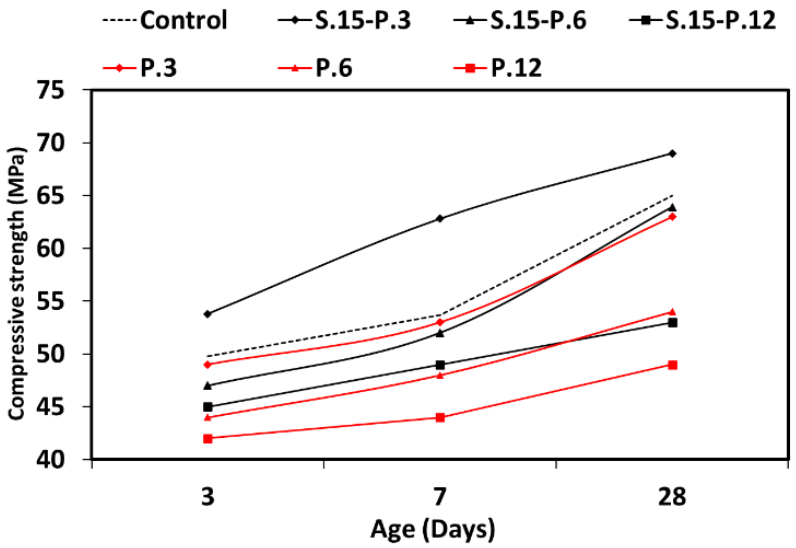

Fig 4.5 Compressive strength for mixtures incorporating various percentages of MPMCs

4.2.5 Shrinkage

Fig 4.6 illustrates the effect of LF and MPCMs incorporation in SCM on the shrinkage test at 28 days. Each point in the curve is the average of three tests. After 28 days, the shrinkage values tend to converge. Generally, The addition of LF and MPCMs tends to increase shrinkage. The mortar mix design made with LF showed higher shrinkage compared to mortar without LF. The increase of shrinkage can be related to the LF effect on accelerating the hydration or formation carboaluimate at an early age, which increased the volume of cement gel (Malhotra and Carette 1985; Adams and Race 1990). Moreover, replacing stiff inclusion, such as sand with compliant inclusion, as MPCMs into the mix, caused an increase in shrinkage (P. Kumar Mehta and Monteiro 2014; Šavija 2018). This increase can be related to the MPCMs role as air void, which does not restrain past shrinkage (Wei et al. 2017).

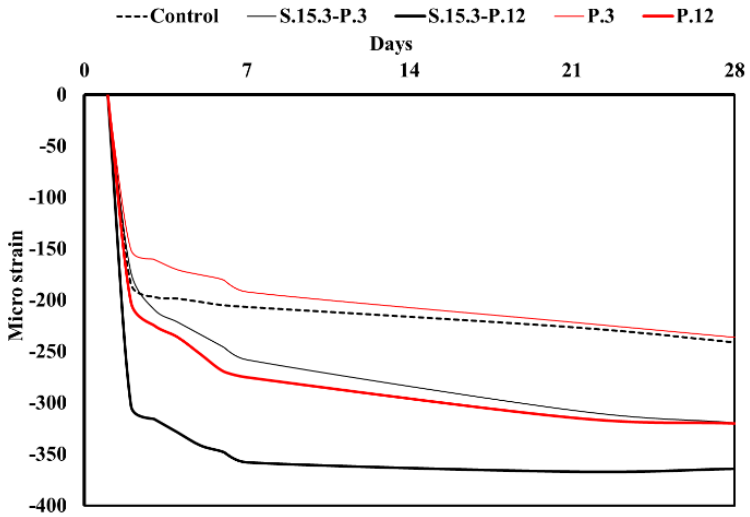

Fig 4.6 Effect of LF and MPCMs content on shrinkage on SCM

4.2.6 Heat Flux

To evaluate the mortar's thermal performance, the heat flux was measured for different percentages of MPCMs (0%, 3%, 6%, 12%) after 28 days. An appropriate temperature range from 23℃ to 35℃ was selected according to the expected range of usage and the transition temperature of the MPCMs. For the given range, a cyclic heating/cooling scan was conducted at a rate of 5℃/min, where the temperature was held for 8 hrs for the maximum and minimum temperature. The first cycle started with heating samples from 23℃ to 35℃, where endothermal conditions higher than the phase transition temperature of the MPCMs. Subsequently, the cooling cycle started in an isothermal condition below the phase transition temperature of the MPCMs.

Fig 4.7 presents the heat flow from mortar made with different percentages of MPCMs. In general, increasing the percentage of MPCM significantly increased the heat capacity and the mortar's heat flux. When the chamber's temperature is above the phase transition temperature, MPCMs incorporated in the samples started to absorb heat through an endothermic process for the first 5 hrs. after that, MPCMs and the samples reached maximum storage capacity. During the cooling down period, an exothermic process took place, and MPCMs started to release absorbed heat over the next 9 hrs. Therefore, incorporating MPCMs significantly improves the thermal performance of mortar. This is due to the increase in the thermal mass and the thermal insulation improvement (i.e. reduction of thermal conductivity).

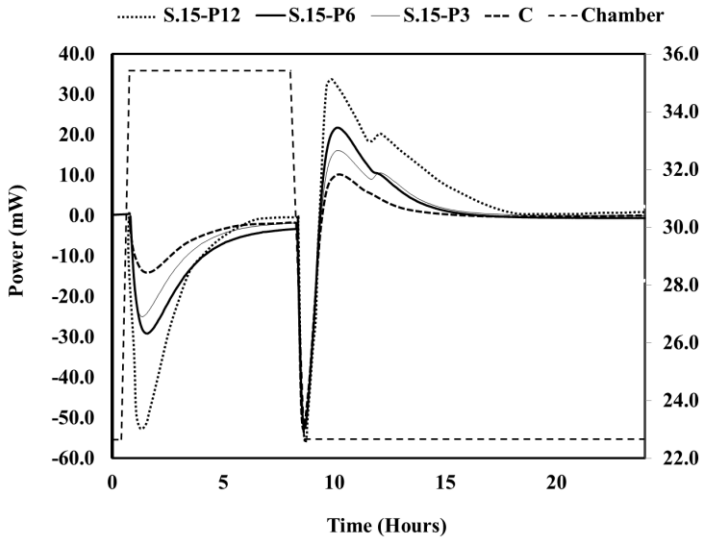

Fig 4.7 Heat flow of Mortar made with different percentage of MPCMs

4.2.7 Thermal conductivity

The thermal conductivity test was used to examine the thermal behaviour of the hardened mixtures. Three samples were prepared with 3%, 6%, 12% of MPCMs, and a measured reference sample. Firstly, the samples are kept at uniform temperature 23℃. After that, the hot plate temperature was raised to 35℃ and 25℃ for the cold plate. The thermal conductivity of the specimens was evaluated after the stabilization period.

Thermal conductivity presented in **Fig 4.8** indicates that incorporating MPCMs into mortar resulted in a reduction in the thermal conductivity. This is due to the low thermal conductivity of the MPCMs compared to sand and their ability to increase the amount of the entrapped air (Hunger et al. 2009; Jayalath et al. 2016).

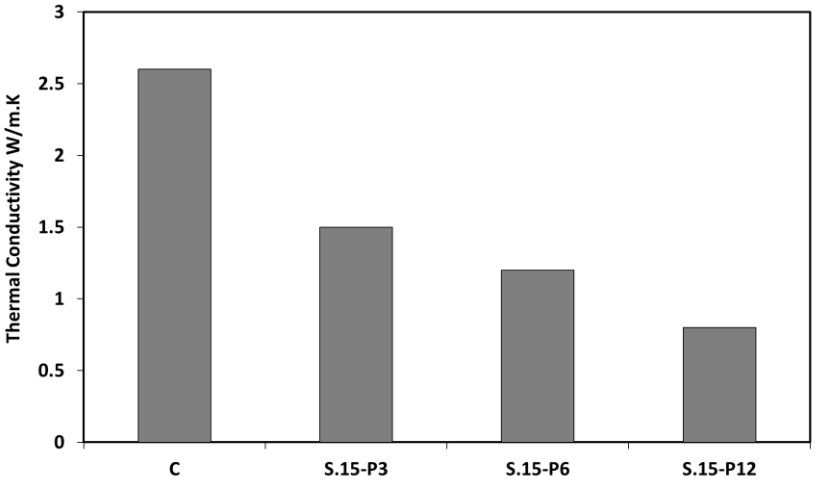

Fig 4.8 Thermal conductivity of MPCMs samples

Chapter 5 A NOVEL PHASE CHANGE MATERIALS CURING SHEET

During the cold winter season, all in-situ construction activities are halted, leading to economic losses. Hence, shifting to precast concrete represents an optimum solution to maintain construction progress during such harsh environments. However, the heat curing process for precast elements represents a challenge for the precast industry due to its high energy consumption. Therefore, this study examines the feasibility of utilizing phase change materials (PCMs) to optimize the heat curing process. A novel phase change material curing sheets were developed and tested. Results showed that covering the specimens during the cooling period had significantly enhanced strength development, even for the shorter heating period. Strength for specimnes exposed to 11 hrs heating curing cycle and covered with PCMs was only 10% lower than 16-hours heated cured specimens. These results prove the feasibility of the idea, leading to a significant saving in energy, allowing the precast industry to advance its sustainability level.

5.1 Significance of Research

The steam curing process has been adopted in the precast industry for a long time. However, the high energy consumption and long-time process represent the main challenges for the precast concrete industry. An excessive amount of research was carried on using and incorporating PCMs in concrete; however, the associated reduction in the mechanical performance did not bode well for broader acceptance. Hence, this study provides a novel application for PCMs that will enhance precast concrete mechanical properties and increase its sustainability

5.2 Experimental Program

5.2.1 Materials and mixture design

General use hydraulic cement, according to CSA-3001-03, was used as the main binding material. Two mixtures were chosen from previous chapters. The first one, Self-compacting

mortar made with 15% Limestone filler as a sand replacement and particle size 3μm. The second one, SCM with 15% LF and 6% of MPCMs. As discussed in the previous chapter, these mixtures showed good mechanical properties (i.e. chapters 3&4). MPCMs with melting points of 43℃ were used. **Table 4.1** summarizes the properties of used MPCM according to the manufacturer.

Table 5.1 MPCM 43°C properties

Manufacture properties	**MCPCM 43**
Melting Point (°C)	43
Heat of Fusion (J/g)	175
Moisture (%)	< 3 %
Appearance	White Powder

5.2.2 Fabrication of the Curing Sheets

Microencapsulated phases change material (MPCM) with a melting point of 43°C was the main component of the prototype fabricated sheets. The used MPCMs have a paraffin core and polymeric outer shell (i.e. the capsule), and particle sizes ranged from 3 to 30 μm. **Table 4.1** summarizes the properties of used MPCM according to the manufacturer. **Fig 5.1** shows MPCMs sheet components; The main idea was to produce a flexible sheet that can be easily used to cover the concrete specimens. Hence, the MPCM was mixed with a binding material and spread inside a flat mold between two thin layers of polythene plastic sheets. Gentle pressure was applied to ensure the sheet has a uniform thickness. The ratio between the MPCMs and binding materials was 80:20, which was selected after several trials to optimize heat entrapping and integrity of the sheet along with maintaining the flexibility. After hardening, the sheet was removed from the mold

and had one side covered by an aluminium adhesive sheet to reduce heat dissipation to the surrounding environment.

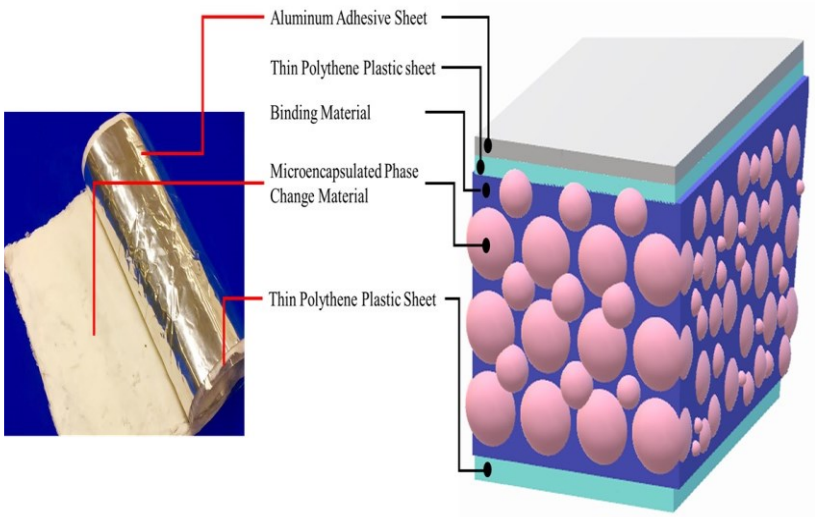

Fig 5.1 PCMs curing sheet

5.2.3 Curing regime

Various curing regimes are illustrated in **Fig 5.2**. For the ambient curing, specimens were kept in the mold for 24 hours. After demolding, specimens were stored in a limewater tank at 23°C until tested (i.e. 1, 3, 7 and 28 days). For the regular steam curing regime, specimens with the molds were stored inside an environmental chamber for 3 hours at 23 °C and 98% relative humidity (RH) (i.e. so-called precast period). The chamber's temperature is then ramped up to 60°C at a 20 °C /hr rate while maintaining the RH at 98%. Temperature and relative humidity were held for 10 hrs (i.e. holding period), then the temperature decreased gradually at a rate of 15 °C/hr. The chamber and specimens' centre temperatures were monitored using type-T thermocouples connected to a data acquisition system. The modified steam curing regime had the same stages as the regular steam curing, except the holding period was shortened to 5 hrs only. Finally, during the cooling

stage, specimens were divided into two groups. One group was exposed to the regular cooling procedure, and the other group was covered by the fabricated MPCMs sheet, as indicated in **Fig 5.2**.

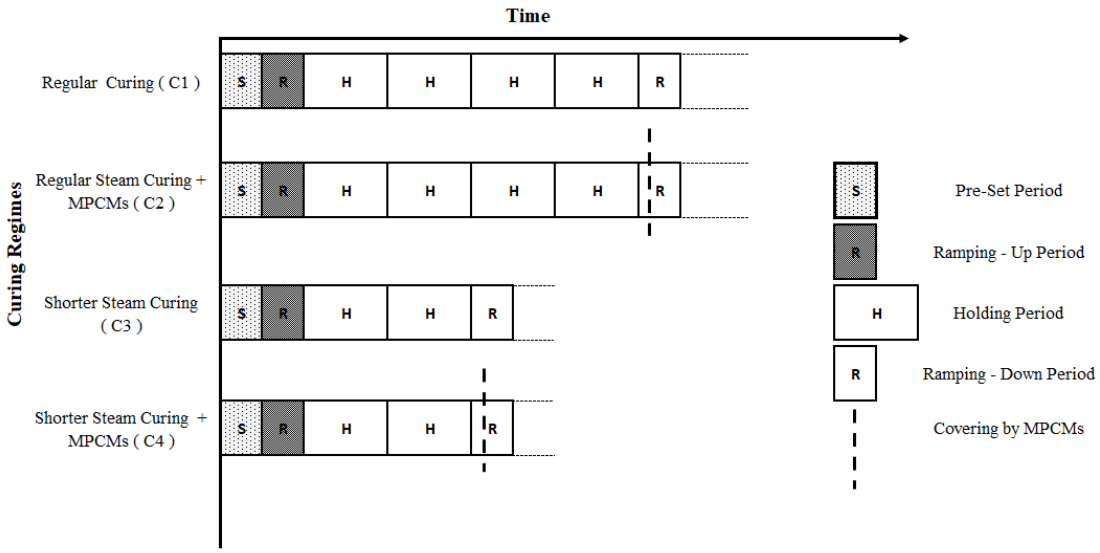

Fig 5.2 Various curing regime

5.2.4 Testing and Specimen Preparation

Compressive strengths at ages 1 and 28 days were evaluated for all tested mixtures using 50 mm cubic specimens according to ASTM C 109 (Standard Test for compressive strength for cement mortar). Specimens' temperatures exposed to various curing regimes were monitored on dummy samples during the first 48 hrs of hydration. Three Type-T thermocouples instrumented in each specimen at different distances along the vertical axis at the specimen's centre. Temperature readings were recorded continuously using a data acquisition system. Replicate specimens indicated a standard deviation of 1.8°C for the maximum specimen temperature. Thermo-gravimetric analysis (TGA) combined with derivative thermo-gravimetric (DTG) was used to monitor the formation of different hydration products (i.e. calcium hydroxide (CH) and non-

evaporable water. This was used as an indication for the hydration progress. At the selected testing age, hydration of samples was stopped using the freeze-drying technique. Then, chunks taken from the centre of the specimens were ground to powder and sieved on No. 200 sieves. Samples weighing approximately 40 mg were heated from 23°C to 1150°C at a 10°C/min heating rate. Collected data and curves were analyzed using a TA Instrument thermal analysis software. The percentage of CH (i.e. approximately the mass loss between 450–500 °C and degree of hydration (subtracting the mass loss associated with calcium carbonate from the loss on ignition of a dried sample weight at 110 °C, normalized by the mass of the dried sample) were used to compare the degree of hydration between various mixtures. This indirect method to quantify the degree of hydration has been commonly used by many researchers (Loukili et al., 1999). Thermal conductivity was measured according to ASTM C518 (Materials 2017), heat flow meter (HFM436, manufactured by NETZSCH) was used to measure the MPCMs sheet's conductivity. The MPCMs sheet with dimensions 300 × 300 mm and thickness 8 mm was placed between the hot and cold plates. Heat flow was calculated according to the Fourier heat flowing **Eq. 1.**

$$q = \frac{Q}{A} = \lambda \frac{\Delta T}{\Delta x} \qquad \textbf{(Eq. 1)}$$

Where q *is the* Heat flux [W/m²], Q is the rate of heat flow [W], A is the specific area [m²], (λ) is the thermal conductivity of the sample, ΔT is the temperature difference of the sample, and (Δx) is the thickness of the sample. The test for each sample was repeated three times, and the results were averaged. Moreover, high-resolution, forward-looking infrared (FLIR) camera, which converts thermal energy into visible light, was used to capture the MPCMs sheet's temperature during the curing process. Scanning Electron Microscopy (SEM) testing was carried out on several specimens to examine the microstructure using a backscattered electron detector on the fracture surface.

5.2.5 Methodology

At the end of the holding period (i.e. the temperature in the chamber is around 60 °C), the specimens were covered by the MPCMs sheets **Fig 5.3**. During this stage, the temperature is higher than the melting point of the MPCMs (i.e. 43°C). Hence, the sheet will start absorbing and storing heat until reaching its heat capacity. Once the chamber's temperature dropped to the melting point of MPCMs, the sheet will start releasing the heat based on the specimen's temperature. Moreover, the aluminum cover will allow the sheet to maintain its temperature and reduce heat loss. As the specimen's temperature dropped below the melting point of MPCMs, the sheet will release heat to maintain the specimen's temperature. This stage will continue until the sheet releases all the stored heat. In other words, the MPCMs sheet will act as an external heat source for the specimens by emitting thermal energy during its solidification process from the liquid state. These stages agreed with the measured changes in temperature profile inside the chamber and the specimens, as illustrated later.

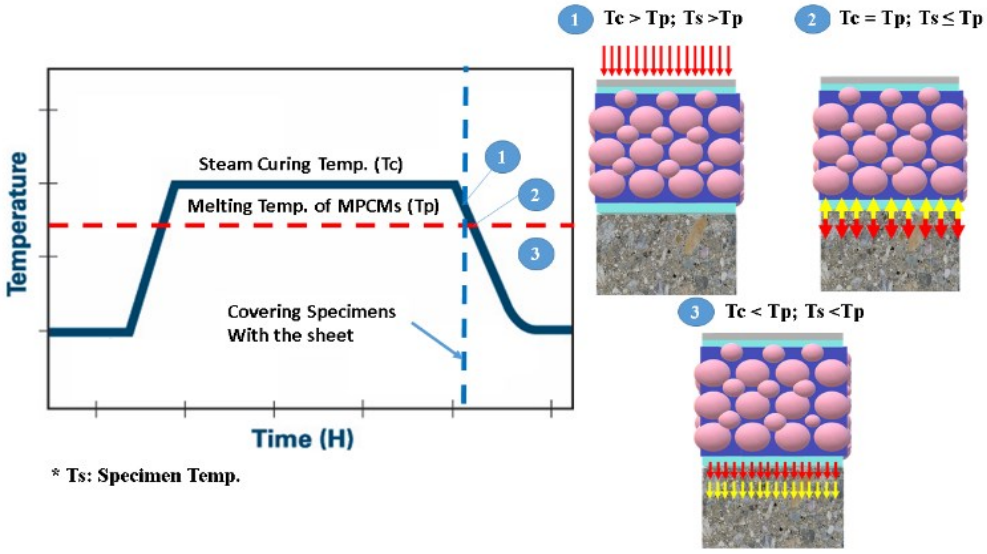

Fig 5.3 Illustration for the curing stages with and without coverage with the sheet (Tc: chamber's temperature, Ts: Specimen's temperature, and Tp: PCM sheet's temperature)

5.3 RESULTS AND DISCUSSION

5.3.1 Heat Profile

Heat profile is used to check the effectiveness of MPCMs sheet for heat storage. The MPCMs sheet temperature and chamber's temperature was monitored for 24 hrs. **Fig 5.4** illustrates the temperature profile of the MPCMs sheet and chamber over time. The chamber's temperature increased by 20 ℃/hr and was held at a maximum temperature of 60 ℃ for 5 hrs. The MPCMs sheet temperature increased gradually with a rate of 7℃/hr until it reached its melting point (i.e. 41℃ ~ 46 ℃), where an endothermic process occurred as MPCMs particles converted from solid to a liquid state and absorbed heat. After 6 hrs, MPCMs sheet temperature increased dramatically with a rate of 9℃/hr. After holding the maximum temperature for 5 hrs, the chamber started to cool down at a rate of 15 ℃/hr. Subsequently, the MPCMs sheet temperature started to drop at a similar rate for the increasing (i.e. 9 ℃/hr) till reaching the melting point. MPCMs particles started the conversion from liquid to the solid-state and released stored heat (i.e. exothermic process). Stored heat was continued to release for around 10 hrs. Moreover, the MPCMs sheet held a temperature above 40 ℃ for more than 7 hrs. Thus, the MPCMs sheet's heat storage capacity is sufficient to conserve energy consumption in different applications.

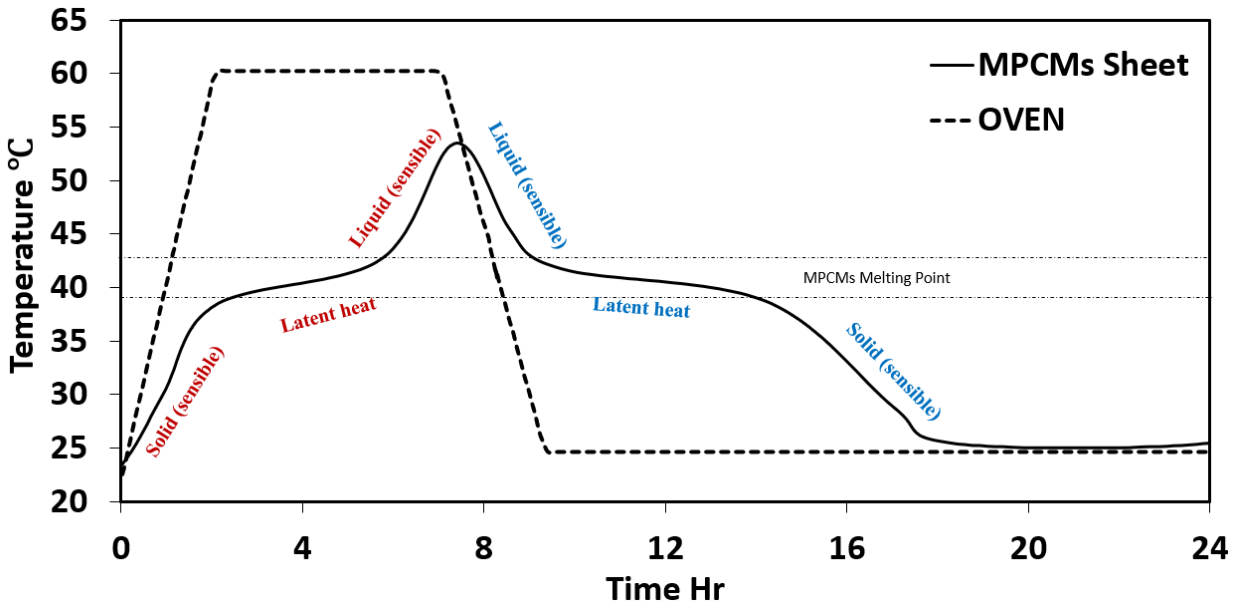

Fig 5.4 Temperature profile of the MPCMs sheet and chamber

Fig 5.5 and **Fig 5.6** show the temperature profile overtime for specimens exposed to various curing regimes. In general, the specimens' temperatures changed following the variation in the chamber's temperature. Initially, the specimens' temperature increased until reaching the maximum temperature during the holding period. Specimens maintained their temperature over the holding period, either the regular (i.e. 10 hours) or the shorter (i.e. 5 hrs) curing regime. Afterward, the specimens' temperature started to drop at the end of the holding period and during the cooling down period, following the same profile for the chamber's temperature.

Initially, specimens covered by the MPCMs sheets followed the same temperature drop profile for uncovered specimens until reaching the melting zone for MPCMs, as shown in **Fig 5.7**. The cooling profile curve for covered specimens started to deviate from that of the uncovered specimens, exhibited a slower temperature drop rate. This extended the curing period at high

temperatures. For instance, specimens covered by the MPCMs sheet took more than 13 hours to reach the ambient temperature compared to 5 hrs for uncovered specimens.

On the other hand, the mortar was made with 6% of MPCM 43 when the champer's temperature reached the MPCMs melting point (i.e. 41- 45°C). The heating curve showed a slight change in the slope associated with a delay in raising the temperature. During the cooling period, the curve showed a change in the slope, resulted in a slight delay in the cooling down period.

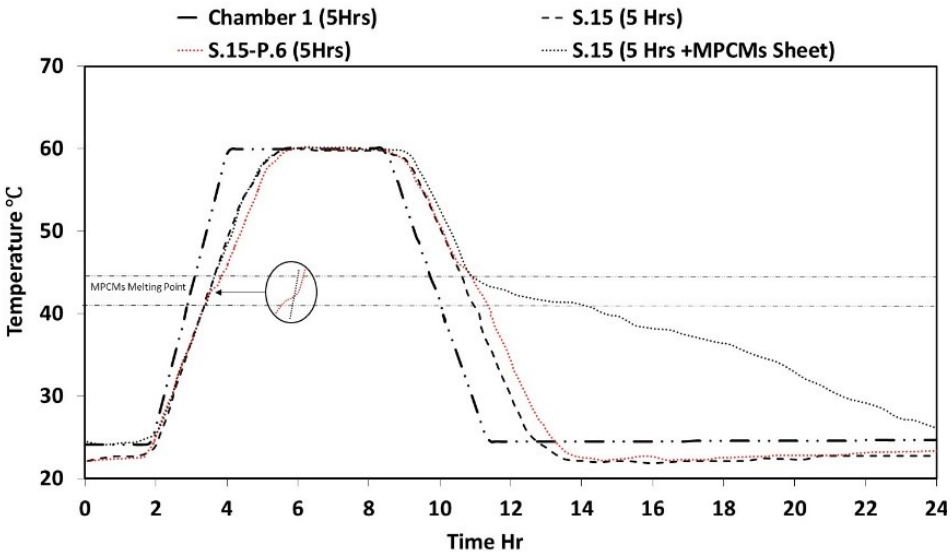

Fig 5.5 Temperature profile for samples at 5 Hrs maximum holding time

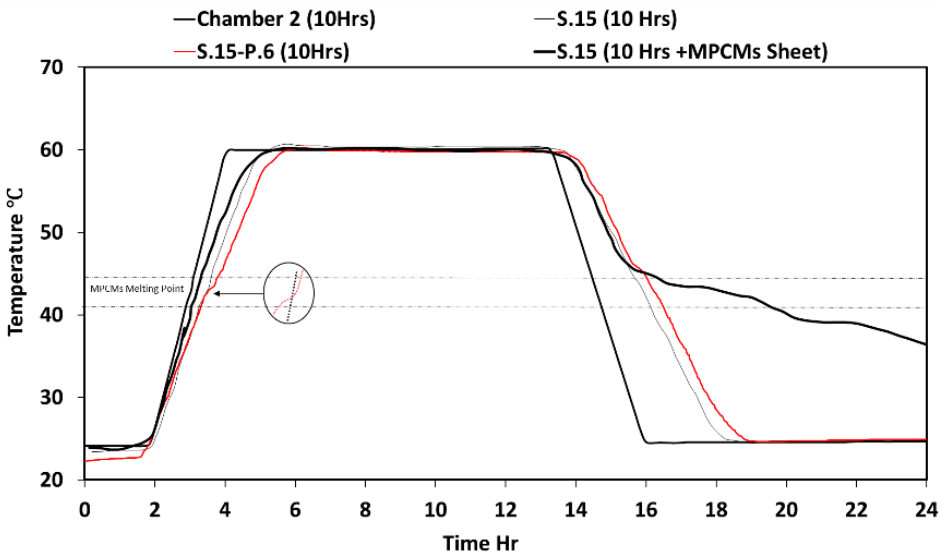

Fig 5.6 Temperature profile for samples at 10 Hrs maximum holding time

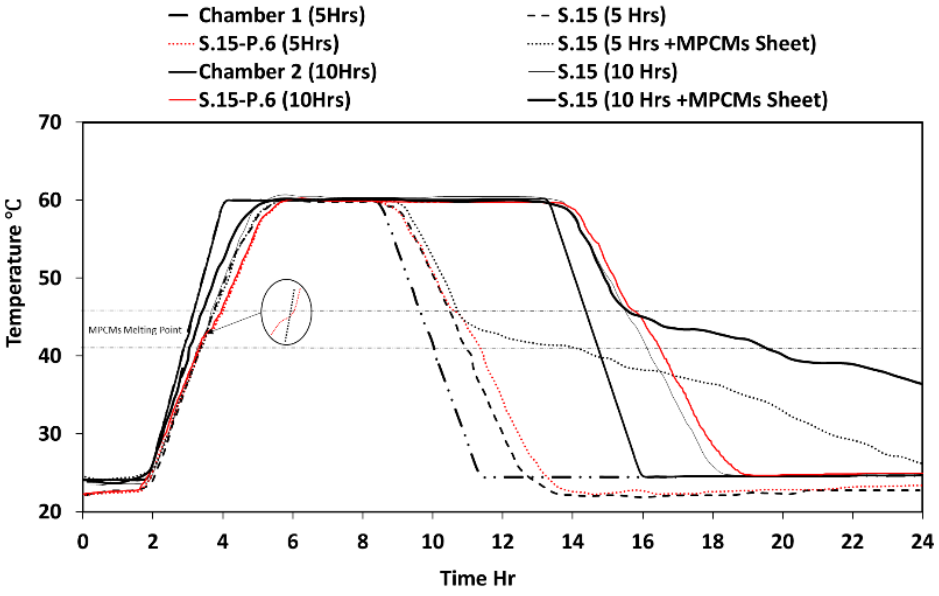

Fig 5.7 Temperature profile of samples at different curing regimes

5.3.2 Cube Compressive Strength

The compressive strength for specimens exposed to various curing regimes is represented in **Fig 5.8**. Each value on the curve represents the average of three replicates with a coefficient of variation less than 3 %. Extending the heat curing period led to a higher strength. For instance, at age 1 day, specimens exposed to steam curing with a holding period of 10 hrs exhibited about 30% higher compressive strength than that exposed to 5 hrs only. This can be attributed to the hydration process enhancement leading to the formation of more hydration products. The same trend was found for specimens covered by the MPCMs sheet. Specimens with a longer holding period exhibited higher strength than those exposed to a shorter holding period. This indicated the uniformity effect of the MPCMs sheet regardless of the curing regime. However, incorporating MPCM caused a reduction in the mechanical properties compared to the control mix. The reduction in compressive strength can be attributed to the soft nature of the MPCMs compared with hard particles of sand, which can not sustain loads, and capsules act as a void (Drissi et al. 2014)

On the other hand, using the MPCMs sheet had improved the achieved strength. For instance, under regular steam curing with 10 hrs holding period, the 1-day strength for specimens covered with MPCMs sheet was 28% higher than uncovered specimens. This can be ascribed to the ability of MPCMs to release heat and to maintain the curing temperature around the specimens for a longer period. Moreover, the MPCMs regulate the reduction in the specimens' temperature at a lower rate. This is anticipated to improve the development of the microstructure.

On the other hand, covering the specimens with MPCMs had compensated the effect of reducing the holding period to 5 hrs. As shown in **Fig 5.8**, reducing the holding period to 5 hrs had led to about 24% reduction in the strength compared to specimens cured to 10 hrs. However, this

reduction was almost null (1.6%) for the same specimens covered by the MPCMs during the cooling period. At later ages, the achieved compressive strength followed a similar trend to that at early age (i.e. 1 day).

As shown in **Fig 5.8**, the development of strength will mainly depend on the curing temperature and period. Hence, the effect of the MPCMs sheet can also be illustrated by applying the maturity concept. Maturity is applied to account for the temperature history of the concrete strength development. Various methods can express it; however, the simplest and most commonly applied is the linear expression for the relationship between temperature and time, as shown in Eq. 2.

$$M = \int_0^t (T_c - T_o)dt \qquad \text{Eq. 2}$$

Where M: maturity; T_c: temperature of concrete; T_o: datum temperature (accepted value: −10 °C). Calculating the maturity for the two curing cycles showed that 5 hrs holding resulted in about 18% reduction compared to the 5 hrs holding. This was corresponding to the 24% reduction in the specimens' strength exposed to 5 hrs holding compared to those cured for the 10 hrs. However, covering the specimens exposed to 5 hrs holding period with the PCMs sheet had reduced the difference in the maturity to only 4.5% with respect to those exposed to 10 hrs holding period. This also agreed with the compressive strength results as the difference was minor (i.e. 1.6%). This again highlighted the efficiency of using PCMs sheets to maintain adequate strength.

On the other hand, applying the PCMs sheets for specimens cured for 10 hrs holding period showed about 12% increase in the maturity with respect to specimens exposed to the same curing

cycle without being covered by the PCMs sheet. This will accelerate the demolding process as specimens achieve the required strength faster. For instance, the compressive strength for specimens cured for 10 hrs holding periods with and without PCMs sheets exhibited 54 MPa and 65 MPa after one day, respectively.

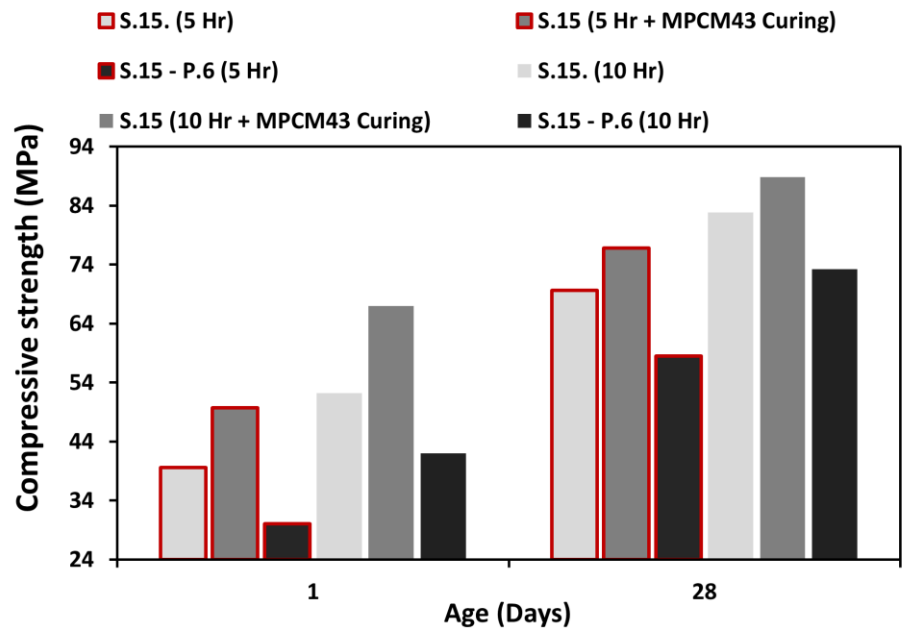

Fig 5.8 Compressive strength for mortar under different curing regimes

5.3.3 Thermal Camera

Thermal imaging was used to investigate the effectiveness of the extended curing technique using the MPCMs sheet. **Fig 5.9** shows the temperature for both sides of the MPCMs sheet. The aluminum isolated adhesive sheet recorded 24°C, while MPCMs maintained a temperature of 40.5°C. The aluminum adhesive cover showed its high efficiency in maintaining MPCMs sheet temperature and reduced heat dissipation, improving the MPCMs sheet thermal performance.

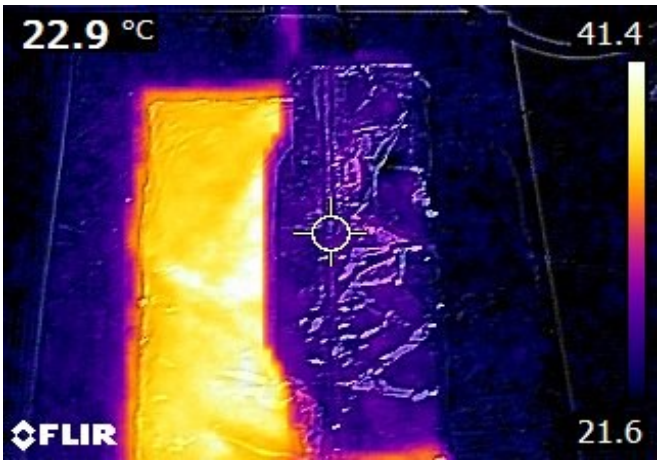

Fig 5.9 the temperature of both sides of the MPCMs sheet

Fig 5.10 illustrates a comparison between temperature evolves from specimen covered and not covered by the MPCMs sheet. After 1 hr, the sample covered with an MPCMs sheet, and the sample under stander cooling down conditions recorded a temperature of around 45℃. Subsequently, the specimen under the stander cooling down condition lost most of the internal heat and recorded a temperature of around 30℃ after 3 hrs and 23℃ after 5 hrs. On the other hand, specimen coved with the MPCMs sheet showed a higher heat retention with a temperature above 42℃ after 3 hrs and 40℃ after 5hrs. These thermal image results matched the heat profile analysis and explain the reported compressive strength improvement.

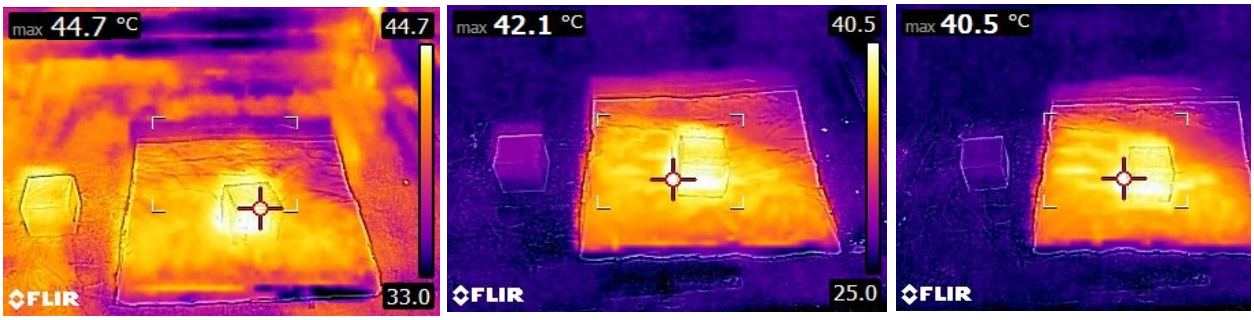

(a) **(b)** **(c)**

Fig 5.10 Thermal image for temperature evolves from specimens covered and not covered by the MPCMs sheet after (a) 1 hr; (b) 3hrs; and (c) 5 hrs

5.3.4 Scanning Electron Microscopy Analysis

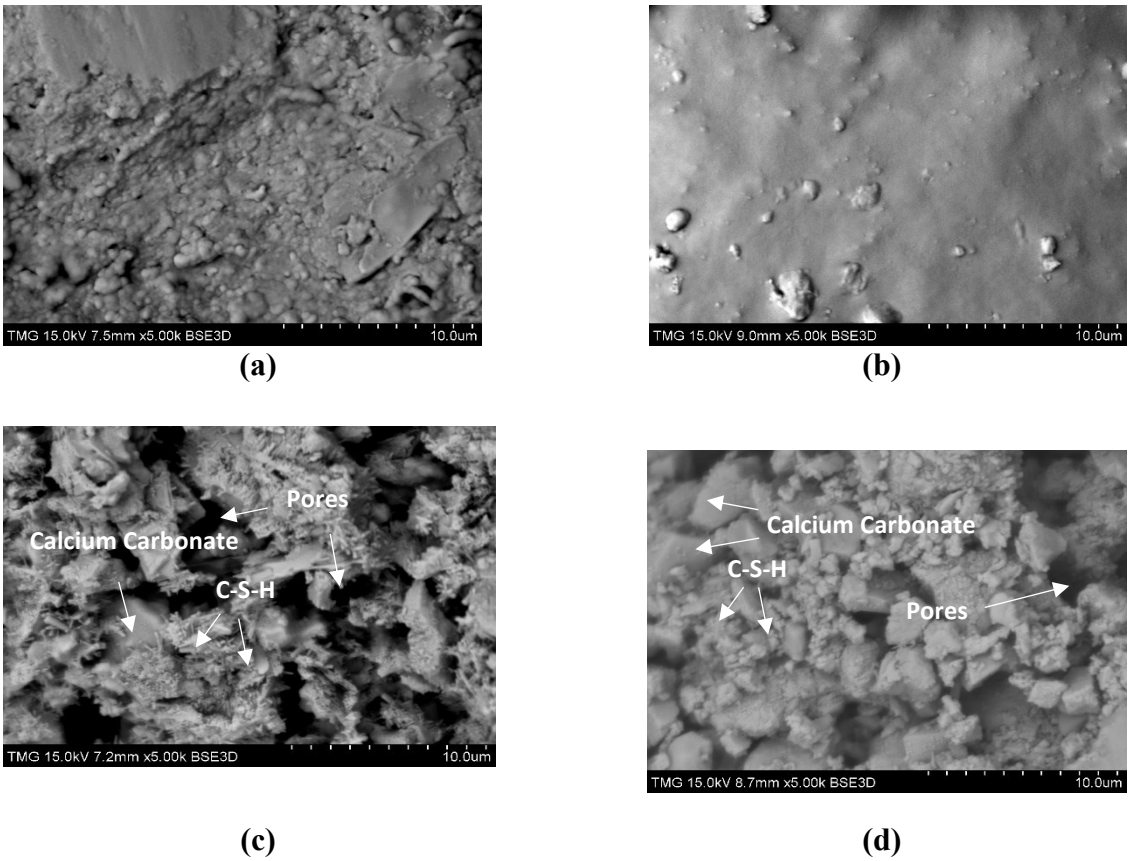

Fig 5.11 SEM photograph of mortar at different curing regimes: (a) 10 hrs; (b) 10 hrs + MPCMs sheet; (c) 5hrs; (d) 5hrs + MPCMs sheet

The hydration process started when cement is mixed with water. During the hydration process, the hydration products formed at the center of cement particles and water filled the pores (Van Breugel 1993). Subsequently, a network of three dimensions is developed gradually, and cement paste is able to resist loading. Thus, the mechanical properties are associated with the formation of microstructure and hydration products (Van Breugel 1993). There are different techniques to investigate the microstructure of the cement paste. The scanning electron microscope (SEM) will

be used to detect the distribution and quantify the contents of different cement phases at different curing regimes.

Fig 5.11 shows the microstructures of the cementitious paste with normal consistency of hydraulic cement, containing 15% limestone replacement at different curing regimes at age one day (i.e. holding maximum temperature for 10 hrs and 5 hrs and covering specimens by preheated MPCMs sheet during the cooling period after 10 hrs and 5hrs). Generally, The pore structures improved by extending the curing time. Also, it was reported that calcium carbonate was held between the hydration products, which enhanced the compact filling through the physical filling.

Fig 5.11 (a) shows the hydration products in the form of flocculent and acicular initially. Moreover, the hydration products were connected by tailing in the shape of plates and blocks. **Fig 5.11 (b)** shows with extending curing time by using MPCM sheet, the flocculent structure disappeared, and honeycomb is formed, and the pore structure significantly improved. **Fig 5.11 (d)** shows a significant improvement in the hydration products, there are no flocculent and honeycomb structures, and the cement particles are connected with a solid layer. Thus, extending the curing time using MPCM sheet increases hydration products' formation and enhances the mechanical properties.

5.3.5 Thermal analysis

Cement past consists of four significant compounds: dicalcium silicate (C_2S), tricalcium silicate (C_3S), tetracalcium aluminoferrite (C_4AF) and tricalcium aluminate (C_3A). The calcium silicate hydrate (C-S-H) and calcium hydroxyde, (CH) is the most critical product of the hydration reactions (Sha, O'Neill, and Guo 1999).

Different researchers pointed out the reactions that occur with increasing temperature in the cement past as follow (Noumowe 1995; 1995; Nonnet, Lequeux, and Boch 1999):

- Between 30 - 105 ℃: most of the bound water evaporates. All the water evaporates at temperature 120℃.
- Between 110- 170 ℃: gypsum and Ettringite decomposed.
- Between 180 – 300 ℃: bound water is lost from the decomposition of calcium silicate and carboaluminate hydrates.
- Between 450 – 550 ℃: Calcium hydroxide (portlandite) is dehydroxylated.
- Between 700 -900: calcium carbonate is decarbonated.

Fig 5.12 presents the derivative of thermogravimetric (DTG) and the thermogravimetric (TG) curves of S.15 samples at different curing regimes (i.e. holding maximum temperature for 10 hrs and 5 hrs and covering specimens by the preheated MPCMs sheet during the cooling period). The DTG curves present the heat flow in (mj/s) during the heating process. The TG curves illustrate the residual weight in (%) for the samples during the heating process.

In the DTG curve, there are two prominent peaks reported at a temperature around 110 ℃, 500℃ and a shoulder peak at 170℃. The first peak corresponds to dehydration of C-S-H gel and Ettringite (Aft) (Le Saoût et al. 2013). The second peak account for the dehydration of calcium hydroxide, which occurred between 450 ℃ and 550 ℃. The Should peak can be related to dehydration of monosulfoaluminate (Trauchessec et al. 2015; Martinelli, Koenders, and Caggiano 2013).

The decomposition occurred in all samples; however, its intensity depends on the curing period, as shown in **Fig 5.12**. The peak value at 110 ℃ and 500 ℃ increased by extending the curing

period and using the preheated MPCM sheet. This means the amount of the C-S-H gel and CH increased by extending the curing period. Moreover, the S.15(10hrs+MPCM sheet) mixture showed a significant higher peak at temperature range 200℃ to 450℃. This can be related to the part of C-S-H gel transformed into a more stable state requiring dehydrating at a higher temperature. Thus, this indicates the influence of the MPCM sheet on the CH content.

In the TG curve, the total weight loss increased with extending curing time. This corresponds to the increase in hydration degree, forming more hydration products with extending curing age. Note that hydration reaction continued with samples covered with the preheated MPCM sheet.Table 5.2 presents the total weight loss in (%) during the TG test. Results show a decrease in residual weight means more hydration dehydrated during the heating process. Thus, this indicates the formation of more hydration products during the curing stage. At the same curing period, the weight loss increased for samples covered with the preheated MPCM sheet since fewer hydration products were produced.

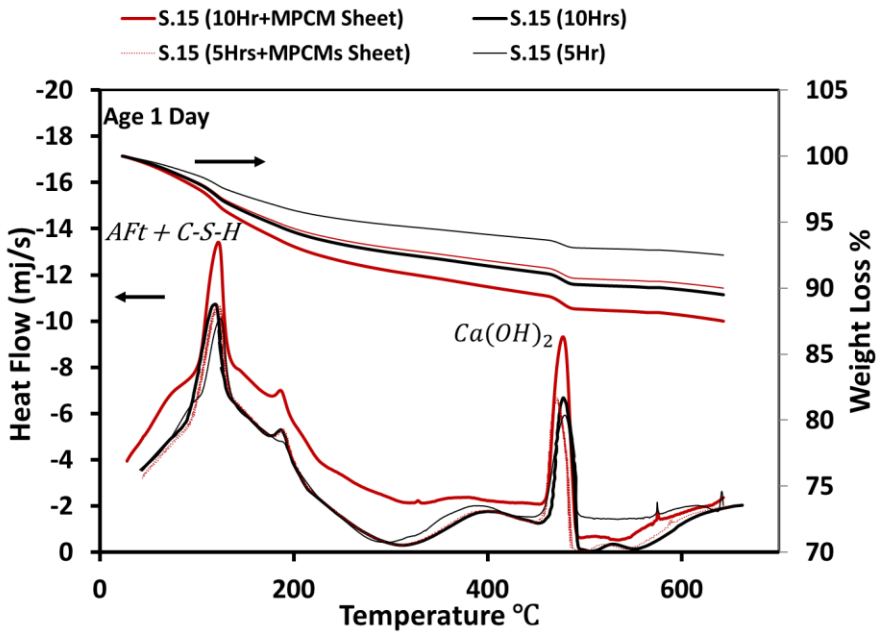

Fig 5.12 TG/DTG curves for self-compacted mortar cured at various curing regimes at 1 Day

Table 5.2 The total weight loss of SCM during the TGA test

Mixture ID	Total weight loss (%)
S.15 (10Hrs +MPCM Sheet)	12.5
S.15 (10Hrs)	10.5
S.15 (5Hrs +MPCM Sheet)	10
S.15 (5Hrs)	7.5

5.3.6 Thermal Conductivity

Fig 5.14 illustrates the thermal conductivity of the MPCM sheet. The heating protocol of the thermal conductivity device was as shown in **Fig 5.13.** Firstly, the MPCM sheet is kept at ambient temperature (i.e. 23℃). After that, the temperature of the upper plate was increased to T_{hot}= 30℃ and the lower plate temperature is lowered to T_{cold}=10℃, thus the obtaining temperature gradient equal to 20℃. When the temperature is stabilized, temperature range (T_{hot}=50℃; T_{cold}=30℃) with the same temperature gradient. T_{mean} shows the mean temperature of the upper and the lower plate.

During each stabilization period, the thermal conductivity was measured. **Fig 5.14** presents the thermal conductivity of the MPCM sheet at different Mean temperatures (i.e. T_{mean} is the average temperature of the upper and the lower plate). The melting point of the MPCMs between 41℃ and 45℃ according to heat profile analysis of the MPCM sheet in **Fig 5.4.** It can be seen when the temperature of the hot plate is higher than melting point of the MPCM sheet, the temperature slowly stabilized due to the solid-liquid transition during phase change. The MPCMs sheet's thermal conductivity slightly decreased when the upper plate's temperature exceeds the melting point of MPCMs from 0.0873 W m^{-1} K^{-1} at a mean temperature of 20 ℃ (i.e., the upper and lower plate's temperature was 30 ℃, and 10 ℃, respectively) to 0.0843 W m^{-1} K^{-1} at mean

temperature 40 ℃ (i.e., the upper and lower plate's temperature was 50 ℃ and 30 ℃, respectively). This due to paraffin's low thermal conductivity properties, which resulted in slow charging and discharging air (Hunger et al. 2009; Jayalath et al. 2016).

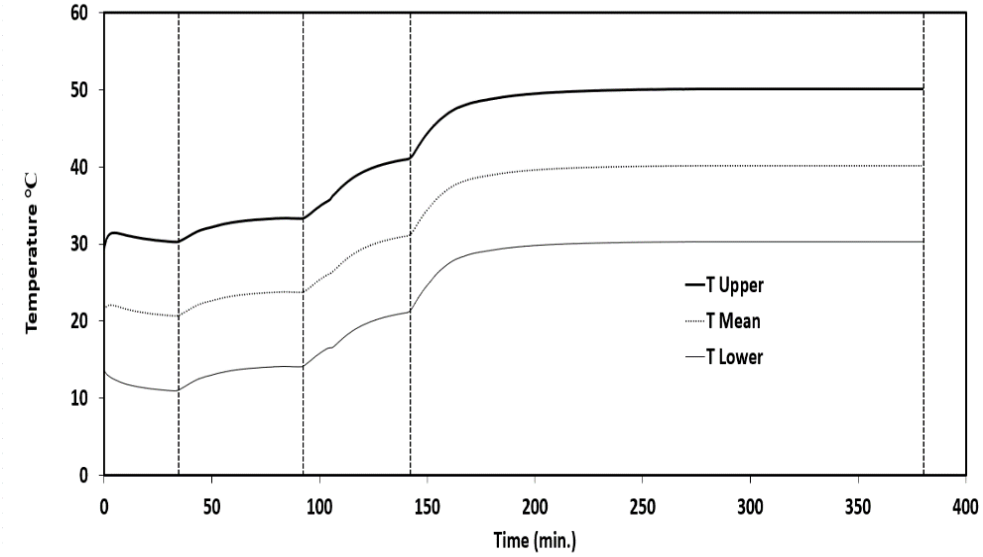

Fig 5.13 Temperature of Upper and lower plate

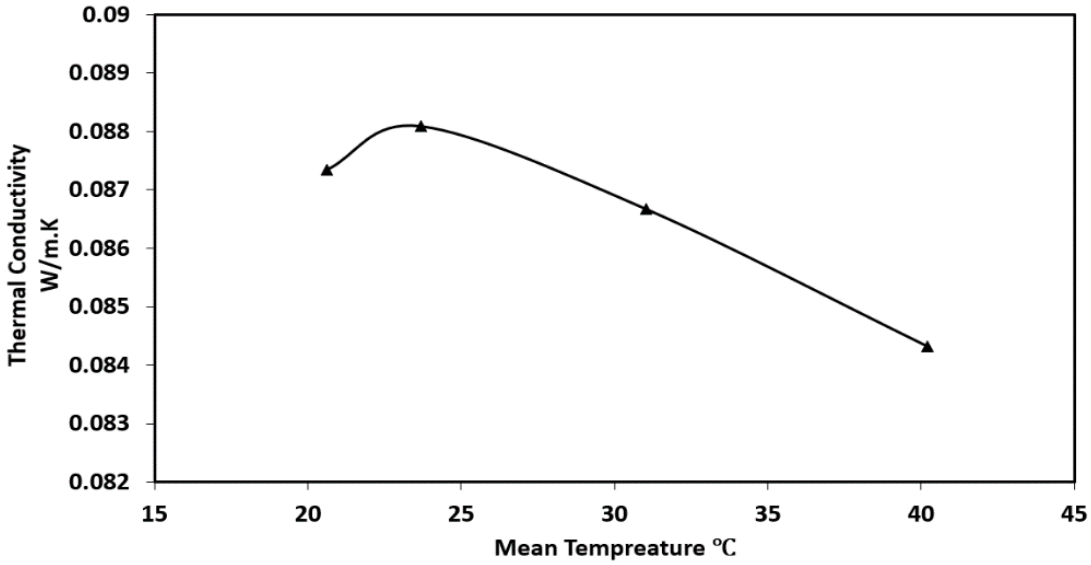

Fig 5.14 Thermal conductivity of MPCMs Sheet at various mean temperatures

Chapter 6 CONCLUSIONS

6.1 Conclusions

- Incorporating Limestone filler in SCM enhanced the flowability when the percentage and size of limestone increased. This improvement in workability was due to replacing LF some of the water inside the voids, which further reduced the internal friction.
- The physical effect and chemical effect of LF improved the early age of hydration and mechanical properties of mortar made with LF sand and cement replacement. This is due to the acceleration effect of LF and the formation of calcium monocarboaluminate, which fills the pores between cement particles. However, the improvement in the mechanical properties was diminished at 28 days for mortar made with LF as cement replacement due to the dilution effect.
- Increasing the percentage of MPCMs increase the viscosity of SCM. This is due to the reduction of free water in the presence of fine particles.
- Limestone filler enhanced the cement-based chemical and physical characteristics and fill the voids between sand and cement particles, decreasing pores volume in the SCM.
- Incorporating LF and MPCMs with smaller sizes stimulates cement hydration and improves the space-filling properties compare to the control mix.
- The amount of the C-S-H gel and CH increased with the increased content of phase change material. This is due to the small size of the PCM particles and LF, which stimulate the hydration reaction and CH content.
- MPCMs dosage affects the mechanical properties of SCM. On the other hand, adding LF enhances the mechanical properties of SCM made with MPCMs. Replacing 15% of sand

with LF and 3% of MPCMs significantly increased compressive strength at all ages by 7% compared to the control mix

- The addition of LF and MPCMs tends to increase shrinkage. The increase of shrinkage can be related to the LF effect on accelerating the hydration or formation carboaluimate at an early age, which increased the volume of cement gel. Moreover, replacing stiff inclusion, such as sand with compliant inclusion, as MPCMs into the mix, caused an increase in shrinkage.
- Incorporating MPCMs significantly improves the thermal performance of mortar. This is due to the increase in the thermal mass and the thermal insulation improvement.
- Incorporating MPCMs into mortar resulted in a reduction in thermal conductivity. This is due to the low thermal conductivity of the MPCMs compared to sand and their ability to increase the amount of the entrapped air.
- The MPCMs sheet is caple to hold temperature above 40 ℃ for more than 7 hrs. Thus, the MPCMs sheet's heat storage capacity is sufficient to conserve energy consumption in different applications.
- Specimens covered with MPCMs sheet during the cooling down period exhibited a slower temperature drop rate. This extended the curing period at high temperatures for more than 13 hours to reach the ambient temperature compared to 5 hrs for uncovered specimens. Thus, they exhibited higher compressive strength and hydration products' formation than those exposed to a shorter holding period.
- Heat curing mortar with 6% of MPCM 43 when the champer's temperature reached the MPCMs melting point (i.e. 41- 45℃). The heating curve showed a slight change in the slope associated with a delay in raising the temperature. During the cooling period, the

curve showed a change in the slope, resulted in a slight delay in the cooling down period. Results showed a reduction in the mechanical properties compared to the control mix. The reduction in compressive strength can be attributed to the soft nature of the MPCMs compared with hard particles of sand, which can not sustain loads, and capsules act as a void.

References

Abhat, A. 1983a. “Low Temperature Latent Heat Thermal Energy Storage: Heat Storage Materials.” *Solar Energy* 30 (4): 313–32.

———. 1983b. “Low Temperature Latent Heat Thermal Energy Storage: Heat Storage Materials.” *Solar Energy* 30 (4): 313–32.

Adams, Lawrence D., and Ronald M. Race. 1990. “Effect of Limestone Additions upon Drying Shrinkage of Portland Cement Mortar.” In *Carbonate Additions to Cement*. ASTM International.

Ahamed, Riyaz, K. A. Pradeep, and M. Plan. 2015. “Experimental Study on Self-Curing Concrete Using Sodium Lignosulphonate.” *Int. J. Emerg. Technol. Eng* 2 (4): 74–78.

Aïtcin, Pierre-Claude. 2011. *High Performance Concrete*. CRC press.

Aïtcin, Pierre-Claude, and P. Kumar Mehta. 1990. “Effect of Coarse Aggregate Characteristics on Mechanical Properties of High-Strength Concrete.” *Materials Journal* 87 (2): 103–7.

Aqel, Mohammad A. 2016. “Steam Cured Self-Consolidating Concrete and the Effects of Limestone Filler.”

Baetens, Ruben, Bjørn Petter Jelle, and Arild Gustavsen. 2010. “Phase Change Materials for Building Applications: A State-of-the-Art Review.” *Energy and Buildings* 42 (9): 1361–68. https://doi.org/10.1016/j.enbuild.2010.03.026.

Benabed, Benchaa, El-Hadj Kadri, Lakhdar Azzouz, and Said Kenai. 2012. “Properties of Self-Compacting Mortar Made with Various Types of Sand.” *Cement and Concrete Composites* 34 (10): 1167–73.

Benachour, Y., Catherine A. Davy, Frédéric Skoczylas, and H. Houari. 2008. “Effect of a High Calcite Filler Addition upon Microstructural, Mechanical, Shrinkage and Transport Properties of a Mortar.” *Cement and Concrete Research* 38 (6): 727–36.

Bentz, Dale P., Ahmad Ardani, Tim Barrett, Scott Z. Jones, Didier Lootens, Max A. Peltz, Taijiro Sato, Paul E. Stutzman, Jussara Tanesi, and W. Jason Weiss. 2015. "Multi-Scale Investigation of the Performance of Limestone in Concrete." *Construction and Building Materials* 75: 1–10.

Berodier, ESKSG, and KJJotACS Scrivener. 2014. "Understanding the Filler Effect on the Nucleation and Growth of C-S-H." *Journal of the American Ceramic Society* 97 (12): 3764–73.

Bertrandy, R., and J. L. Chabernaud. 1971. "Study of the Influence of Calcareous Fillers on Concrete." *Travaux* 437: 38–52.

Billberg, Peter. 1999. "Fine Mortar Rheology in Mix Design of SCC." In *Proceedings of the First International RILEM Symposium on Self-Compacting Concrete, Edited by Å. Skarendahl and Ö. Petersson, Stockholm*, 47–58.

Bonavetti, V. L., and E. F. Irassar. 1994. "The Effect of Stone Dust Content in Sand." *Cement and Concrete Research* 24 (3): 580–90.

Bosiljkov, Violeta Bokan. 2003. "SCC Mixes with Poorly Graded Aggregate and High Volume of Limestone Filler." *Cement and Concrete Research* 33 (9): 1279–86.

Boyd, Andrew J., Sidney Mindess, and Jan P. Skalny. 2002. *Materials Science of Concrete: Cement and Concrete-Trends and Challenges*. Vol. 56. Wiley-American Ceramic Society.

Brutschin, Elina, and Andreas Fleig. 2016. "Innovation in the Energy Sector–The Role of Fossil Fuels and Developing Economies." *Energy Policy* 97: 27–38.

Bullard, Jeffrey W., Hamlin M. Jennings, Richard A. Livingston, Andre Nonat, George W. Scherer, Jeffrey S. Schweitzer, Karen L. Scrivener, and Jeffrey J. Thomas. 2011. "Mechanisms of Cement Hydration." *Cement and Concrete Research* 41 (12): 1208–23.

Cabeza, Luisa F. 2008. *Heat And Cold Storage With PCM: An Up To Date Introduction Into Basics And Applications. Heat and Mass Transfer*. Springer.

Camiletti, J., A. M. Soliman, and M. L. Nehdi. 2013. "Effects of Nano-and Micro-Limestone Addition on Early-Age Properties of Ultra-High-Performance Concrete." *Materials and Structures* 46 (6): 881–98.

Castell, A., I. Martorell, M. Medrano, G. Pérez, and L. F. Cabeza. 2010. "Experimental Study of Using PCM in Brick Constructive Solutions for Passive Cooling." *Energy and Buildings* 42 (4): 534–40. https://doi.org/10.1016/j.enbuild.2009.10.022.

Chang, Xu, Cheng-Kui Huang, and Ya-Juan Chen. 2009. "Mechanical Performance of Eccentrically Loaded Pre-Stressing Concrete Filled Circular Steel Tube Columns by Means of Expansive Cement." *Engineering Structures* 31 (11): 2588–97.

Chatterji, S., and J. W. Jeffery. 1966. "The Volume Expansion of Hardened Cement Paste Due to the Presence of 'Dead-Burnt' CaO." *Magazine of Concrete Research* 18 (55): 65–68.

Chatterji, S. t, and J. W. Jeffery. 1963. "A New Hypothesis of Sulphate Expansion." *Magazine of Concrete Research* 15 (44): 83–86.

Chen, Bing, and Juanyu Liu. 2008. "Damage in Carbon Fiber-Reinforced Concrete, Monitored by Both Electrical Resistance Measurement and Acoustic Emission Analysis." *Construction and Building Materials* 22 (11): 2196–2201.

Chen, J. J., A. K. H. Kwan, and Y. Jiang. 2014. “Adding Limestone Fines as Cement Paste Replacement to Reduce Water Permeability and Sorptivity of Concrete.” *Construction and Building Materials* 56: 87–93.

Chi, C., Y. Wu, and C. Riefler. 2004. “The Use of Crushed Dust Production of Selfconsolidating Concrete (SCC).” *Recycling Concrete and Other Materials for Sustainable Development, ACI International SP-219*.

Costoya Fernández, Maria Mercedes. 2008. “Effect of Particle Size on the Hydration Kinetics and Microstructural Development of Tricalcium Silicate.” EPFL.

Cui, Yaping, Jingchao Xie, Jiaping Liu, and Song Pan. 2015. “Review of Phase Change Materials Integrated in Building Walls for Energy Saving.” *Procedia Engineering* 121: 763–70.

Cusson, D., Z. Lounis, and L. Daigle. 2010. “Benefits of Internal Curing on Service Life and Life-Cycle Cost of High-Performance Concrete Bridge Decks–A Case Study.” *Cement and Concrete Composites* 32 (5): 339–50.

De Schutter, Geert. 2011. “Effect of Limestone Filler as Mineral Addition in Self-Compacting Concrete.” In *36th Conference on Our World in Concrete & Structures:’Recent Advances in the Technology of Fesh Concrete’(OWIC’S 2011)*, 49–54. Ghent University, Department of Structural engineering.

De Weerdt, K., M. Ben Haha, G. Le Saout, K. O. Kjellsen, H. Justnes, and B. Lothenbach. 2012. “The Effect of Temperature on the Hydration of Composite Cements Containing Limestone Powder and Fly Ash.” *Materials and Structures* 45 (7): 1101–14.

Domone, P. L., and J. Jin. 1999. “Properties of Mortar for Self-Compacting Concrete.” In *PRO 7: 1st International RILEM Symposium on Self-Compacting Concrete*, 7:107. RILEM Publications.

Donza, H., O. Cabrera, and E. F. Irassar. 2002. “High-Strength Concrete with Different Fine Aggregate.” *Cement and Concrete Research* 32 (11): 1755–61.

Donza, H., M. Gonzalez, and O. Cabrera. 1999. “Influence of Fine Aggregate Mineralogy on Mechanical Properties in High Strength Concrete.” In *Second International Conference on High Performance Concrete, Gramado, Brazil*.

Drissi, Sarra, Anissa Eddhahak-Ouni, Sabine Caré, and Jamel Néji. 2014. “Effect of Phase Change Materials (PCMs) on the Hydration Reaction and Kinetic of PCM-Mortars.” In *Materials for Energy & Environment International Conference and Exhibition (MEET Tunisia 2014)*.

EFNARC, Specification. 2002. “Guidelines for Self-Compacting Concrete.” *London, UK: Association House* 32: 34.

Erdem, Tahir Kemal, Kamal H. Khayat, and Ammar Yahia. 2009. “Correlating Rheology of Self-Consolidating Concrete to Corresponding Concrete-Equivalent Mortar.” *ACI Materials Journal* 106 (2): 154.

Escadeillas, Gilles, Jean-Emmanuel Aubert, Maximiliano Segerer, and William Prince. 2007. “Some Factors Affecting Delayed Ettringite Formation in Heat-Cured Mortars.” *Cement and Concrete Research* 37 (10): 1445–52.

Esping, Oskar. 2008. “Effect of Limestone Filler BET (H2O)-Area on the Fresh and Hardened Properties of Self-Compacting Concrete.” *Cement and Concrete Research* 38 (7): 938–44.

Eura, S., Y. Yamazaki, and T. Monji. 1975. “Influence of Initial Drying on the Change of Length of Mortar with Expansive Admixture.” In *CAJ Review of the 29th General Meeting*, 29:428–31.

Ezziane, K., E. H. Kadri, A. Hallal, and R. Duval. 2010. “Effect of Mineral Additives on the Setting of Blended Cement by the Maturity Method.” *Materials and Structures* 43 (3): 393–401.

Felekoğlu, Burak. 2008. “A Comparative Study on the Performance of Sands Rich and Poor in Fines in Self-Compacting Concrete.” *Construction and Building Materials* 22 (4): 646–54.

Felekoğlu, Burak, Kamile Tosun, Bülent Baradan, Akın Altun, and Bahadır Uyulgan. 2006. “The Effect of Fly Ash and Limestone Fillers on the Viscosity and Compressive Strength of Self-Compacting Repair Mortars.” *Cement and Concrete Research* 36 (9): 1719–26.

Fernandes, Fabio, Shilpa Manari, Mathew Aguayo, Kevin Santos, Tandre Oey, Zhenhua Wei, Gabriel Falzone, Narayanan Neithalath, and Gaurav Sant. 2014. “On the Feasibility of Using Phase Change Materials (PCMs) to Mitigate Thermal Cracking in Cementitious Materials.” *Cement and Concrete Composites* 51 (August): 14–26. https://doi.org/10.1016/j.cemconcomp.2014.03.003.

Frigione, Mariaenrica, Mariateresa Lettieri, and Antonella Sarcinella. 2019. “Phase Change Materials for Energy Efficiency in Buildings and Their Use in Mortars.” *Materials* 12 (8): 1260. https://doi.org/10.3390/ma12081260.

Fujiwara, Hiromi, Shigeyoshi Nagataki, Nobuaki Otsuki, and Hideki Endo. 1996. “Study on Reducing Unit Powder Content of High-Fluidity Concrete by Controlling Powder Particle Size Distribution.” *Concrete Library of JSCE* 28: 117–28.

Gambhir, Murari Lal. 2013. *Concrete Technology: Theory and Practice*. Tata McGraw-Hill Education.

Gandhi, Mukesh V., and B. D. Thompson. 1992. *Smart Materials and Structures*. Springer Science & Business Media.

Ghorpade, Vaishali G., Koneru Venkata Subash, and Lam Chaitanya Anand Kumar. 2015. "Development of Mix Proportions for Different Grades of Metakaolin Based Self-Compacting Concrete." In *Advances in Structural Engineering*, 1733–45. Springer.

Gjorv, Odd E., and Koji Sakai. 1999. *Concrete Technology for a Sustainable Development in the 21st Century*. CRC Press.

Gosselin, Clément, Romain Duballet, Ph Roux, Nadja Gaudillière, Justin Dirrenberger, and Ph Morel. 2016. "Large-Scale 3D Printing of Ultra-High Performance Concrete–a New Processing Route for Architects and Builders." *Materials & Design* 100: 102–9.

Gunnelius, K. R., T. C. Lundin, J. B. Rosenholm, and J. Peltonen. 2014. "Rheological Characterization of Cement Pastes with Functional Filler Particles." *Cement and Concrete Research* 65: 1–7.

Gupta, Sumit, Jesus G. Gonzalez, and Kenneth J. Loh. 2017. "Self-Sensing Concrete Enabled by Nano-Engineered Cement-Aggregate Interfaces." *Structural Health Monitoring* 16 (3): 309–23.

Han, Baoguo, Yunyang Wang, Siqi Ding, Xun Yu, Liqing Zhang, Zhen Li, and Jinping Ou. 2017. "Self-Sensing Cementitious Composites Incorporated with Botryoid Hybrid Nano-Carbon Materials for Smart Infrastructures." *Journal of Intelligent Material Systems and Structures* 28 (6): 699–727.

Han, Baoguo, Yunyang Wang, Sufen Dong, Liqing Zhang, Siqi Ding, Xun Yu, and Jinping Ou. 2015. “Smart Concretes and Structures: A Review.” *Journal of Intelligent Material Systems and Structures* 26 (11): 1303–45.

Han, Baoguo, Liqing Zhang, and Jinping Ou. 2017a. “General Introduction of Smart and Multifunctional Concrete.” In *Smart and Multifunctional Concrete Toward Sustainable Infrastructures*, 1–9. Springer.

———. 2017b. “Self-Curing Concrete.” In *Smart and Multifunctional Concrete Toward Sustainable Infrastructures*, 55–66. Springer.

———. 2017c. “Self-Curing Concrete.” In *Smart and Multifunctional Concrete Toward Sustainable Infrastructures*, 55–66. Springer.

———. 2017d. “Self-Expanding Concrete.” In *Smart and Multifunctional Concrete Toward Sustainable Infrastructures*, 37–53. Springer.

———. 2017e. “Self-Shaping Concrete.” In *Smart and Multifunctional Concrete Toward Sustainable Infrastructures*, 67–80. Springer.

Hasnain, S. M. 1998. “Review on Sustainable Thermal Energy Storage Technologies, Part I: Heat Storage Materials and Techniques.” *Energy Conversion and Management* 39 (11): 1127–38.

Hawes, D. W., D. Banu, and D. Feldman. 1992. “The Stability of Phase Change Materials in Concrete.” *Solar Energy Materials and Solar Cells* 27 (2): 103–18.

Hawkins, Peter, Paul D. Tennis, and Rachel Jean Detwiler. 1996. *The Use of Limestone in Portland Cement: A State-of-the-Art Review*. Portland Cement Association.

Heikal, M., H. El-Didamony, and M. S. Morsy. 2000. “Limestone-Filled Pozzolanic Cement.” *Cement and Concrete Research* 30 (11): 1827–34.

Heritage, Ian, Fouad M. Khalaf, and John G. Wilson. 2000. “Thermal Acceleration of Portland Cement Concretes Using Direct Electronic Curing.” *Materials Journal* 97 (1): 37–40.

Hooton, R. D., M. Nokken, and M. D. A. Thomas. 2007. “Portland-Limestone Cement: State-of-the-Art Report and Gap Analysis for CSA A 3000.” *Report Prepared for St. Lawrence Cement*.

Hossain, Md, Altynay Zhumabekova, Suvash Chandra Paul, and Jong Ryeol Kim. 2020. “A Review of 3D Printing in Construction and Its Impact on the Labor Market.” *Sustainability* 12 (20): 8492.

Hunger, M., A. G. Entrop, I. Mandilaras, H. J. H. Brouwers, and M. Founti. 2009. “The Behavior of Self-Compacting Concrete Containing Micro-Encapsulated Phase Change Materials.” *Cement and Concrete Composites* 31 (10): 731–43.

Hwang, Soo-Duck, Rami Khatib, Hoi Keun Lee, Seung-Hoon Lee, and Kamal H. Khayat. 2012. “Optimization of Steam-Curing Regime for High-Strength, Self-Consolidating Concrete for Precast, Prestressed Concrete Applications.” *PCI Journal* 57 (3): 48.

Iida, Hideo. 1976. *Prestressed Concrete Pipe*. Google Patents.

Irassar, E. F. 2009. “Sulfate Attack on Cementitious Materials Containing Limestone Filler—A Review.” *Cement and Concrete Research* 39 (3): 241–54.

Isogai, J. 1975. “Long Term Properties of Hardened Concrete of (3CaO+ 3A1 2 O 3 CaSO 4–CaSO 4–CaO) Series Expansive Cement.” *Cem. Tech. Ann. Rep* 29: 126–30.

Jayalath, Amitha, Rackel San Nicolas, Massoud Sofi, Robert Shanks, Tuan Ngo, Lu Aye, and Priyan Mendis. 2016. “Properties of Cementitious Mortar and Concrete Containing Micro-Encapsulated Phase Change Materials.” *Construction and Building Materials* 120: 408–17.

Jensen, Ole Mejlhede, and Per Freiesleben Hansen. 2001. “Water-Entrained Cement-Based Materials: I. Principles and Theoretical Background.” *Cement and Concrete Research* 31 (4): 647–54.

Jeon, Jisoo, Jung-Hun Lee, Jungki Seo, Su-Gwang Jeong, and Sumin Kim. 2013. “Application of PCM Thermal Energy Storage System to Reduce Building Energy Consumption.” *Journal of Thermal Analysis and Calorimetry* 111 (1): 279–88.

Juilland, Patrick, Emmanuel Gallucci, Robert Flatt, and Karen Scrivener. 2010. “Dissolution Theory Applied to the Induction Period in Alite Hydration.” *Cement and Concrete Research* 40 (6): 831–44.

Kang, Sung-Hoon, Yeonung Jeong, Kiang Hwee Tan, and Juhyuk Moon. 2019. “High-Volume Use of Limestone in Ultra-High Performance Fiber-Reinforced Concrete for Reducing Cement Content and Autogenous Shrinkage.” *Construction and Building Materials* 213: 292–305.

Kara, Y. A., A. Kurnucß, and C. Arslanturk. 2009. “Solar Energy Storage in Building Structure for Solar Space Heating.” In *SET2009–8th International Conference on Sustainable Energy Technologies, Aachen, Germany*.

Kenai, S., B. Menadi, and M. Ghrici. 2006. “Performance of Limestone Cement Mortar.” In *Eight CANMET/ACI International Conference on Recent Advances in Concrete Technology*, 39.

Kenai, Said, Wolé Soboyejo, and Alfred Soboyejo. 2004. “Some Engineering Properties of Limestone Concrete.” *Materials and Manufacturing Processes* 19 (5): 949–61.

Kesler, Clyde E., and Donald W. Pfeifer. 1970. *Expansive Cement Concretes-Present State of Knowledge*.

Khadiran, Tumirah, Mohd Zobir Hussein, Zulkarnain Zainal, and Rafeadah Rusli. 2016. "Advanced Energy Storage Materials for Building Applications and Their Thermal Performance Characterization: A Review." *Renewable and Sustainable Energy Reviews* 57: 916–28.

Khudhair, Amar M., and Mohammed M. Farid. 2004. "A Review on Energy Conservation in Building Applications with Thermal Storage by Latent Heat Using Phase Change Materials." *Energy Conversion and Management* 45 (2): 263–75.

Kim, Hyeong-Ki. 2015. "Chloride Penetration Monitoring in Reinforced Concrete Structure Using Carbon Nanotube/Cement Composite." *Construction and Building Materials* 96: 29–36.

Knop, Yaniv, Alva Peled, and Ronen Cohen. 2014. "Influences of Limestone Particle Size Distributions and Contents on Blended Cement Properties." *Construction and Building Materials* 71: 26–34.

Kreston, Max S. 1970. *Method of Manufacturing Self-Stressed Concrete Pipe*. Google Patents.

Lane, George A. 1983a. "Solar Heat Storage: Latent Heat Materials."

———. 1983b. "Solar Heat Storage: Latent Heat Materials."

Lawrence, Philippe, Martin Cyr, and Erick Ringot. 2003. "Mineral Admixtures in Mortars: Effect of Inert Materials on Short-Term Hydration." *Cement and Concrete Research* 33 (12): 1939–47.

Le Saoût, Gwenn, Barbara Lothenbach, Akihiro Hori, Takayuki Higuchi, and Frank Winnefeld. 2013. "Hydration of Portland Cement with Additions of Calcium Sulfoaluminates." *Cement and Concrete Research* 43: 81–94.

Li, Ming, Yujia Yang, Meng Liu, Xiaoyang Guo, and Song Zhou. 2015. "Hybrid Effect of Calcium Carbonate Whisker and Carbon Fiber on the Mechanical Properties and Microstructure of Oil Well Cement." *Construction and Building Materials* 93: 995–1002.

Lim, Sungwoo, Richard A. Buswell, Thanh T. Le, Simon A. Austin, Alistair GF Gibb, and Tony Thorpe. 2012. "Developments in Construction-Scale Additive Manufacturing Processes." *Automation in Construction* 21: 262–68.

Lin, Feng, and Christian Meyer. 2009. "Hydration Kinetics Modeling of Portland Cement Considering the Effects of Curing Temperature and Applied Pressure." *Cement and Concrete Research* 39 (4): 255–65.

Lin, Shu-Kun. 1999. *Modern Thermodynamics: From Heat Engines to Dissipative Structures.* Molecular Diversity Preservation International.

Liu, Shuhua, Lihua Li, Meijuan Rao, and Zhiyang Gao. 2012. "Effect of Limestone Powder on Microstructure and Strength of Ultra High Performance Cement-Based Materials." *Advanced Science Letters* 15 (1): 475–79.

Lothenbach, Barbara, Gwenn Le Saout, Emmanuel Gallucci, and Karen Scrivener. 2008a. "Influence of Limestone on the Hydration of Portland Cements." *Cement and Concrete Research* 38 (6): 848–60.

———. 2008b. "Influence of Limestone on the Hydration of Portland Cements." *Cement and Concrete Research* 38 (6): 848–60.

Lu, Shilei, Yiran Li, Xiangfei Kong, Bo Pang, Yafei Chen, Shaoqun Zheng, and Linwei Sun. 2017. "A Review of PCM Energy Storage Technology Used in Buildings for the Global Warming Solution." In *Energy Solutions to Combat Global Warming*, 611–44. Springer.

Lucas, S. S., V. M. Ferreira, and JL Barroso De Aguiar. 2013. “Latent Heat Storage in PCM Containing Mortars—Study of Microstructural Modifications.” *Energy and Buildings* 66: 724–31.

Lucas, S., L. Senff, V. M. Ferreira, JL Barroso De Aguiar, and J. A. Labrincha. 2010. “Fresh State Characterization of Lime Mortars with PCM Additions.” *Applied Rheology* 20 (6).

Luo, Fu Jia, Li He, Zhu Pan, Wen Hui Duan, Xiao Ling Zhao, and Frank Collins. 2013. “Effect of Very Fine Particles on Workability and Strength of Concrete Made with Dune Sand.” *Construction and Building Materials* 47: 131–37.

Malhotra, V. M., and G. G. Carette. 1985. “Performance of Concrete Incorporating Limestone Dust as Partial Replacement for Sand.” In *Journal Proceedings*, 82:363–71.

Malier, Yves. 1992. *High Performance Concrete: From Material to Structure*. CRC Press.

Manual, Highway Design. 2002. *New York State Department of Transportation*. April.

Marland, G., T. A. Boden, and R. J. Andres. 2003. “Global, Regional, and National CO2 Emissions in Trends: A Compendium of Data on Global Change.” *Carbon Dioxide Information Analysis Center, Oak Ridge National Laboratory, US Department of Energy, Oak Ridge, TN*.

Martinelli, Enzo, Eduardus AB Koenders, and Antonio Caggiano. 2013. “A Numerical Recipe for Modelling Hydration and Heat Flow in Hardening Concrete.” *Cement and Concrete Composites* 40: 48–58.

Materials, American Society for Testing and. 2017. *Standard Test Method for Steady-State Thermal Transmission Properties by Means of the Heat Flow Meter Apparatus*. ASTM International.

Mehta, P. Kumar, and Paulo JM Monteiro. 2014. *Concrete: Microstructure, Properties, and Materials*. McGraw-Hill Education.

Mehta, Povindar Kumar. 1973. "Mechanism of Expansion Associated with Ettringite Formation." *Cement and Concrete Research* 3 (1): 1–6.

Mizuma, Katsuhisa. 1972. *Steel Wire Cage Wire for Chemically Prestressed Concrete Pipe*. Google Patents.

Moosberg-Bustnes, Helena, Björn Lagerblad, and Eric Forssberg. 2004. "The Function of Fillers in Concrete." *Materials and Structures* 37 (2): 74.

Nagataki, S., and H. Gomi. 1998. "Expansive Admixtures (Mainly Ettringite)." *Cement and Concrete Composites* 20 (2–3): 163–70.

Naik, Tarun R., Rudolph N. Kraus, Yoon-moon Chun, Fethullah Canpolat, and Bruce W. Ramme. 2005. "Use of Limestone Quarry By-Products for Developing Economical Self-Compacting Concrete." In *Published at the CANMET/ACI International Symposium on Sustainable Developments of Cement and Concrete, Toronto, Canada*.

Nehdi, Moncef, Sidney Mindess, and Pierre-Claude Aïtcin. 1996. "Optimization of High Strength Limestone Filler Cement Mortars." *Cement and Concrete Research* 26 (6): 883–93.

Newman, John, and Ban Seng Choo. 2003. *Advanced Concrete Technology Set*. Elsevier.

Nguyen, Van-Huong, Nordine Leklou, Jean-Emmanuel Aubert, and Pierre Mounanga. 2013. "The Effect of Natural Pozzolan on Delayed Ettringite Formation of the Heat-Cured Mortars." *Construction and Building Materials* 48: 479–84.

Nishibayashi, S., A. Yoshino, S. Inoue, and T. Kuroda. 2004. “Effect of Properties of Mix Constituents on Rheological Constants of Self-Compacting Concrete.” In *Production Methods and Workability of Concrete*, 267–74. CRC Press.

Nonnet, Emmanuel, Nicolas Lequeux, and Philippe Boch. 1999. “Elastic Properties of High Alumina Cement Castables from Room Temperature to 1600 C.” *Journal of the European Ceramic Society* 19 (8): 1575–83.

Noumowe, Albert. 1995. “Effet de Hautes Températures (20-600° C) Sur Le Béton: Cas Particulier Du Béton a Hautes Performances.” Lyon, INSA.

Okamuara, H., and M. Ouchi. 1999. “Self-Compacting Concrete-Development, Present and Future.” In *FIRST INTERNATIONAL RILEM SYMPOSIUM ON SELF-COMPACTING CONCRETE. Sweden*, 3–14.

Okushima, Masaichi. 1968. “Development of Expansive Cement with Calcium Sulphoaluminous Cement Clinker.” In *Proc. of the 5th Inter. Symp. on the Chem. of Cement*, 419–38.

Pacheco-Torgal, Fernando, S. Jalali, Joao Labrincha, and V. M. John. 2013. *Eco-Efficient Concrete*. Elsevier.

Pasupathy, A_, R. Velraj, and R. V. Seeniraj. 2008. “Phase Change Material-Based Building Architecture for Thermal Management in Residential and Commercial Establishments.” *Renewable and Sustainable Energy Reviews* 12 (1): 39–64.

Perrot, Arnaud, Damien Rangeard, and Alexandre Pierre. 2016. “Structural Built-up of Cement-Based Materials Used for 3D-Printing Extrusion Techniques.” *Materials and Structures* 49 (4): 1213–20.

Poitevin, P. 1999. “Limestone Aggregate Concrete, Usefulness and Durability.” *Cement and Concrete Composites* 21 (2): 89–97.

Pomianowski, Michal, Per Heiselberg, and Yinping Zhang. 2013. “Review of Thermal Energy Storage Technologies Based on PCM Application in Buildings.” *Energy and Buildings* 67 (December): 56–69. https://doi.org/10.1016/j.enbuild.2013.08.006.

Ramachandran, Vangipuram Seshachar, Peter J. Sereda, and R. F. Feldman. 1964. “Mechanism of Hydration of Calcium Oxide.” *Nature* 201 (4916): 288–89.

Ramirez, J. L., J. M. Barcena, and J. I. Urreta. 1987. “Sables Calcaires à Fines Calcaires et Argileuses: Influence et Nocivité Dans Les Mortiers de Ciment.” *Materials and Structures* 20 (3): 202–13.

———. 1990. “Proposal for Limitation and Control of Fines in Calcareous Sands Based upon Their Influence in Some Concrete Properties.” *Materials and Structures* 23 (4): 277–88.

Regin, A. Felix, S. C. Solanki, and J. S. Saini. 2008. “Heat Transfer Characteristics of Thermal Energy Storage System Using PCM Capsules: A Review.” *Renewable and Sustainable Energy Reviews* 12 (9): 2438–58.

Richardson, Alan, Ashraf Heniegal, and Jess Tindall. 2017. “Optimal Performance Characteristics of Mortar Incorporating Phase Change Materials and Silica Fume.” *Journal of Green Building* 12 (2): 59–78.

Saafi, Mohamed. 2009. “Wireless and Embedded Carbon Nanotube Networks for Damage Detection in Concrete Structures.” *Nanotechnology* 20 (39): 395502.

Saafi, Mohamed, Kelly Andrew, Pik Leung Tang, David McGhon, Steven Taylor, Mahubur Rahman, Shangtong Yang, and Xiangming Zhou. 2013. “Multifunctional Properties of Carbon Nanotube/Fly Ash Geopolymeric Nanocomposites.” *Construction and Building Materials* 49: 46–55.

Sanfelix, Susana G., Isabel Santacruz, Anna M. Szczotok, Luis Miguel O. Belloc, G. Angeles, and Anna-Lena Kjøniksen. 2019. “Effect of Microencapsulated Phase Change Materials on the Flow Behavior of Cement Composites.” *Construction and Building Materials* 202: 353–62.

Šavija, Branko. 2018. “Smart Crack Control in Concrete through Use of Phase Change Materials (PCMs): A Review.” *Materials* 11 (5): 654.

Schneider, Eric D., and James J. Kay. 1995. “Order from Disorder: The Thermodynamics of Complexity in Biology.” *What Is Life? The next Fifty Years: Speculations on the Future of Biology*, 161–72.

Schossig, P., H.-M. Henning, S. Gschwander, and T. Haussmann. 2005. “Micro-Encapsulated Phase-Change Materials Integrated into Construction Materials.” *Solar Energy Materials and Solar Cells* 89 (2–3): 297–306.

Schwartz, Mel. 2008. *Smart Materials*. CRC press.

Scrivener, Karen Louise. 1984. “The Development of Microstructure during the Hydration of Portland Cement.”

Sha, WEAZ, E. A. O’Neill, and Z. Guo. 1999. “Differential Scanning Calorimetry Study of Ordinary Portland Cement.” *Cement and Concrete Research* 29 (9): 1487–89.

Soares, Nelson Miguel Lopes. 2016. “Thermal Energy Storage with Phase Change Materials (PCMs) for the Improvement of the Energy Performance of Buildings.”

Taylor, H. F. W., C. Famy, and K. L. Scrivener. 2001. “Delayed Ettringite Formation.” *Cement and Concrete Research* 31 (5): 683–93.

Telkes, MARIA. 1975. “Thermal Storage for Solar Heating and Cooling.” In *Proceedings of the Workshop on Solar Energy Storage Subsystems for the Heating and Cooling of Buildings, Charlottesville (Virginia, USA)*.

Tennis, P. D., M. D. A. Thomas, and W. J. Weiss. 2011. “State-of-the-Art Report on Use of Limestone in Cements at Levels of up to 15%.” *PCA R&D SN3148, Portland Cement Association, Skokie, IL*.

Transportation (WSDOT), Washington State Dept of. 2010. “Annual Traffic Report.”

Trauchessec, Romain, J.-M. Mechling, André Lecomte, A. Roux, and B. Le Rolland. 2015. “Hydration of Ordinary Portland Cement and Calcium Sulfoaluminate Cement Blends.” *Cement and Concrete Composites* 56: 106–14.

Tyagi, V. V., S. C. Kaushik, S. K. Tyagi, and T. Akiyama. 2011. “Development of Phase Change Materials Based Microencapsulated Technology for Buildings: A Review.” *Renewable and Sustainable Energy Reviews* 15 (2): 1373–91.

Valcuende, M., E. Marco, C. Parra, and P. Serna. 2012. “Influence of Limestone Filler and Viscosity-Modifying Admixture on the Shrinkage of Self-Compacting Concrete.” *Cement and Concrete Research* 42 (4): 583–92.

Van Breugel, Klaas. 1993. “Simulation of Hydration and Formation of Structure in Hardening Cement-Based Materials.”

Vance, Kirk, Aditya Kumar, Gaurav Sant, and Narayanan Neithalath. 2013. “The Rheological Properties of Ternary Binders Containing Portland Cement, Limestone, and Metakaolin or Fly Ash.” *Cement and Concrete Research* 52: 196–207.

Villarreal, Victor H., and David A. Crocker. 2007. “Better Pavements through Internal Hydration.” *Concrete International* 29 (2): 32–36.

Von Paumgartten, Paul. 2003. “The Business Case for High Performance Green Buildings: Sustainability and Its Financial Impact.” *Journal of Facilities Management*.

Waqas, Adeel, and Zia Ud Din. 2013. “Phase Change Material (PCM) Storage for Free Cooling of Buildings—A Review.” *Renewable and Sustainable Energy Reviews* 18 (February): 607–25. https://doi.org/10.1016/j.rser.2012.10.034.

Wei, Zhenhua, Gabriel Falzone, Bu Wang, Alexander Thiele, Guillermo Puerta-Falla, Laurent Pilon, Narayanan Neithalath, and Gaurav Sant. 2017. “The Durability of Cementitious Composites Containing Microencapsulated Phase Change Materials.” *Cement and Concrete Composites* 81: 66–76.

Whitman, Catherine A., Michel B. Johnson, and Mary Anne White. 2012. “Characterization of Thermal Performance of a Solid–Solid Phase Change Material, Di-n-Hexylammonium Bromide, for Potential Integration in Building Materials.” *Thermochimica Acta* 531: 54–59.

Wu, Z. W., and H. Z. Zhang. 1990. “Expansive Concrete.” *China Railway Publishing House* 248: 17–18.

Yan, Z., and C. P. Pantelides. 2011. “Concrete Column Shape Modification with FRP Shells and Expansive Cement Concrete.” *Construction and Building Materials* 25 (1): 396–405.

Yuan, Wen Hua, Qin Yong Ma, and Peng Bo Cui. 2011. “Test and Analysis of Expansive Deformation for Shrinkage-Compensating Steel Fiber Reinforced Shotcrete.” In *Advanced Materials Research*, 287:747–53. Trans Tech Publ.

Zalba, Belen, Jose Ma Marın, Luisa F. Cabeza, and Harald Mehling. 2003. “Review on Thermal Energy Storage with Phase Change: Materials, Heat Transfer Analysis and Applications.” *Applied Thermal Engineering* 23 (3): 251–83.

Zeng, Qiang, Mingyong Luo, Xiaoyun Pang, Le Li, and Kefei Li. 2013. “Surface Fractal Dimension: An Indicator to Characterize the Microstructure of Cement-Based Porous Materials.” *Applied Surface Science* 282: 302–7.

Zhang, Jingchuan, Jialiang Wang, Sufen Dong, Xun Yu, and Baoguo Han. 2019. “A Review of the Current Progress and Application of 3D Printed Concrete.” *Composites Part A: Applied Science and Manufacturing* 125: 105533.

Zhou, Dan, Chang-Ying Zhao, and Yuan Tian. 2012. “Review on Thermal Energy Storage with Phase Change Materials (PCMs) in Building Applications.” *Applied Energy* 92: 593–605.